molecular-beam electric-resonance studies of linear triatomic molecules

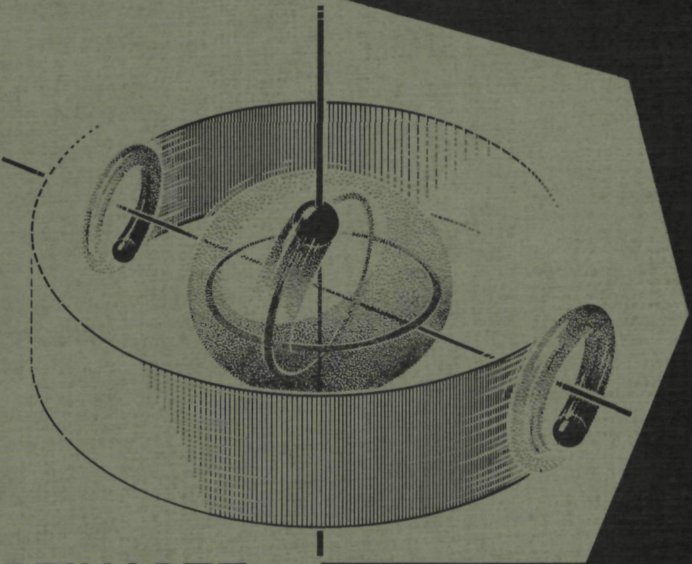

J.M.L.J. REINARTZ

MOLECULAR–BEAM ELECTRIC–RESONANCE
STUDIES OF
LINEAR TRIATOMIC MOLECULES

PROMOTOR PROF DR A DYMANUS

MOLECULAR–BEAM ELECTRIC–RESONANCE STUDIES OF LINEAR TRIATOMIC MOLECULES

PROEFSCHRIFT

ter verkrijging van de graad van doctor
in de wiskunde en natuurwetenschappen
aan de Katholieke Universiteit te Nijmegen,
op gezag van de Rector Magnificus
prof. dr. A.J.H. Vendrik
volgens besluit van het College van Decanen
in het openbaar te verdedigen
op donderdag 2 december 1976
des namiddags te 4 uur

door

JEAN MARIE LEON JOSEPH REINARTZ
geboren te Rimburg

1976

druk: krips repro meppel

Van de velen die bijgedragen hebben aan de tot standkoming van dit proefschrift wil ik enkelen in het bijzonder bedanken.

Dr. L. Meerts voor zijn dagelijkse interesse in het onderzoek en zijn daadwerkelijke steun bij het oplossen van vele problemen.

De Heren J. Holtkamp, L. Hendriks en C. Sikkens, F. van Rijn en E. van Leeuwen voor hun technische hulp.

Dr. O.B. Dabbousi from who I learned not only to hope for better signal to noise ratios but also the experimental techniques to achieve them.

Dr. R. van Wachem en Dr. F.H. de Leeuw die mij ingewijd hebben in de elektrische-resonantie-techniek.

Dr. J. Reuss voor de stimulerende gesprekken op momenten dat beslissende wendingen in het onderzoek noodzakelijk waren.

Allen, die behoorden tot de Werkgroep Atoom- en Molekuulfysika tijdens mijn promotieperiode, voor de prettige samenwerking.

De dienstverlenende afdelingen wil ik graag bedanken in de personen van de Heren H. Verschoor, P. Walraven en J. van Langen.

Het manuscript werd getypt door Mevr. E. Remers-Dreuning.

De figuren werden vervaardigd door de afdeling illustratie door de Heren M. Groos en J. Gerritsen en de afdeling fotografie onder leiding van de Heer H. Spruyt.

De faciliteiten, verleend door de Offsetdrukkerij van de Faculteit der Wiskunde en Natuurwetenschappen onder leiding van de Heer J. Geertsen maakten de druk van dit proefschrift mede realiseerbaar.

aan mijn ouders

aan Gerrie

CONTENTS

Page
INTRODUCTION 9

CHAPTER 1 MBER SPECTROSCOPY 14
1.1 Principle of the MBER method 14
1.2 The MBER spectrometer 15
1.3 State selection 18
1.4 Qualitative treatment on signal and noise contributions 21
1.5 Molecular beams 26
  1.5.1 Nozzle beams 26
  1.5.2 Composition of a KCN beam 31

CHAPTER 2 THEORY

2.1 Introduction 34
2.2 Hamiltonian and wavefunctions 35
2.3 Matrix elements of the hyperfine Hamiltonian 40
  2.3.1 Electric quadrupole interactions 41
  2.3.2 Spin-rotation interactions 43
  2.3.3 Spin-spin interaction 45
2.4 Electric field interactions 45
  2.4.1 Stark effect 45
  2.4.2 Electric polarizability interaction 46
2.5 Magnetic field interactions 47
  2.5.1 Molecular Zeeman effect 47
  2.5.2 Magnetic susceptibility 48
  2.5.3 Nuclear Zeeman effect 48
  2.5.4 Translational Stark effect 50
2.6 Special cases 50

CHAPTER 3 EXPERIMENTAL RESULTS

3.1 Introduction 53
3.2 Ground vibrational state measurements; introduction 54
  3.2.1 Carbonyl sulphide ($^{18}O^{12}C^{32}S$ and $^{16}O^{12}C^{33}S$) Stark spectra 54
  3.2.2 Nitrous Oxide ($^{14}N_2{}^{16}O$) 58
    3.2.2a Stark spectra 58
    3.2.2b Stark-Zeeman spectra 62
  3.2.3 Cyanogen chloride ($^{35}Cl^{12}C^{14}N$) 64
    3.2.3a Stark spectra 65
    3.2.3b Stark-Zeeman spectra 67
3.3 First excited bending vibrational state measurements 69

Page
3.3.1 OCS isotopes 70
3.3.1a Zero field spectra 70
3.3.1b Stark spectra 74
3.3.1c Zeeman spectra 77
3.3.2 Nitrous Oxide 80
3.3.2a Zero field spectra 80
3.3.2b Stark spectra 85
3.3.2c Zeeman spectra 86
3.3.3 Cyanogen Chloride 87
3.3.3a Zero field spectra 87
3.3.3b Stark spectra 90
3.4 Measurements and results on KCN and CsOH 91

CHAPTER 4 DISCUSSION OF RESULTS

4.1 Introduction 94
4.2 Molecular quadrupole moments 94
4.3 Sign of the electric dipole moments 96
4.4 Determination of the nuclear shielding factors of ClCN, N_2O and OCS 97
4.5 Anisotropies for axes perpendicular to the molecular axis. Probable molecular structure for excited vibrational states 99
4.6 l-doubling constants; especially OCS 102
4.7 Bending vibrational effects on nuclear quadrupole moments and electric dipole moments 104
4.8 MBER spectroscopy at high temperatures 108
4.9 Final remarks 111

APPENDIX 113
REFERENCES 116

SAMENVATTING 122

Curriculum vitae 125

INTRODUCTION

Molecular-beam electric-resonance (MBER) spectroscopy is one of the most powerful techniques for the determination of the hyperfine structure of molecules and of their electric and magnetic properties. Until quite recently most of the efforts were restricted to the study of stable diatomic alkali halides coherent with the detection techniques available at that time. A complete review of this group of molecules is given by Lovas and Lide (LOV 71). With the introduction of the universal beam detectors for MBER spectrometers around 1960 new fields of investigations were opened. Recent MBER studies on diatomic molecules have been performed on HF, HCl and HBr (KAI 70, LEE 71,73 and DAB 73), on CO (LEE 71, MUE 75, MEE 76a) and on SiO and GeO (DAV 74), all stable $^1\Sigma$ molecules. Studies on diatomic open-shell molecules have been performed on NO, OH, OD, SH and SD (MEE 72, 75a, 75b, 76b) all with a $^2\Pi$ ground state and on LiO (FRE 72). The metastable $^3\Pi$ CO molecule has been studied by MBER spectroscopy by Wicke *et al*. (WIC 72).

The step from diatomic to polyatomic molecules for MBER research appears to be larger than expected at first glance. Major difficulties of research on larger molecules stem from very large density of spectra and the low population of especially the lower quantum states. The simplest polyatomic molecules are the linear triatomics. When the present investigations were started the only triatomic molecules studied with MBER were OCS (MUE 68, LEE 70,71) and HCN (TOM 70, see also DYK 74) at low temperatures, 100-300 ^{o}K. Other polyatomic molecules succesfully studied by the MBER method are some asymmetric and symmetric top molecules all thoroughly reviewed by Dyke and Muenter (DYK 74). These authors also give a complete survey of the study of weakly bound chemical species like dimers and van der Waals molecules, a new development in molecular beam spectroscopy.

The primary goal of the present investigations was the extension of high temperature (∿1000 °K) MBER spectroscopy to polyatomic molecules. This extension turned out to be a very difficult step. Thus far the only triatomic "linear" molecule that has been studied by MBER spectroscopy is LiOH (FRE 70, see also DYK 74). All the other alkali hydroxides have been studied only by microwave absorption techniques; NaOH and KOH by Pearson and Trueblood (PEA 73b, 73a) and by Kuijpers *et al*. (KUI 76a,75), RbOH by Matsumura and Lide (MAT 69) and CsOH by Lide and Kuczkowski (LID 67). Difficulties in chemical preparation and handling of the alkali hydroxides at high temperatures and weak line intensities made the spectra especially of the lighter compounds undetectable until recently. By employing special container and cell materials which come into contact with the hot vapours and liquids and by application of special detection techniques (TOR 73) those difficulties could succesfully be overcome for some molecules.

All the spectra observed indicated that the alkali hydroxides are subject to unusually strong vibration-rotation effects for the bending vibrations caused by the large amplitudes of the bending motion (LID 69). The spectra could be interpreted satisfactorily only on the basis of a linear equilibrium geometry for the molecules. A bent structure leading to an asymmetric rotor spectrum could, however, be ruled out for those molecules.

Probably the same pertains also to another group of high temperature compounds, the alkali cyanides. From mass spectrometric studies on NaCN (POR 61) it is known that the compound evaporates as a mixture of monomers and dimers at 1000 °K. From recent mass spectrometric and electric deflection studies on KCN beams at about 1000 °K (see Sect. 1.5.2) it was found that the neutral beam consists of monomers for at least 60%. The remaining fraction of the beam consists mainly of free

K atoms produced by decomposition reactions of liquid or gaseous KCN with the oven materials. Other workers (see e.g. ZOR 73) observed numerous weak radio-frequency transitions but could not analyze them in terms of KCN structure. Recently microwave spectra have been obtained by Kuijpers et al. (KUI 76b). The interpretation of the spectra tends to a structure containing a polytopic bond between the K atom and the cyano group. Clementi et al. (CLE 73) have predicted a similar structure for LiCN.

As the prospects of obtaining well resolved spectra for molecules like KCN and CsOH did not look bright it was decided to achieve first more insight in spectra and structure of linear triatomic molecules at lower temperatures (∿300 ^{o}K) before extending to higher temperatures.

One of the most characteristic properties of linear triatomic molecules as compared with diatomic molecules is the presence of, in principle, four modes of vibration. In addition to two stretching modes with motions along the molecular axis also two degenerate bending vibrations are possible. From classical point of view these two motions perpendicular both mutually and to the molecular axis can, with proper phasing, be seen as a rotation around the axis. If also rotation of the nuclear frame around an axis perpendicular to the molecular axis is considered different Coriolis forces for the different directions of vibration result in a distortion of the symmetry around the axis. This phenomenon, revealed by a slight splitting of the rotational energy levels, is known as l-type doubling, the split levels as l-doublet. The special behaviour of these l-doublet states forms the major problem in obtaining high resolution spectra of triatomic molecules as will be explained in details in Sect. 1.4. An extensive investigation of triatomic molecules in the excited bending vibrations at low temperatures forms a proving ground for development of techniques for high temperature studies.

In the present work the MBER technique has been employed to investigate the spectra of the high temperature species KCN and CsOH and at low temperatures the spectra of five different isotopic species of OCS in natural mixture and the most abundant isotopic species of N_2O and ClCN. For the low temperature species spectra in the ground state and in the first excited state of the bending mode have been obtained. Bending vibrational effects on hyperfine constants and on electric and magnetic constants have been deduced from these spectra. The introduction of nozzle beam sources has been a factor of great importance for this study. For the ground states high resolution spectra have been obtained both in external electric and in combined parallel electric and magnetic fields. These spectra could well be explained by the known theories for molecules in a $^1\Sigma$ state to within an experimental accuracy of about 50-150 Hz. Extension of the theory needed for the interpretation of the spectra for excited bending states is given in Chap. 2. Hyperfine properties and electric and magnetic constants have been obtained with very high accuracy from the analysis of the frequencies of the observed transitions within one rotational state ($\Delta J=0$ transitions).

The first chapter (Chap. 1) describes the general features of MBER-spectroscopy and -spectrometer and gives a survey of the problems especially at high temperatures. The production of intense molecular beams by the application of nozzle sources for this spectroscopic technique is demonstrated. Production of hot beams and the determination of their composition by mass spectrometric and beam deflection techniques is discussed. The Hamiltonian used for the interpretation of the spectra is given in Chap. 2. Experimental results on spectra and molecular constants are collected in Chap. 3. In the last chapter (Chap. 4) some new molecular properties are derived from the present results and discussed in terms of electronic properties of the relevant molecules. A complete survey of the measured molecular constants together with the quantities derived from them (in Chap. 4) are given in the Appendix.

CHAPTER 1

MBER SPECTROSCOPY

1.1 PRINCIPLE OF THE MBER METHOD.

A schematic diagram of an MBER spectrometer is given in Fig. 1.1. Its main components are: the source producing and shaping the molecular beam, the detector whose output is proportional with the number of molecules which enter it, the state polarizing (selecting) and analyzing inhomogeneous electric fields A and B, respectively, and a homogeneous electric (for historical reasons called)C-field. The latter fields incorporates some structure inducing transitions between selected quantum states.

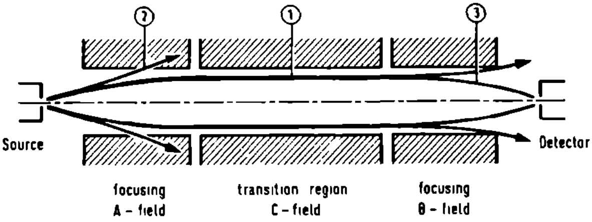

Fig. 1.1 Possible trajectories of polar molecules in an MBER spectrometer for flop-out operation. The numbers are explained in the text.

By the action of the polarizing A-field the beam molecules in a certain state or states are deflected in such a way as to form an essentially parallel beam traveling through the C-field region (see trajectories 1 in Fig. 1.1); molecules in other states are deflected out of the beam (trajectories 2). In an ideal situation all molecules traveling through the C-field region are in one well specified state. If no transition is induced in this field, the B-field, which is identical to the A-field, focuses the molecules on the entrance slit of the detector (trajectories 1-3). On the other hand, if a transition is induced in the C-field from a state selected by the A-field to a state rejected from the beam by this field the molecules which made the transition are deflected out of the beam and there is a decrease in the number of molecules reaching the detector. Whether a transition takes place and hence a decrease of detector output signal is observed or not, depends on the frequency of the radiation applied to the C-field. Sweeping the frequency through regions where the transitions can be expected yields the spectrum of the induced transition as in the classical absorption spectroscopy. This spectrum mostly consists of just several spectral lines whose frequencies contain information about the energy levels of the molecule in question.

It is clear from the foregoing that the most important feature of the MBER spectrometers is the state selection. Its principle and practical realization are discussed in some details in Sect. 1.3.

Molecular-beam resonance spectroscopy has some advantages with respect to both conventional microwave spectroscopy and to other techniques, e.g. beam absorption and beam-masers. In the first place a very high resolution can be achieved in the MBER spectrometers. In principle the only limit for resolution is the time τ for a molecule to pass through the resonance region. The line width $\Delta\nu$ defined as the full width at half maximum (FWHM) of a spectral line is inversely proportional to τ with a proportionality constant of about unity. Normally line widths of 2 to 8 kHz are obtained if the transition field is 10 cm long. Another advantage is the large frequency range extending from less than 50 kHz to submillimeter wave region, which can be covered without resonant structures. Because the flux of molecules is monitored and not the spectroscopic radiation, the sensitivity of the spectrometer does not depend on the frequency.

This is especially advantageous at low (radio) frequencies where all other techniques fail for sensitivity reasons (except in a few special cases). Spectra of molecules not yet studied by more conventional microwave techniques can easily be obtained by MBER spectroscopy. Rapid searching for transitions is possible by broadening the spectral line on purpose by mixing white noise to the RF signal or by saturation broadening of the line at increased RF power levels. This technique facilitates considerably the search for the lines because broadened lines are much more easily detected and saturation generally yields the highest line intensity. The price paid for all this is of course some loss in resolution, but after a rough indication of the presence of the line accurate high resolution recordings can be made. Because of the possibility of applying external electric and/or magnetic fields to the C-field region also Stark and Zeeman spectra can be obtained yielding electric and magnetic moments of the molecules. Moreover identification of spectral lines can be made by observing their behaviour in those fields.

Disadvantages of the MBER method are the need of a rather complicated instrumentation, its lower sensitivity at high frequencies as compared with for instance absorption spectroscopy; the requirement of state selection and its difficult applicability to large molecules.

1.2 THE MBER SPECTROMETER.

The molecular-beam electric-resonance spectrometer used to study the high temperature species was essentially the machine designed and constructed by van Wachem (WAC 67a). The spectrometer, equipped with a hot-wire detector, is described in details in the reference cited. This machine will be indicated in the next chapters as EBR I machine. The only essential modification was the addition of a universal detector employing electron bombardment ionization and a quadrupole mass filter, so

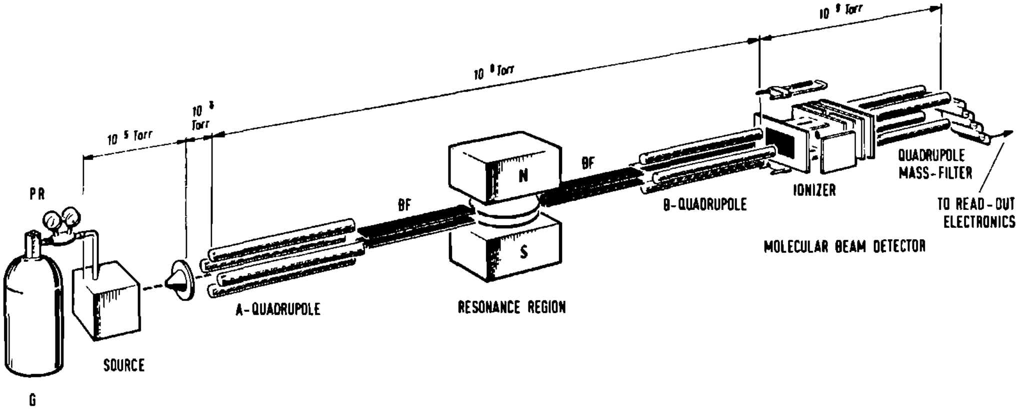

Fig. 1.2 Schematic diagram of the spectrometer (modification of the version of de Leeuw (LEE 71,73) and Meerts (MEE 75a). (G) gas reservoir, (PR) pressure regulator, (BF) buffer fields.

that also zero-field and Stark spectra of OCS could be obtained. For the measurements on N_2O and ClCN and for all Zeeman measurements mainly another spectrometer, called EBR II machine, has been used. This machine, schematically shown in Fig. 1.2, is described in full detail by de Leeuw (LEE 71,73). The most prominent features of the EBR II spectrometer are a sensitive universal beam detector, a relatively long transition region (30 cm), an external magnetic field and state selectors especially designed to sustain high voltages. All components are housed in ultra high vacuum chambers pumped by ion getter pumps. High ionization efficiency has been achieved by the application (MEE 75a) of an electron bombardment ionizer designed by Stolte (STO 72).

Application of nozzle sources with small nozzle diameters (100μ) and high backing pressures, resulted in the production of strong supersonic beams. The population of rotational levels in these beams does no longer correspond to the equilibrium distributions characterized by the source temperature (Sect. 1.5.1).

1.3 STATE SELECTION.

State selection of molecules in an MBER spectrometer is performed with inhomogeneous electric A and B fields. Those fields exert forces on the electric dipole moment of polar molecules directed towards regions of lower energy. The force is given by

$$\vec{F} = -\text{grad } W = - \frac{\partial W}{\partial E} \text{grad } E \qquad (1.1)$$

where W is the Stark interaction energy. The quantity $(\frac{\partial W}{\partial E})$ is often called effective dipole moment. The Stark energy of a polar molecule can be written as a power series

$$W(E) = \alpha E + \frac{1}{2} \beta E^2 + \frac{1}{3} \gamma E^3 + \ldots \qquad (1.2)$$

with coefficients α, β, γ ... depending on the quantum state. The effective dipole moment for $^1\Sigma$ diatomic and triatomic linear molecules in the ground vibrational state is proportional to E (α=0)

$$\mu_{eff} = \beta E = \frac{-3\,\mu_{el}^2 E}{hBJ(J+1)}\;\frac{3M_J^2-J(J+1)}{3(2J-1)(2J+3)} \qquad (1.3)$$

in fields where higher orders can be disregarded. However molecules in an excited bending vibrational state experience essentially linear Stark effect (only $\alpha \neq 0$) and in field regions where no higher order corrections have to be considered a constant effective dipole moment is found:

$$\mu_{eff} = \alpha = -\frac{\mu_{el} M_J l}{J(J+1)} \qquad (1.4)$$

In expressions (1.3) and (1.4) μ_{el} is the electric dipole moment, B is the rotational constant, h is Planck's constant, J is the rotational quantum number, M_J and l is the quantum number of the projection of the total angular momentum $\underline{J}$ along the external field and the molecular axis, respectively. From Eq. 1.4 it can be seen that the effective dipole moment for excited bending vibrational states does not depend on the electric field strength but only on molecular parameters. Furthermore many different states yield exactly the same μ_{eff}. For example all excited v_2 states with l=1 and J=1 M_J=1 yield $\mu_{eff} = -\frac{1}{2}\mu_{el}$, as also do all v_2 states with l=2, J=3, M_J=3; l=3, J=3, M_J=2 and J=5, M_J=5; l=4, J=7, M_J=7; l=5, J=5, M_J=3, and so on. This phenomenon is responsible for severe problems when selection of single states is required. In Sect. 1.4 the consequences of this bad separation of the different states are discussed in terms of signal and noise contributions, especially for molecules with linear Stark effect.

As focusing fields electric quadrupoles and hexapoles have been used with the cylindrically symmetric field gradients we have

- for 4-poles

$$|E_4(r)| = \frac{2V_o}{r_o^2}\, r \quad \text{and} \qquad \text{grad}\ |E_4(r)| = \frac{2V_o}{r_o^2}\, \frac{\vec{r}}{r} \qquad (1.5)$$

- for 6-poles

$$|E_6(r)| = \frac{3V_o}{r_o^3}\, r^2 \quad \text{and} \qquad \text{grad}\ |E_6(r)| = \frac{6V_o}{r_o^3}\, \vec{r} \qquad (1.6)$$

where $+V_o$ and $-V_o$ is the potential of adjacent bars of the four or six pole field, r_o is the distance of an electrode to the n-pole axis and $\vec{r}$ is the radius vector perpendicular to the axis. Though Eqs. 1.5 and 1.6 are only satisfied in case of hyperbolic electrodes they are also valid in first approximation when cylindrical rods, as in the present experiment, are used. From Eqs. 1.1 through 1.6 the focusing force on a dipole is (with α and β defined in Eqs. 1.3 and 1.4, respectively):

4-pole.

$$\text{first order Stark effect } \vec{F} = -\frac{2\alpha V_o}{r_o^2}\, \frac{\vec{r}}{r} \qquad (1.7)$$

$$\text{second order Stark effect } \vec{F} = -\frac{4\beta V_o^2}{r_o^4}\, \vec{r} \qquad (1.8)$$

6-pole:

$$\text{first order Stark effect } \vec{F} = -\frac{6\alpha V_o}{r_o^3}\, \vec{r} \qquad (1.9)$$

$$\text{second order Stark effect } \vec{F} = -\frac{18\beta V_o^2}{r_o^6}\, r^2 \vec{r} \qquad (1.10)$$

The trajectories of molecules entering an n-pole at its axis under a certain angle γ and with a given velocity v are obtained by solving the radial equation of motion $\vec{F}_r = m\, \frac{d^2\vec{r}}{dt^2}$.

A force F_r proportional with r as in Eqs. 1.8 and 1.9 yields harmonic motion independent of the entrance angle γ; a force F_r independent of the magnitude of r as in Eq. 1.7 results in parabolic trajectories (REI 69) and the force F_r of Eq. 1.10 yields a force proportional to r^3 (ENG 71). The force is directed (1) towards the beam axis for $\mu_{eff} > 0$ and (2) away from it for $\mu_{eff} < 0$. Molecules in states yielding the first case are focused on the axis, those yielding the second case are deflected out of the beam. Given a certain geometry of the state selector the trajectories of the molecules for the considered cases depend strongly on the velocity of a molecule and on the voltage V_o.

It has been shown theoretically (REI 69, REI 70a) as well as experimentally (REI 72c) that molecules with linear Stark effect can be focused with 4-pole and with 6-pole fields. The optimum obtainable signal to noise ratio of the $v_2=1$, J=1 l-doublet transition of OCS was a factor of about 1.6 better with 6-poles than with 4-poles. Molecules with second order Stark effect turned out to be almost ideally focused with quadrupole fields. Use of quadrupoles is the best compromize when molecular states with first and/or second order Stark effect have to be investigated with a single state selector.

1.4 QUALITATIVE TREATMENT ON SIGNAL AND NOISE CONTRIBUTIONS.

A molecule in a particular quantum state leaving the source with velocity v making an angle γ with the machine axis will reach the detector only for certain values of γ. The limits for γ (γ_{min} and γ_{max}) depend on machine geometry, state selector voltages V_o and the effective dipole moment which we now write as $\mu_{eff} = \rho\mu_{el}$. In the case of focusing a state with linear Stark effect by means of electric quadrupole fields it has been shown that γ_{min} and γ_{max} depend on the quantity $\rho V_o/v^2$ (REI 69). For other combinations of Stark field dependence and selector geometries analogous quantities can be defined. This means that in the chosen example the detector signal, which is proportional with the solid angle $S=\pi\ (\gamma^2_{max} - \gamma^2_{min})$, at the applied voltages V_o is a function of the quantity ρ/v^2. The function $S(\rho V_o,v)$ is known as the velocity acceptance of the machine.

The focused signal at velocity v depends also on the probability I(v) of finding molecules with that particular velocity in the beam. The function I(v) represents the velocity distribution of the source. The focused detector signal for a certain velocity v is proportional to

$$R(\rho V_o,v) = \frac{S(\rho V_o,v)I(v)}{\int_o^\infty I(v)dv} \tag{1.11}$$

This signal depends strongly on source properties and on the Stark effect of the particular molecule. For a molecule of mass 65 (KCN) at a source temperature of 1000 ^oK, and a Maxwell-Boltzmann velocity distribution in the beam the function $S(\rho V_o,v)$ and I(v) are depicted in Fig. 1.3 for the geometry shown in the inset. For the calculation of $S(\rho V_o,v)$ the machine configuration of WAC 67a and state selector voltages V_o of 1 kV have been chosen for $\rho=\frac{1}{2}$ ($J=1$, $l=1$, $M_J=1$) (REI 69). The state selector voltages V_o are optimum when $\int_o^\infty R(\rho_o V_o,v)dv$ reaches a maximum for a particular ρ_o. A voltage V' gives optimum conditions for a ρ' value satisfying the relation $\rho'V' = \rho_o V_o$. The distribution function $S(\rho'V',v)$ calculated for the voltage V' than exactly coincides with $S(\rho_o V_o,v)$ at V_o. Strictly speaking molecules with only one axial velocity are focused on the axis at the detector; molecules with lower (higher) axial velocities are focused in front of (beyond) the detector. In our example $R(\rho V_o,v)$ is a function of ρ/v^2 for a given V_o. This means that molecules in quantum states with slightly lower (higher) ρ values experience also optimum conditions for slightly lower

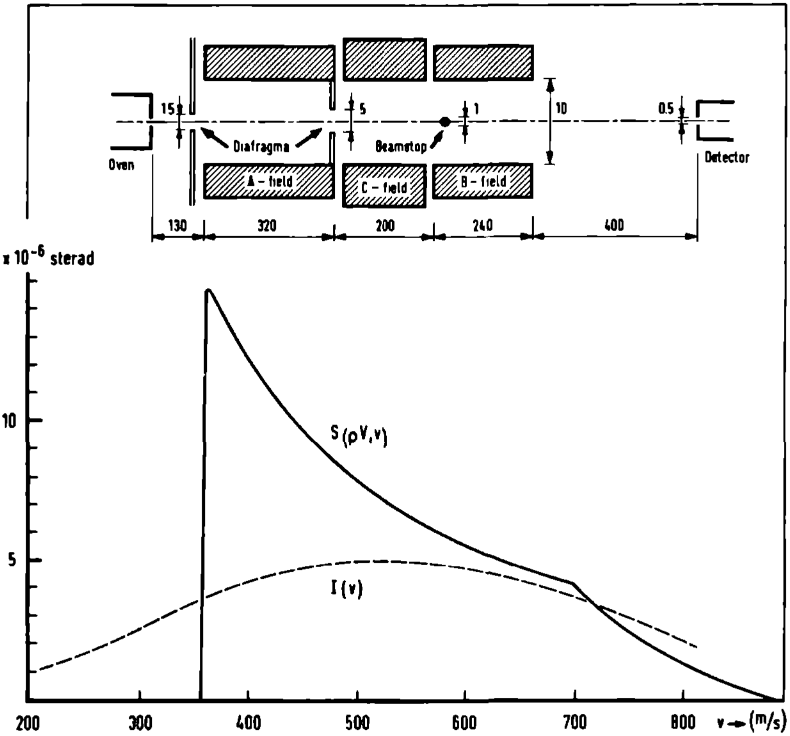

Fig. 1.3 Transmission probability S(ρV,v) (in sterad) for a fixed value of ρ (=½) and optimum voltage V, and a Maxwell-Boltzmann velocity distribution I(v) (in arbitrary units) for a molecular beam at 1000 $^{\circ}$K and molecular mass of 65. The upper figure illustrates the machine configuration used in the calculations of S(ρV,v). All distances are in mm.

(higher) velocities. The function $R(\rho V_o,v)$ at a certain velocity v therefore can be considered as a weighting factor for the degree of focusation of ρ at optimum focusation conditions for ρ_o. Whether or not the ρ's in the neighbourhood of ρ_o really do contribute to the focused signal depends strongly on their population. The population $f(\rho)$ of a given ρ is determined as the sum of populations of all states with quantum numbers v_2,J,l,M_J for which the value of ρ fell within a given interval. We arbitrarily used an interval width $\Delta\rho = 0.01$ for the calculation.

The major difficulty in obtaining MBER spectra of linear triatomic molecules (especially when heated up to several hundreds degrees) is the large number of vibrational states populated at these temperatures. Since electric field state selectors do not discriminate effectively between the different vibrational states to which a certain J,l,M_J-state belongs, many are present in the focused beam. Also individual rotational states can generally not be separated; at best a group of states with nearly the same effective dipole moments may be selected. This can be readily seen from the distribution functions $f(\rho)$ for CsOH and KCN as given in Figs. 1.4 and 1.5, respectively, for normal working temperatures of 1000 ^oK. If the population distributions are compared with the distribution for OCS at room temperature as shown in Fig. 1.6 it turns out that for KCN and CsOH more highly populated states with nearly equal effective dipole moments occur especially in the higher ρ regions. Higher ρ's belong to just the states we are primarily interested in. For CsOH at 900 ^oK a list of states with all ρ-values greater or equal to 0.45 and their population is given elsewhere (REI 71a). Most of the states tabulated there belong to low l values; in principle all states with $v_2 \geqslant 1$ contribute, because l can take values $l = -v_2, -v_2+2, \ldots, \ldots, v_2$, and also

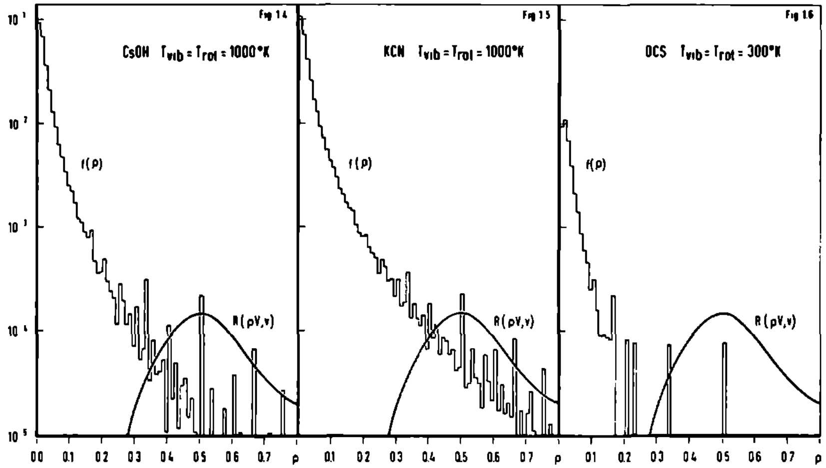

Fig. 1.4, 1.5 and 1.6 Population distribution functions f(ρ) for CsOH at 1000 °K (Fig. 1.4), for KCN at 1000 °K (Fig. 1.5) and for OCS at 300 °K (Fig. 1.6). The function R(ρV,v)(in arbitrary units) is chosen so that optimum focusation is obtained for ρ=½.

the higher M_J values of the lower J states. As we are interested in selection of one single state, for instance the $v_2=1$, J=1, l=1, $M_J=1$ state with ρ=½, other highly populated states with ρ=½ or with ρ's in the neighbourhood of ½ as for instance the J=2, l=2, $M_J=2$ states with ρ=0.67; J=3, l=2, $M_J=3$ states with ρ=0.5; J=3, l=3, $M_J=2$ states with ρ=0.5; J=4, l=3, $M_J=3$ states with ρ=0.45; J=4, l=3, $M_J=4$ states with ρ=0.6 and many others, are also focused and thus are responsible for the large noise contributions. Apart from large noise contributions this multiplicity of focused states can also give rise to very dense spectra if vibrational and rotational effects are not large. A qualitative discussion of possible improvement in the signal to noise ratio for ''high temperature molecules" making use of the functions f(ρ) and R(ρV;v) will be given in Sect. 4.8.

1.5 MOLECULAR BEAMS.

For the formation of the beams in the present investigations two types of sources have been used: the two-chamber oven of van Wachem (WAC 67a) for the high temperature beams and a simple nozzle source for the low temperature species. The nozzle source was a gas container with an easily replaceable front piece in which the nozzle hole was drilled or sparked. Performance of this nozzle source is compared with that of a simple effusive source in Sect. 1.5.1.

For beams of OCS, N_2O and ClCN the most intense peaks in the mass spectrum were found at m/e=60, 44 and 61 respectively. These m/e-values correspond with the single ionized monomers so that polymers, if present in the beam and if not dissociatively ionized, did generally not contribute to the detected beam signal.

Beams of KCN, and also other alkali containing compounds, mostly were detected with a hot wire detector because of its high ionization efficiency (∿100%) for these species. The detector output was proportional to all alkali containing products of the reaction at the surface of the hot wire. In this case all polymers present contribute to the beam signal. In the early stage of the experiment on KCN it appeared necessary to know what fraction of neutral monomers in the KCN beam was sufficient for spectroscopic research. Therefore the molecular composition of the beam has been examined using the mass detector and the quadrupole fields of the MBER machine to deflect a beam of polar molecules. This experiment is described in Sect. 1.5.2.

1.5.1 Nozzle beams.

Nozzle sources are attractive for production of supersonic beams for MBER spectroscopy because of the rotational cooling, increased intensity in the forward direction and more effective focusing as a result of the much narrower distribution of velocities in the beam. In order to get more insight in the properties of such supersonic beams, velocity distributions, beam intensities and spectral line intensity of the $v_2=0$, $J=1 \rightarrow 1$, $|\Delta M_J|=1$ Stark transitions of OCS have been measured as a function of the pressure for several nozzle diameters.

Velocity distribution measurements have been performed on a machine especially designed for molecular cluster production (DEU 76) using a nozzle diameter $d=28\mu$ and optimum conditions for nozzle beam formation. The beam velocity distribution was supposed to be proportional to

$$v^3\, e^{-m(v-\omega_e)^2/2kT_e}, \tag{1.12}$$

where v is the velocity, m the molecular mass, ω_e the stream velocity and T_e the stream temperature related to the three dimensional velocity distribution. As the detector signal is proportional to v^{-1} the measured distribution, h(v), is proportional to $v^2 \exp(-m(v-\omega_e)^2/2kT_e)$. A slotted disc type velocity selector of length l has been used with a transmission function $I(v,v_o)$ of the form

$$I(v,v_o) = \left(1-3\left|\frac{v_o-v}{v}\right|\right) \text{for } 3/4\ v_o < v < 3/2\ v_o \tag{1.13}$$

and $\qquad I(v,v_o) = 0 \qquad$ otherwise.

The rotation frequency of the selector was $\omega_o=2\pi\ v_o/l$. The detector signal is then given by

$$g(v_o) = \frac{1}{N} \int_{3/4\ v_o}^{3/2\ v_o} h(v)I(v,v_o)dv \tag{1.14}$$

where N is a proper normalisation factor (REI 72c). Velocity distributions have been measured for OCS at inlet pressures from 10 to 4000 Torr and brought into agreement with the theoretical curves by adjusting ω_e and T_e. The experimental results, shown in Fig. 1.7, include the most probable velocity

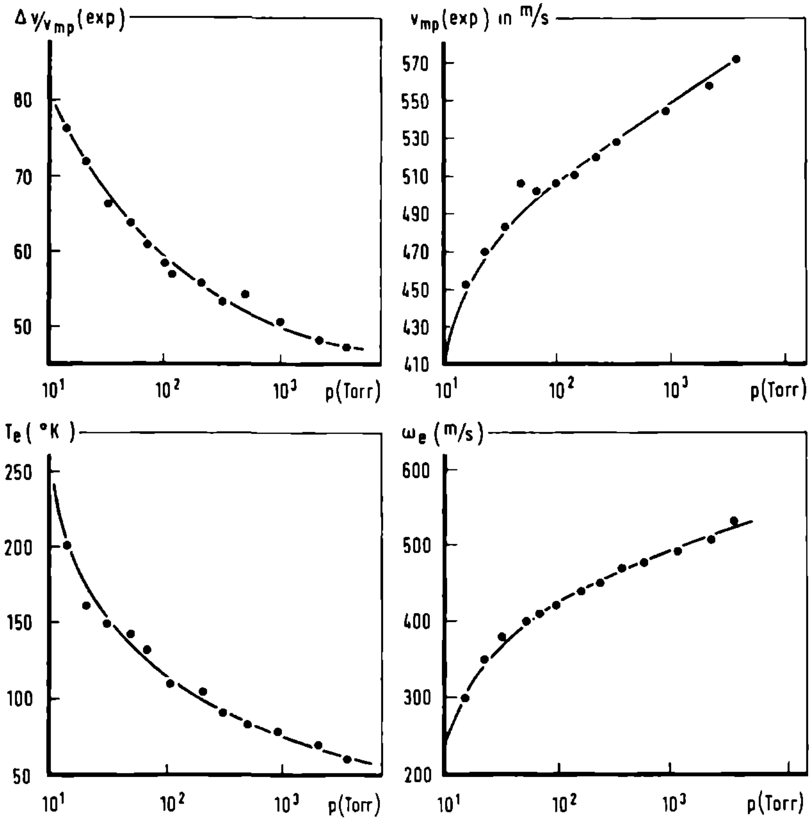

Fig. 1.7 Experimentally obtained $\Delta v/v_{mp}$ and v_{mp} as a function of the backing pressure using a 28μ nozzle diameter. The lower curves represent the best-fit values for translational temperature (T_e) and stream velocity (ω_e) as a function of the backing pressure.

(v_{mp}) and $\Delta v/v_{mp}$ where Δv is the full width at half maximum of the distribution curve. The same figure shows the adjusted stream temperature (T_e) and stream velocity (ω_e) as function of the inlet pressure. The population of the rotational states in the beam can be determined for the different inlet pressures if we assume that the rotational and translational (or stream) temperature do not differ very much.

In earlier experiments an effusive source has been used for the formation of the beams operating at room temperature and with inlet pressures of less than 10 Torr. Signal to noise ratio of the $v_2=0$, $J=1 \rightarrow 1$, $|\Delta M_J|=1$ transitions of OCS obtained under these source conditions were about 15 at RC=0.1 s. Beam and line intensity measurements have been performed on EBR I machine using nozzle diameters of 400, 120 and 60µ and inlet pressures up to 300 Torr. Results are collected in Fig. 1.8. Using the smaller nozzle diameters a maximum gain in signal to noise ratio (S/N) for the $v_2=0$, $J=1 \rightarrow 1$, $|\Delta M_J|=1$ transitions of OCS of about 20 was obtained as compared with these earlier measurements performed at room temperature and with a 400µ "nozzle". For the $v_2=1$ $J=1$ l-doublet transition also a gain in the ratio S/N of about 10 was measured. A rotational temperature of about 80 ^{o}K as deduced from Fig. 1.7 indicates that an improvement in the S/N ratio by a factor of 3-4 can be explained from rotational cooling. Another factor of 3 - 5 originates from the increased forward directed beam intensity and/or the increased focused beam signal. The effect of rotational cooling is clearly seen in Fig. 1.8 at high inlet pressures. At pressures higher than about 50 Torr and nozzle diameters less than about 100µ the beam intensity starts to decrease because of scattering due to the limited pumping capacity but the line intensity still increases as a result of rotational cooling.

Without the gain in the S/N ratio obtained thanks to the use of nozzle sources most of the measurements presented in this thesis would have been impossible.

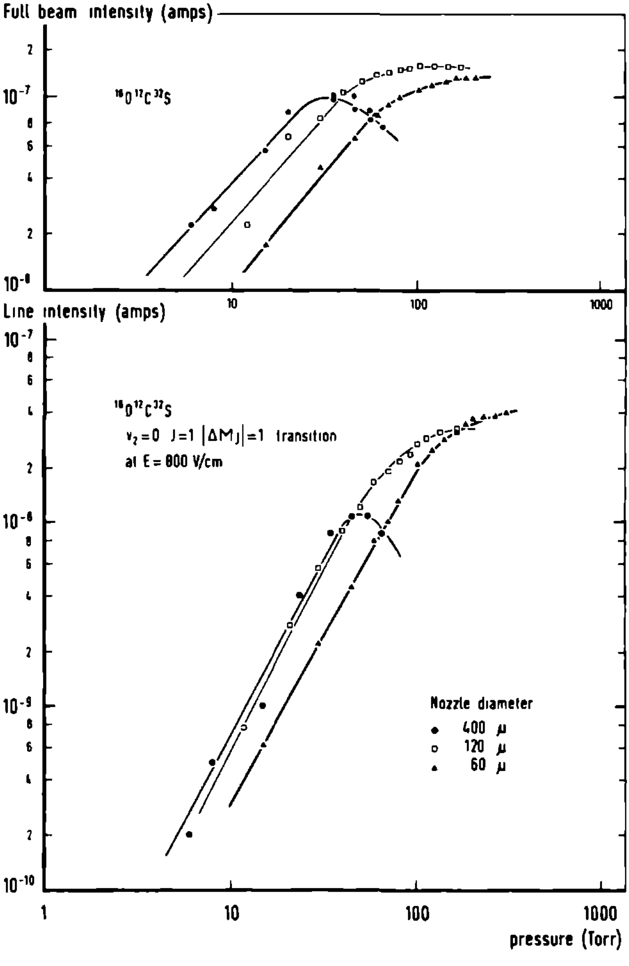

Fig. 1.8 Intensities of full beam and of the $v_2=0$, $J=1$, $|\Delta M_J|=1$ transition line of $^{16}O^{12}C^{32}S$ for several nozzle diameters against backing pressure.

1.5.2 Composition of a KCN beam.

In 1939 Kusch et al (KUS 39) used molecular beams of NaCN, KCN and RbCN for the determination of the nuclear magnetic moment of ^{14}N. At temperatures of 1000 °K they found considerable dissociation ; alkali atoms constituting about 50% of the beam. In 1961 Porter (POR 61) measured the mass spectrum of NaCN around 1000 °K. Much resemblance with sodium halide and hydroxide vapours which exhibit high polymerisation, was found. In the present investigations therefore it appeared necessary to determine the molecular composition of a KCN beam.

At oven temperatures of 900-1100 °K the mass spectrum of the beam has been examined yielding the ion beam composition. To derive from the latter the composition of the neutral molecular beam we need some more information. To this end the beam stop is placed in such a way that it optically blocks the beam from the detector (see e.g. the inset in Fig. 1.3). If a voltage is applied to the state selectors polar molecules which interact strongly with the field may follow curved trajectories around the stop wire onto the detector. The signal intensity, measured with beam stop in and electric quadrupole voltages on, has been studied with and without a field free region between the state selectors. The difference between the two intensities originates mainly from states with second order Stark effect because these states mix in those regions of the beampath where guiding fields are absent. Focused states with linear Stark effect, however, remain occupied and do not mix in field free regions so that the difference in signal with and without C-field voltage on is an indication of the relative number of molecules with second order Stark effect coming from the ground and excited stretching vibrational state.

The most important ion masses are m/e=39 (K^+), 65 (KCN^+) and 104 (K_2CN^+) (REI 72b). In all mass spectrometric measurements of alkali salts (MX), thoroughly reviewed in REI 71a,72b, it was found that the M_2X^+-ion was formed by dissociative ionization of M_2X_2 and hence the intensity on mass 104 can be seen as a measure of the amount of dimers in the beam. Since no refocused signal was observed it has to be concluded that the dimers are nonpolar in accordance with measurements on alkali halides and hydroxides (BUC 64,67).

Two possible reactions in the ionization region may be responsible for the contribution to the signal on mass 65

$$KCN + e^- \rightarrow KCN^+ + 2e^- \qquad (1.15)$$

$$(KCN)_n + e^- \rightarrow KCN^+ + \text{other fragments} \qquad (1.16)$$

with $n \geqslant 2$

Because of the already relatively low dimer signal on m/e=104 it was concluded that contributions in Eq. 1.16 for $n > 2$ are negligible. In combination with electric deflection measurements it is not difficult to show (see REI 72b) that also reaction for n=2 does not give any measurable contribution, so that in principle only reaction 1.15 takes place.

Contributions at mass 39 of K^+ are generally a factor of 20 higher than at mass 65. From deflection and appearance potential measurements ion intensities can be explained by the two possible different reactions

$$K + e^- \rightarrow K^+ + 2e^- \qquad (1.17)$$

$$KCN + e^- \rightarrow K^+ + \text{other fragments} \qquad (1.18)$$

As the behaviour of monomers can be deduced from intensity variations as monitored at mass 65 the magnitude of the contribution of the dissociatively ionized monomers to the ion intensity at m/e=39 can be estimated from deflection measurements. It was found that at least 40% of the signal at this mass originates from neutral monomers in the beam. High alkali atom concentrations are caused probably by reaction of the liquid or gaseous potassium cyanide at high temperature with the oven materials (stainless steel). Coating only the oven crucible with a thin silver layer diminished the reduction reaction (1.17) appreciably, resulting in a percentage of ion intensity on 39 of 60% from neutral KCN molecules.

The conclusion from these mass spectroscopic and electric deflection experiments is that KCN beams do possess enough monomers and are sufficiently intense for the resonance measurements.

CHAPTER 2

THEORY

2.1 INTRODUCTION

The Hamiltonian suitable for the description of the hyperfine structure, Stark effect and Zeeman effect in the spectra of $^1\Sigma$ polar diatomic molecules has been extensively treated by many authors (see e.g. SCH 61, LEE 71). A more general treatment concerning any $^1\Sigma$ molecule, may be found in VER 69 and DYM 76. Thus the Hamiltonian given in the references cited is also valid for linear triatomic molecules in the ground vibrational state. However, in excited states of the degenerate vibration some modification of this Hamiltonian is required. For these states an additional angular momentum (of vibration) along the molecular axis can be defined (HOW 70,71) and the molecule can be considered as a symmetric top. Coupling between vibrational and rotational angular momenta results in a slight splitting of the degenerate rotational energy levels, called l-type doubling. This doubling is in many ways similar to the splitting of symmetric top levels by a slight asymmetry. Besides vibrational effects on rotational energies also hyperfine structure, Stark and Zeeman energies in excited vibrational states will be different from those of the ground vibrational state.

A quantum mechanical description of vibration-rotation interaction in linear molecules has first been given by Nielsen (NIE 43,51) and since then generally accepted and applied by many workers to linear polyatomic molecules (see e.g. YAR 57, TOR 61, DOR 64, MAK 67,73).

In the following section explicit expressions for the vibrational-rotational and hyperfine energies for ground and excited bending vibrational states are given assuming the Born-Oppenheimer approximation to be valid.

2.2 HAMILTONIAN AND WAVEFUNCTIONS.

The molecular Hamiltonian used for the interpretation of the spectra can be written in the form

$$\underline{H} = \underline{H}_o + \underline{H}_{VR} + \underline{H}_{hfs} + \underline{H}_{E,H} \qquad (2.1)$$

In this equation $\underline{H}_o$ represents the electronic and pure vibrational contributions to the Hamiltonian which are not of interest for the present investigations. The next terms represent the vibration-rotation contribution (except for the pure vibrational part), nuclear hyperfine interactions and interactions with an external electric ($\underline{E}$) and magnetic ($\underline{H}$) field. The capital H will be used for the magnetic field strength instead of B to avoid confusion with the B as used for the rotational constant.

The vibration-rotation term of the Hamiltonian can be evaluated starting from the expression

$$\underline{H}_{VR} = B\, \tilde{\underline{N}}^2 \qquad (2.2)$$

where $\tilde{\underline{N}}$ is defined by $\tilde{\underline{N}} = \tilde{\underline{J}} - \tilde{\underline{G}}$ with $\tilde{\underline{N}}$ representing the rotational angular momentum of the nuclear framework and B the rotational constant; $\tilde{\underline{J}}$ and $\tilde{\underline{G}}$ are the total and the vibrational angular momentum, respectively, of the molecule. It is assumed that the electronic angular momentum $\tilde{\underline{L}}$ can be disregarded in a $^1\Sigma$ molecule in first approximation. Operators denoted with tildes, as in $\tilde{\underline{J}}, \tilde{\underline{G}}, \tilde{\underline{N}}$, are defined in the molecule fixed frame of reference (MFFR), and without tildes in the space fixed frame of reference (SFFR).

If the molecular axis is accepted as the z-axis of the MFFR, then $\tilde{\underline{N}}_z = 0$ is a good approximation, and the Hamiltonian (2.2) can be expanded in the form

$$\underline{H}_{VR} = B(\underline{\tilde{J}}^2 - \underline{\tilde{J}}_z^2) + B(\underline{\tilde{G}}_x^2 + \underline{\tilde{G}}_y^2) - 2B(\underline{\tilde{J}}_x\underline{\tilde{G}}_x + \underline{\tilde{J}}_y\underline{\tilde{G}}_y) \qquad (2.3)$$

Basis wavefunctions for the calculation of the matrix elements of this part of the Hamiltonian can be written as products:

$$|v_1 v_2^l v_3 J\rangle = |v_1 v_2^{|l|} v_3\rangle |J l M_J\rangle \qquad (2.4a)$$

where $|v_1 v_2^{|l|} v_3\rangle$, abbreviated as $|vl\rangle$ is the vibrational wavefunction and

$$|JlM_J\rangle = \sqrt{\frac{2J+1}{8\pi^2}}\, D^{(J)}_{lM_J}(\alpha\beta\gamma) \qquad (2.4b)$$

is the rotational wavefunction of a symmetric top molecule (EDM 60). For a triatomic linear molecule there are three normal vibrations whose quantum numbers are v_1, v_2, v_3 and the corresponding energies $\hbar\omega_1(v_1+\frac{1}{2})$, $\hbar\omega_2(v_2+1)$ and $\hbar\omega_3(v_3+\frac{1}{2})$ with ω_1 and ω_3 as stretching vibrational frequencies and ω_2 the bending vibration frequency. The function $|vl\rangle$, defined e.g. by Townes (TOW 55), depends only on $|l|$. In $|JlM_J\rangle, M_J$ represents the quantum number of the component of the total angular momentum along the external z-axis and l that of the component of J along the molecular axis, taking the values $-v_2, -v_2 + 2, -v_2 + 4, \ldots\ldots, + v_2-2, v_2$.

In the representation (2.4) the contribution of the first term of Eq.(2.3) to the energy is given by $B[J(J+1)-l^2]$. The term $B(\underline{\tilde{G}}_x^2+\underline{\tilde{G}}_y^2) = \frac{1}{2}B(\underline{\tilde{G}}_+\underline{\tilde{G}}_- + \underline{\tilde{G}}_-\underline{\tilde{G}}_+)$ is diagonal in $|l|$ and independent of J so that its contribution can be included in $\underline{H}_o$. The term $-2B(\underline{\tilde{J}}_x\underline{\tilde{G}}_x + \underline{\tilde{J}}_y\underline{\tilde{G}}_y)$ is rewritten as

$$\underline{H}_1 = -B(\underline{\tilde{J}}_+\underline{\tilde{G}}_- + \underline{\tilde{J}}_-\underline{\tilde{G}}_+) \qquad (2.5)$$

For the operation of $\underline{\tilde{J}}_\pm$ on the wavefunction (2.4) the following result holds (FRE 66, Eq. 5.2)

$$\underline{\tilde{J}}_\pm \, |JlM_J\rangle = [J(J+1)-l(l\mp1)]^{\frac{1}{2}}|J(l\mp1)M_J\rangle \qquad (2.6)$$

With the knowledge of Eq. (2.6) and that for a certain v_2 and J state only $\Delta l = 2$ interactions are possible, it can be shown that $\underline{H}_l$ in the representation (2.4) yields contributions to the rovibrational energy matrix offdiagonal in l only in second order. This term is responsible for the l-type doubling.

The most appropriate representation for the calculation of the l-doubling is a set of symmetrized wavefunctions

$$|vJlM_J\pm\rangle = 1/\sqrt{2}\left[|vl\rangle|JlM_J\rangle \pm (-1)^J|vl\rangle|J(-l)M_J\rangle\right] \tag{2.7}$$

where l takes only positive values.

The second order contribution to the Hamiltonian can be defined as

$$\underline{H}^{(2)}_{VR} = \sum_{v'l'} \frac{\underline{H}_{VR}|vJlM_J\pm\rangle\langle v'Jl'M_J\pm|\underline{H}_{VR}}{E_{v'l'} - E_{vl}} \tag{2.8}$$

Because we are interested only in contributions for the case l=1 the non-vanishing matrix elements offdiagonal in l appearing in $\langle\pm|\underline{H}^{(2)}_{VR}|\pm\rangle$ generated by $\underline{H}_l$ are

$$\begin{aligned} \langle vJ1M_J\pm|\underline{H}_l|v'J0M_J\pm\rangle &= [\,a\pm\delta_{l1}(-1)^J b]\; B\sqrt{J(J+1)} \\ \langle vJ1M_J\pm|\underline{H}_l|v'J2M_J\pm\rangle &= cB\sqrt{J(J+1)-2} \end{aligned} \tag{2.9}$$

Contributions of second order terms of $\underline{H}_{VR}$ are diagonal in l and can be absorbed in the rotational energy. Their effects are non-detectable in the present investigations as only transitions within a state with the same J and l are observed. The constants a, b and c appearing in Eq. 2.9 are independent of J so that the contribution to the vibration-rotation matrix in second order is

$$\begin{aligned} &\langle vJ1M_J\pm|\underline{H}^{(2)}_{VR}|vJ1\;M_J\pm\rangle = \\ &\quad X + YJ(J+1)\pm\;\delta_{l1}(-1)^J\frac{B^2}{\omega_2}J(J+1)Z \end{aligned} \tag{2.10}$$

where X,Y and Z are functions of the vibrationally dependent a's, b's and c's from Eq. (2.9) and hence of v_2. The definition of Z has been given by Nielsen (NIE 51):

$$\frac{B^2}{\omega_2} Z = \tfrac{1}{2}\, q_{vJ}(v_2+1) = \frac{B^2}{\omega_2}(v_2+1)\Big[\Big(1+\sum_{i\neq 2} 4\xi_{2i}^2 \frac{\omega_2^2}{\omega_i^2-\omega_2^2}\Big) + \text{higher orders in } v\Big] \tag{2.11}$$

where q_{vJ} represents the l-doubling constant. This constant may include measurable higher order effects in J(J+1) and is normally written as (MAK 67)

$$q_{vJ} = q_v - \mu_v J(J+1) + \Delta H\, J^2(J+1)^2 \tag{2.12}$$

with $$q_v = q_e + \sum_{i=1,3} q_{v_i}(v_i+\tfrac{1}{2}d_i) \tag{2.13}$$

and analogous expressions for μ_v and ΔH. In Eqs. (2.12) and (2.13) q_v is the l-doubling constant in the vibrational state v and q_e the l-doubling constant in the equilibrium state, while the constants q_{v_i} are the vibrational corrections and d_i the degree of degeneracy of the v_i state. The Coriolis coupling constants in Eq. (2.11), ξ_{2i}, satisfy the sum rule $\xi_{21}^2 + \xi_{23}^2=1$ and can be determined experimentally by measuring q_{vJ} in several vibration and rotational states. Present investigations concern only excited v_2 states so that additional information is required to obtain the ξ_{2i}^2 's.

Though for one molecule (OCS) also spectra in the $v_2=2$ excited vibrational state have been obtained (COR 73 and see also FAB 74) we restrict ourselves in this section to the theoretical treatment of the $v_2=0$ and $v_2=1$ states. The explanation of the $v_2=2$ spectra requires inclusion of $\Delta l=4$ interactions as given e.g. by Maki and Lide (MAK 67).

The appropriate basis functions for the calculation of the hyperfine sublevels are constructed as linear combinations:

$$|F_1 I_2 F M_F \pm\rangle = \sum_{M_{F_1} M_{I_2}} |F_1 M_{F_1} I_2 M_{I_2} \pm\rangle\langle F_1 M_{F_1} I_2 M_{I_2} | F_1 I_2 F M_F\rangle \qquad (2.14)$$

with $|F_1 M_{F_1} I_2 M_{I_2} \pm\rangle = |F_1 M_{F_1} \pm\rangle |I_2 M_{I_2}\rangle$

and $|F_1 M_{F_1} \pm\rangle = \sum_{M_{I_1}, M_J} |J l M_J I_1 M_{I_1} \pm\rangle\langle J l M_J I_1 M_{I_1} | F_1 M_{F_1}\rangle$

To simplify notation the vibrational indices of the symmetrized functions (2.7) have been dropped in (2.14). The wavefunctions (2.14) are based on the coupling scheme $\underline{I}_1+\underline{J}=\underline{F}_1$ and $\underline{F}_1+\underline{I}_2 = \underline{F}$ which is appropriate if only two non-zero spins are considered. The subscript 1(2) of the nuclear spin vector $\underline{I}$ refers to the nucleus in the molecule which causes the largest (smallest) contributions of $\underline{H}_{hfs}$ to the energy; $M_F (M_{F_1}, M_{I_1}, M_{I_2}, M_J)$ is the component of the angular momentum $\underline{F} (\underline{F}_1, \underline{I}_1, \underline{I}_2, \underline{J})$ along the space-fixed z-axis.

The largest contributions to the hyperfine structure for a singlet electronic state, comprising the Hamiltonian $\underline{H}_{hfs}$, are

$$\underline{H}_{hfs} = \sum_K \underline{Q}_K \cdot \underline{V}_K + \sum_K \underline{I}_K \cdot \underline{M}_K \cdot \underline{J} + \sum_{L>K} \underline{I}_K \cdot \underline{D}_{KL} \cdot \underline{I}_L \qquad (2.15)$$

The first term represents the interaction of the nuclear quadrupole tensor $\underline{Q}_K$ with the gradient tensor $\underline{V}_K$ of the electric field at the position of nucleus K; The second term of Eq. (2.15) is the spin-rotation interaction and the third the interaction between nuclear spins; $\underline{M}_K$ and $\underline{D}_{KL}$ are the nuclear spin-rotation and spin-spin interaction tensor, respectively, and the summation is over all nuclei with $I \geq 1$ in the first term, and with $I \geq \frac{1}{2}$ in the remaining two terms. Cartesian components of the hyperfine tensors as also for the electric and magnetic tensor operators entering below are presented elsewhere (see e.g. VER 69, LEE 71, DIJ 71).

Contributions to the Hamiltonian in external electric (or Stark) fields are

$$\underline{H}_{\underline{E}} = -\underline{\mu}_{el}.\underline{E} - \tfrac{1}{2}\underline{E}.\underline{\alpha}.\underline{E} \qquad (2.16)$$

where the first term represents the Stark effect with μ_{el} the electric dipole moment and where the second term describes the contribution to the energy because of the electric polarizability with α as the polarizability tensor. Magnetic (or Zeeman) field interactions contributing to $\underline{H}_{\underline{H}}$ can be written as

$$\underline{H}_{\underline{H}} = -\underline{H}.\underline{G}.\underline{J} - \tfrac{1}{2}\underline{H}.\chi.\underline{H} - \sum_{K} \frac{\mu_K}{I_K} \underline{I}_{\underline{K}}.(\underline{1}-\underline{\sigma}_{\underline{K}}).\underline{H} - \underline{\mu}_{el}.\underline{v}x\underline{H} \qquad (2.17)$$

The terms of Hamiltonian (2.17) describe in this order the energy contribution because of molecular Zeeman effect, magnetic susceptibility, nuclear Zeeman effect and translational Stark effect. In Eq. (2.17) the usual symbols are used for the magnetic rotational tensor ($\underline{G}$), the magnetic susceptibility ($\underline{\chi}$) tensor, the magnetic dipole moment of nucleus K(μ_K), the nuclear shielding tensor ($\underline{\sigma}_{\underline{K}}$) and the molecular velocity ($\underline{v}$).

Spherical tensor operator techniques (EDM 60, JUD 63) have been applied to calculate the matrix elements of the Hamiltonian (2.1) using basis functions (2.14). If in the case of v_2=0 (and thus l=0) the wavefunctions $|(I_1J)F_1I_2FM_F\rangle$ are defined in the same way as the v_2=1 functions, then the matrix elements for v_2=0 are obtained by taking the v_2=1 results and putting l=0.

2.3 MATRIX ELEMENTS OF THE HYPERFINE HAMILTONIAN.

Typical contributions to the energy of the molecule of the various terms of the hyperfine Hamiltonian (2.15) are 10^2-10^6 kHz for the nuclear quadrupole, 1-10^3 kHz for the nuclear spin-rotation and 10^{-1}-10^2 kHz for the spin-spin interaction. In this sequence of contribution to the energy with descending order of magnitude the expressions for the matrix elements are presented. Detailed derivations of the matrix elements is given elsewhere (REI 74a).

2.3.1 Electric quadrupole interactions.

As the present investigations deal only with molecules with at most two nonzero nuclear spins the quadrupole contribution ($\underline{H}_Q$) to the Hamiltonian (2.15) consists of the terms

$$\underline{H}_Q = \underline{Q}_1 \cdot \underline{V}_1 + \underline{Q}_2 \cdot \underline{V}_2 \qquad (2.18)$$

General matrix element of $\underline{Q}_1 . \underline{V}_1$ can be deduced from the theorems given by Edmonds (EDM 60) or Judd (JUD 63, chap.3) as

$$<(I_1 J l) F_1 I_2 F M_F | \underline{Q}_1 \cdot \underline{V}_1 | (I_1 J' l') F'_1 I_2 F' M'_F> =$$

$$\delta(M'_F, M_F)\,\delta(F'_1, F_1)\,\delta(F'_1, F)\,(-1)^{I_1+I_2+2F_1+F+J}\,[(2F+1)(2F_1+1)]^{\frac{1}{2}} \times$$

$$\begin{Bmatrix} F & 0 & F' \\ F'_1 & I_2 & F_1 \end{Bmatrix} \begin{Bmatrix} I_1 & J' & F_1 \\ J & I_1 & 2 \end{Bmatrix} <I_1||(Q_1)^{(2)}||I_1><Jl||(V_1)^{(2)}||J'l'>$$

$$(2.19)$$

The reduced matrix elements in Eq. (2.19) are evaluated with the aid of Wigner Eckart theorem

$$<I_1||(Q_1)^{(2)}||I_1> = \frac{eQ_1}{2}\left[\frac{(2I_1+3)(2I_1+2)(2I_1+1)}{2I_1(2I_1-1)}\right]^{\frac{1}{2}} \qquad (2.20)$$

with

$$eQ_1 = 2\sqrt{6}\ <I_1 I_1|(Q_1)^{(2)}_0|I_1 I_1>$$

The quantity Q_1 is known as the nuclear electric quadrupole moment of nucleus 1, e is the elementary charge.

The components of a general interaction tensor, $\underline{T}^{(k)}_q$, are transformed from the SFFR to the MFFR (EDM 60), in which the components are denoted by tildes, $\tilde{\underline{T}}^{(k)}_q$, by the relation

$$\underline{T}^{(k)}_{q} = \sum_{q'} \underline{\tilde{T}}^{(k)}_{q'}\, D^{(k)}_{q'q}(\alpha\beta\gamma) \qquad (2.21)$$

The functions $D^{(k)}_{q'q}(\alpha\beta\gamma)$ are defined in EDM 60(Eq. 4.1.12). Evaluation of the reduced matrix element of $(\underline{V}_1)^{(2)}$ using Eq. 2.21 gives

$$\langle J1||(\underline{V}_1)^{(2)}||J'1'\rangle = (-1)^{J-1}\,[(2J+1)(2J'+1)]^{\frac{1}{2}} \sum_q \begin{pmatrix} J & 2 & J' \\ -1 & q & 1' \end{pmatrix} (\tilde{V}_1)^{(2)}_q \qquad (2.22)$$

Herein the spherical tensor components $(\tilde{V}_1)^{(2)}_q$ can be written in terms of molecular coupling constants. The relations between spherical and Cartesian components are given by YUT 62 page 106 or LEE 71. Substituting results of Eq. (2.20) and Eq.(2.22) into Eq. (2.19) yields the general matrix element of $\underline{Q}_1 \cdot \underline{V}_1$ now in the representation (2.14)

$$\begin{aligned}
&\langle (I_1J1)F_1I_2FM_F\pm|\underline{Q}_1\cdot\underline{V}_1|(I_1J'1)F_1'I_2F'M_F'\pm\rangle = \\
&\delta(F_1',F_1)\,\delta(F',F)\,\delta(M_F',M_F)\,(-1)^{I_1+2J+F+1} \quad \times \\
&\left[\frac{(2J+1)(2J'+1)(2I_1+3)(2I_1+2)(2I_1+1)}{2I_1(2I_1-1)}\right]^{\frac{1}{2}} \begin{Bmatrix} F_1 & J' & I_1 \\ 2 & I_1 & J \end{Bmatrix} \times \\
&\tfrac{1}{2}\left[\begin{pmatrix} J & 2 & J' \\ -1 & 0 & 1 \end{pmatrix} eQ_1q_{11} \pm (-1)^J \frac{1}{\sqrt{6}} \begin{pmatrix} J & 2 & J' \\ -1 & 2 & -1 \end{pmatrix} eQ_1q_{12}\right]
\end{aligned} \qquad (2.23)$$

The constants q_{11} and q_{12} are defined in terms of the electric field gradients as

$$q_{11} = (\tilde{V}_1)_{zz} = -\frac{\partial^2 V_1}{\partial z^2} \qquad (2.24)$$

and

$$q_{12} = (\tilde{V}_1)_{xx} - (\tilde{V}_1)_{yy} = -\left(\frac{\partial^2 V_1}{\partial x^2} - \frac{\partial^2 V_1}{\partial y^2}\right),$$

where V_1 is the potential at nucleus 1 produced by all other charges in the molecule.

The expression (2.23) gives both diagonal and offdiagonal contributions in J. The latter are important because energy shifts of the J-levels can amount 10 kHz or more depending on the values of the eQq's and the rotational constant B. Because of symmetry properties of the wavefunctions (2.7) matrix elements $<\pm|\underline{O}|\mp>$ between states with different symmetry all vanish and are not further considered.

By an analogous treatment the matrix contribution of the second quadrupole term of (2.18) may be written as

$$<(I_1J1)F_1I_2FM_F\pm|\underline{Q}_2\cdot\underline{V}_2|(I_1J'1)F_1'I_2F'M_F'\pm> \;=$$

$$\delta(F',F)\,\delta(M_F',M_F)\,(-1)^{I_1+I_2+F_1+F_1'+F+J+J'+1} \quad \mathrm{x}$$

$$\frac{1}{4}\left[\frac{(2J+1)(2J'+1)(2I_2+3)(2I_2+2)(2I_2+1)}{2I_2(2I_2-1)}\right]^{\frac{1}{2}}\left[(2F_1+1)(2F_1'+1)\right]^{\frac{1}{2}} \;\mathrm{x}$$

$$\begin{Bmatrix} F_1' & I_2 & F \\ I_2 & F_1 & 2 \end{Bmatrix} \begin{Bmatrix} F_1 & 2 & F_1' \\ J' & I_1 & J \end{Bmatrix} \left[\begin{pmatrix} J & 2 & J' \\ -1 & 0 & 1 \end{pmatrix} eQ_2q_{21} \pm (-1)^J \frac{1}{\sqrt{6}} \begin{pmatrix} J & 2 & J' \\ -1 & 2 & -1 \end{pmatrix} eQq_{22}\right] \tag{2.25}$$

With this expression also elements with $J'\neq J$ can be calculated because also for this quadrupole term offdiagonal elements in J yield non-negligible contributions to the hyperfine energies. The constants Q_2 and q_{21} and q_{22} of nucleus 2 are defined in the same way as the constants for nucleus 1 (see Eqs. (2.20) and (2.24)). So, the first index (i) of q_{ij} refers to the i-th nucleus while the second index (j) refers to the zz-component of q if j=1 and to the anisotropy for axes perpendicular to the z-axis (the difference $q_{xx}-q_{yy}$) if j=2.

2.3.2 Spin-rotation interactions.

The second hyperfine term ($\underline{H}_{IJ}$) of the Hamiltonian (2.15) involves in the present case contributions of two different nuclei, i.e.

$$\underline{H}_{IJ} = \underline{I}_1 \cdot \underline{M}_1 \cdot \underline{J} + \underline{I}_2 \cdot \underline{M}_2 \cdot \underline{J} \tag{2.26}$$

Because offdiagonal elements do not give measurable effects on the transition frequencies with todays sensitivity of the MBER spectrometer only expressions for $\Delta J = J' - J = 0$ matrix elements will be given. The results for the contribution of nucleus 1 and 2 are

$$\begin{aligned}
&<(I_1 J l) F_1 I_2 F M_F \pm | \underline{I}_1 \cdot \underline{M}_1 \cdot \underline{J} | (I_1 J l) F_1' I_2 F' M_F' \pm> = \\
&\delta(F_1', F_1)\, \delta(F', F)\, \delta(M_F', M_F) \times \tfrac{1}{2} [F_1(F_1+1) - I_1(I_1+1) - J(J+1)] \times \\
&[c_\perp^{(1)} + \frac{l^2}{J(J+1)} (c_\parallel^{(1)} - c_\perp^{(1)}) \pm (-1)^J \delta_{l1} \tfrac{1}{2} (c_{xx}^{(1)} - c_{yy}^{(1)})]
\end{aligned} \tag{2.27}$$

$$\begin{aligned}
&<(I_1 J l) F_1 I_2 F M_F \pm | \underline{I}_2 \cdot \underline{M}_2 \cdot \underline{J} | (I_1 J l) F_1' I_2 F' M_F' \pm> = \\
&\delta(F'; F)\, \delta(M_F', M_F)\, (-1)^{I_1 + I_2 + F_1 + F_1' + F + J + 1} \times \\
&\begin{Bmatrix} F_1' & I_2 & F \\ I_2 & F_1 & 1 \end{Bmatrix} \begin{Bmatrix} F_1 & 1 & F_1' \\ J & I_1 & J \end{Bmatrix} [(2I_2+1)(I_2+1) I_2 (2F_1+1)(2F_1'+1)(2J+1)(J+1)J]^{\frac{1}{2}} \times \\
&[c_\perp^{(2)} + \frac{l^2}{J(J+1)} (c_\parallel^{(2)} - c_\perp^{(2)}) \pm (-1)^J \delta_{l1} \tfrac{1}{2} (c_{xx}^{(2)} - c_{yy}^{(2)})]
\end{aligned} \tag{2.28}$$

The superscripts of the c-constants in the last two expressions refer to the different nuclei, while the subscript $\parallel$ and $\perp$ refers to the components parallel and perpendicular, respectively to the molecular (z-)axis:

$$\begin{aligned}
c_\parallel^{(i)} &= c_{zz}^{(i)} \\
c_\perp^{(i)} &= \tfrac{1}{2}(c_{xx}^{(i)} + c_{yy}^{(i)})
\end{aligned} \tag{2.29}$$

with $c_{aa}^{(i)} = (\tilde{M}_i)_{aa}$ for $a = x, y, z$.

2.3.3 Spin-spin interaction.

The last term of Hamiltonian (2.15), the spin-spin interaction, contains only contributions due to $\underline{D}_{12}$, because in the considered cases at most two non-zero spins occur. The matrix elements of this contribution for $\Delta J=0$ interactions are obtained by the same procedure as used for the spin-rotation interaction.

The result is

$$<(I_1 Jl)F_1 I_2 F M_F \pm | \underline{I}_1 \cdot \underline{D}_{12} \cdot \underline{I}_2 | (I_1 Jl)F_1' I_2 F' M_F' \pm> =$$

$$\delta(F',F)\,\delta(M_F',M_F)\,(-1)^{F_1+I_2+F+1} \times \sqrt{30} \times$$

$$[(2F_1+1)(2F_1'+1)I_1(I_1+1)(2I_1+1)I_2(I_2+1)(2I_2+1)]^{\frac{1}{2}} \times$$

$$\left[\frac{J(J+1)(2J+1)}{(2J-1)\ (2J+3)}\right]^{\frac{1}{2}} \begin{Bmatrix} F_1' & I_2 & F \\ I_2 & F_1 & 1 \end{Bmatrix} \begin{Bmatrix} J & I_1 & F_1 \\ J & I_1 & F_1' \\ 2 & 1 & 1 \end{Bmatrix} \times$$

$$\left[- \frac{3l^2 - J(J+1)}{J(J+1)}\, d_T \pm \tfrac{1}{2}\, (-1)^J\, \delta_{l1}\, (d_{xx} - d_{yy})\right] \qquad (2.30)$$

In this expression the spin-spin interaction constant d_T has been defined as

$$d_T = 1/6\ \left((\tilde{D}_{12})_{xx} + (\tilde{D}_{12})_{yy} - 2(\tilde{D}_{12})_{zz}\right)$$

For the spin-spin tensor the relation $\sum_{g=x,y,z} (\tilde{D}_{12})_{gg} = 0$ is satisfied so that the expression for d_T simplifies to $d_T = -\frac{1}{2}\ (\tilde{D}_{12})_{zz}$.

2.4 ELECTRIC FIELD INTERACTIONS.

2.4.1 Stark effect.

The Stark operator $\underline{H}_E = - \underline{\mu}_{el} \cdot \underline{E}$ written in spherical tensor components is

$$\underline{H}_E = -\mu_{el} E D^{(1)}_{00}(\alpha\beta\gamma)$$

assuming that the electric field is along the space fixed z-axis and the permanent dipole moment along the molecular z-axis. This operator gives non-vanishing matrix elements only between $|\pm\rangle$ and $|\mp\rangle$ states:

$$\langle (I_1Jl)F_1I_2FM_F\pm| -\underline{\mu}.\underline{E}|(I_1J'l)F_1'I_2F'M_F'\mp\rangle =$$

$$\delta(M_F',M_F)(-1)^{F-M_F}\begin{pmatrix} F & 1 & F' \\ -M_F & 0 & M_F \end{pmatrix} \times$$

$$(-1)^{2F_1+I_1+I_2+F'+J'+J+1} \times [(2F+1)(2F'+1)(2F_1+1)(2F_1'+1)(2J+1)(2J'+1)]^{\frac{1}{2}} \times$$

$$\begin{Bmatrix} F & 1 & F' \\ F_1' & I_2 & F_1 \end{Bmatrix}\begin{Bmatrix} F_1 & 1 & F_1' \\ J' & I_1 & J \end{Bmatrix}\begin{pmatrix} J & 1 & J' \\ -1 & 0 & 1 \end{pmatrix}\mu_{el}E \qquad (2.31)$$

In the v_2=1 case (in which l=1) non-vanishing matrix elements diagonal in J do occur and yield the first order or linear Stark effect. For v_2=0, ΔJ=0, all elements vanish so that the largest contributions come from ΔJ=∓1 elements resulting in second order or quadratic Stark effect.

2.4.2 Electric polarizability interaction.

The expressions for the matrix elements of the electric polarizability tensor can readily be obtained by taking the corresponding expression for the magnetic susceptibility as presented below in Eq. (2.33) by replacing χ and H by α and E respectively. The contribution of the α_{av} does not depend on any quantum number and does not contribute to the transition frequencies. The anisotropy in the polarizability $(\alpha_{\parallel} - \alpha_{\perp})$ with definition of the Cartesian components given e.g. in

DIJ 71, is important if accurate electric dipole measurements in the $v_2=0$ state are performed.

2.5 MAGNETIC FIELD INTERACTIONS.

The first three contributions to the Zeeman Hamiltonian (2.17) originate, in the sequence indicated, in the interactions of the rotational magnetic moment $\underline{G}.\underline{J}$, of the induced magnetic moment $\underline{H}.\underline{X}$, and in the electron shielded nuclear magnetic moments $\frac{\mu_K}{I_K}\ \underline{I}_K.(\underline{1} - \underline{\sigma}_K)$, respectively with the applied external homogeneous field $\underline{H}$. The last term of Eq. (2.17) represents the translational Stark effect.

2.5.1 Molecular Zeeman effect.

Making use of the wavefunctions (2.14) the contributing matrix elements of $-\underline{H}.\underline{G}.\underline{J}$ are

$$<(I_1Jl)F_1I_2FM_F\pm|-\underline{H}.\underline{G}.\underline{J}|(I_1Jl)F_1'I_2F'M_F\pm> \;=$$

$$\delta(M_F',M_F)(-1)^{F-M_F}\begin{pmatrix} F & 1 & F' \\ -M_F & 0 & M_F \end{pmatrix}(-1)^{2F_1+I_1+I_2+F'+J+1} \quad \mathrm{x}$$

$$[(2F+1)(2F'+1)(2F_1+1)(2F_1'+1)J(J+1)(2J+1)]^{\frac{1}{2}}\begin{Bmatrix} F & 1 & F' \\ F_1' & I_2 & F_1 \end{Bmatrix}\begin{Bmatrix} F_1 & 1 & F_1' \\ J & I_1 & J \end{Bmatrix}\mathrm{x}$$

$$[g_\perp + \frac{l^2}{J(J+1)}(g_\parallel - g_\perp) \pm \tfrac{1}{2}\,\delta_{l1}(-1)^J(g_{xx}-g_{yy})]H \qquad (2.32)$$

Herein $g_{aa} = \tilde{G}_{aa}$ for a=x,y,z; $g_\parallel=g_{zz}$ and $g_\perp=\frac{1}{2}(g_{xx}+g_{yy})$. The contribution of matrix elements offdiagonal in J at the relatively low magnetic fields (up to 8.7 kG) used in the present experiment is below the limit of resolution and has been disregarded in the fit.

2.5.2 Magnetic susceptibility.

The general matrix element of the contribution of the induced magnetic moment (diamagnetic susceptibility) is:

$$<(I_1Jl)F_1I_2FM_F\pm\,|-\tfrac{1}{2}\underline{H}.\underline{\chi}.\underline{H}|\,(I_1Jl)F_1'I_2F'M_F'\pm> \;=$$

$$\tfrac{1}{2}\,\chi_{av}H^2 + \delta(M_F',M_F)(-1)^{F-M_F}\begin{pmatrix}F & 2 & F'\\ -M_F & 0 & M_F\end{pmatrix}(-1)^{2F_1+I_1+I_2+F'+J+1}\;\mathrm{x}$$

$$[(2F+1)(2F'+1)(2F_1+1)(2F_1'+1)]^{\frac{1}{2}}\left[\frac{J(J+1)(2J+1)}{(2J-1)(2J+3)}\right]^{\frac{1}{2}}\;\mathrm{x}$$

$$\begin{Bmatrix}F & 2 & F'\\ F_1' & I_2 & F_1\end{Bmatrix}\begin{Bmatrix}F_1 & 2 & F_1'\\ J & I_1 & J\end{Bmatrix}\Big[\frac{3l^2 - J(J+1)}{3J(J+1)}\;(\chi_{\parallel} - \chi_{\perp}) \pm$$

$$\tfrac{1}{4}\,\delta_{l1}(-1)^J(\chi_{xx} - \chi_{yy})\Big]H^2 \qquad (2.33)$$

The first terms containing $\chi_{av} = 1/3(\chi_{xx} + \chi_{yy} + \chi_{zz})$ does not depend on molecular orientations and consequently can not be obtained from resonance experiments.

2.5.3 Nuclear Zeeman effect.

As there are two nuclei with non-zero spins the nuclear Zeeman effect yields two contributions to the energy:

$$<(I_1Jl)F_1I_2FM_F\pm\,|\frac{\mu_1}{I_1}\;\underline{I}_1.(\underline{1}-\underline{\sigma}_1).\underline{H}|\,(I_1Jl)F_1'I_2F'M_F'\pm> \;=$$

$$\delta(M_F',M_F)(-1)^{F-M_F}\begin{pmatrix}F & 1 & F'\\ -M_F & 0 & M_F\end{pmatrix}(-1)^{F_1+I_2+F'}$$

$$[(2F+1)(2F'+1)(2F_1+1)(2F_1'+1)]^{\frac{1}{2}}\;\mathrm{x}$$

$$[(2I_1+1)(I_1+1)I_1]^{\frac{1}{2}}\;\mathrm{x}\;\frac{\mu_1}{I_1}\begin{Bmatrix}F & 1 & F'\\ F_1' & I_2 & F_1\end{Bmatrix}$$

$$\Big[(-1)^{I_1+J+F_1'+1}\begin{Bmatrix}I_1 & I_1 & 1\\ F_1 & F_1' & J\end{Bmatrix}(1-\sigma_{av}^{(1)}) \;+$$

$$\begin{Bmatrix} I_1 & I_1 & 1 \\ J & J & 2 \\ F_1 & F_1' & 1 \end{Bmatrix} \sqrt{30}\ \left[\frac{J(J+1)(2J+1)}{(2J-1)(2J+3)}\right]^{\frac{1}{2}} \left[\frac{3l^2-J(J+1)}{3J(J+1)} \left(\sigma^{(1)}_{\parallel}-\sigma^{(1)}_{\perp}\right)\right.$$

$$\left.\left. \pm \tfrac{1}{2}\ \delta_{l1}(-1)^J\left(\sigma^{(1)}_{xx} - \sigma^{(1)}_{yy}\right)\right]\ \right] H \qquad (2.34)$$

for nucleus 1, and

$$<(I_1Jl)F_1I_2FM_F\pm\left|\frac{\mu_2}{I_2}\ \underline{I}_2\cdot(\underline{1}-\underline{\sigma}_2)\cdot\underline{H}\right|(I_1Jl)F_1'I_2F'M_F'\pm> \ =$$

$$\delta(M_F',M_F)\,(-1)^{F-M_F}\begin{pmatrix} F & 1 & F' \\ -M_F & 0 & M_F \end{pmatrix}(-1)^{F_1+I_1} \quad \times$$

$$\left[(2I_2+1)(I_2+1)I_2(2F+1)(2F'+1)(2F_1+1)(2F_1'+1)\right]^{\frac{1}{2}} \ \times$$

$$\frac{\mu_2}{I_2}\left[(-1)^{I_1+I_2+2F_1+F}\ \frac{\delta(F_1',F_1)}{(2F_1+1)}\begin{Bmatrix} F_1' & F & 1 \\ I_2 & I_2 & F_1 \end{Bmatrix}\left(1-\sigma^{(2)}_{av}\right) \ +\right.$$

$$\begin{Bmatrix} F_1 & F_1' & 2 \\ I_2 & I_2 & 1 \\ F & F' & 1 \end{Bmatrix} \begin{Bmatrix} F_1 & 2 & F' \\ J & I_1 & J \end{Bmatrix} \sqrt{30}\ \left[\frac{J(J+1)(2J+1)}{(2J-1)(2J+3)}\right]^{\frac{1}{2}} \left[\frac{3l^2-J(J+1)}{3J(J+1)}\left(\sigma^{(2)}_{\parallel}-\sigma^{(2)}_{\perp}\right)\right.$$

$$\left.\left.\pm\ \tfrac{1}{2}\ \delta_{l1}(-1)^J\left(\sigma^{(2)}_{xx}-\sigma^{(2)}_{yy}\right)\right]\ \right] H \qquad (2.35)$$

for nucleus 2. In Eqs. (2.34) and (2.35) μ_i/I_i for i=1 and 2 is defined as the nuclear g - factor in units of nuclear magneton. In high magnetic fields, where I-J coupling is broken down, the matrix elements (2.34) and (2.35) are proportional to M_{I_i} (the component of I_i for i=1 or 2 along the external z-axis). As the quantum number M_{I_i} can not be changed by electric dipole transitions only $\Delta M_{I_i}=0$ lines can be observed at high fields. In sufficiently low H-fields also $\Delta M_{I_i} \neq 0$ transitions can be observed.

2.5.4 Translational Stark effect.

The last term of Hamiltonian (2.17) arises from coupling of the electric dipole moment of the molecule and the $\underline{v}\times\underline{H}$ electric field "seen" by the molecule travelling through the magnetic field $\underline{H}$ at a velocity $\underline{v}$. In our configuration with parallel electric and magnetic fields the $\underline{v}\times\underline{H}$ term is perpendicular to those fields and to the beam. The induced linear Stark effect causes shifts of a few kHz and is essential in analyzing the spectra.

With the $-\underline{\mu}_{el}\cdot\underline{v}\times\underline{H}$ operator expressed in spherical tensor components

$$-\underline{\mu}_{el}\cdot\underline{v}\times\underline{H} = 1/\sqrt{2}\mu_{el}vH(D^{(1)}_{01}-D^{(1)}_{0-1})$$

and the result of Eq. (2.31) the following expression is derived for the general matrix element

$$\langle(I_1J1)F_1I_2FM_F\pm|-\underline{\mu}_{el}\cdot\underline{v}\times\underline{H}|(I_1J'1)F_1'I_2F'M_F'\mp\rangle =$$

$$(-1)^{F-M_F}\left[\begin{pmatrix} F & 1 & F' \\ -M_F & -1 & M_F' \end{pmatrix} - \begin{pmatrix} F & 1 & F' \\ -M_F & 1 & M_F' \end{pmatrix}\right](-1)^{2F_1+I_1+I_2+F'+J'+J+1} \times$$

$$[(2F+1)(2F'+1)(2F_1+1)(2F_1'+1)(2J+1)(2J'+1)]^{\frac{1}{2}} \times$$

$$\begin{Bmatrix} F & 1 & F' \\ F_1' & I_2 & F_1 \end{Bmatrix}\begin{Bmatrix} F_1 & 1 & F_1' \\ J' & I_1 & J \end{Bmatrix}\begin{pmatrix} J & 1 & J' \\ -1 & 0 & 1 \end{pmatrix}\frac{1}{\sqrt{2}}\mu_{el}vH \qquad (2.36)$$

Herein only $\Delta M_F = M_{F'} - M_F = \pm 1$ elements are non-zero.

2.6 SPECIAL CASES.

Species like $O^{13}CS$ and $OC^{33}S$ with only one nuclear spin different from zero reduce the basis functions (2.14) to (REI 74c):

$$|(IJ1)FM_F\pm\rangle = \frac{1}{\sqrt{2}}[\,|(IJ1)FM_F\rangle \pm (-1)^J|(IJ-1)FM_F\rangle] \qquad (2.37)$$

With these functions rather simple expressions for the hyperfine matrix elements are obtained for $\Delta J=0$ contributions;

$$<\pm|\underline{Q}.\underline{V} + \underline{I}.\underline{M}.\underline{J}|'\pm> \;=\; \delta(F',F)\,\delta(M_F',M_F) \quad x$$

$$\frac{3/4C(C+1)-I(I+1)J(J+1)}{2I(2I-1)(2J-1)(2J+3)}\left[\frac{3l^2-J(J+1)}{J(J+1)}\,eQq_{11} \pm \tfrac{1}{2}\,\delta_{l1}(-1)^J eQ\,q_{12}\right]$$
$$+ \tfrac{1}{2}\,C\left[c_{\perp}^{(1)} + \frac{l^2}{J(J+1)}\,(c_{\parallel}^{(1)} - c_{\perp}^{(1)}) \pm \tfrac{1}{4}\,\delta_{l1}(-1)^J(c_{xx}^{(1)} - c_{yy}^{(1)})\right] \tag{2.38}$$

where $C=F(F+1)-I(I+1)-J(J+1)$. For $v_2=1$ states it is easy to obtain simple analytical expressions for the transition frequencies. In the case of all nuclear spins being zero matrix elements of the Stark and Zeeman interactions reduce to simple expressions. The expressions provide a good insight in the rather complicated formulae of Sect. 2.4 and 2.5. Using as wavefunctions (REI 72d)

$$|JlM\pm> = \frac{1}{\sqrt{2}}\;[\;|JlM> \pm(-1)^J|J\text{-}lM\;>\;] \tag{2.39}$$

with $M=M_J$ as the component along the external field axis, the following expressions are obtained for the relavant matrix elements:

$$<JlM\pm|\;-\;\underline{\mu}_{el}.\underline{E}|\;JlM\mp> \;=\; \frac{-\;Ml}{J(J+1)}\;\mu_{el}E \tag{2.40}$$

$$<JlM\pm|\;-\;\underline{\mu}_{el}.\underline{E}\;|(J+1)l\;M\;\mp> \;=$$

$$-\;\frac{\mu_{el}E}{J\;+\;1}\;\left[\frac{(J+M+1)(J-M+1)(J+l+1)(J-l+1)}{(2J+1)(2J+3)}\right]^{\frac{1}{2}} \tag{2.41}$$

$$<JlM\pm|-\;\underline{H}.\underline{G}.\underline{J}|JlM\pm> \;=$$
$$-\;HM\;\left[g_{\perp} + \;\frac{l^2}{J(J+1)}\;(g_{\parallel} - g_{\perp}) \pm \tfrac{1}{4}\;\delta_{l1}(-1)^J(g_{xx}-g_{yy})\right] \tag{2.42}$$

$$\langle J l M\pm | -\tfrac{1}{2}\, \underline{H}.\underline{\chi}.\underline{H} | J l M\pm \rangle =$$

$$-H^2 \; \frac{3M^2-J(J+1)}{(2J-1)(2J+3)} \quad x$$

$$\left[\frac{3l^2-J(J+1)}{3J(J+1)} (\chi_{\parallel} - \chi_{\perp}) \pm \tfrac{1}{4}\, \delta_{l1} (-1)^J (\chi_{xx} - \chi_{yy})\right] \tag{2.43}$$

As before the matrix elements for the electric polarizability can be obtained by replacing in Eq.(2.42) χ and H by α and E respectively.

CHAPTER 3

EXPERIMENTAL RESULTS.

3.1 INTRODUCTION.

This chapter deals with the measurements and analysis of Stark field and combined Stark-Zeeman field spectra of $^{18}O^{12}C^{32}S$, $^{16}O^{12}C^{33}S$, $^{14}N^{14}N^{16}O$, and $^{35}Cl^{12}C^{14}N$ in the ground vibrational state, for J=1. Zero field and Stark field measurements have also been performed in the first excited state of the bending vibration of five isotopic species of OCS and of N_2O and ClCN. Zeeman spectra in this state have been obtained for $^{16}O^{12}C^{32}S$ and N_2O.

Theoretical expressions for the energies and for the transition frequencies in terms of the coupling constants have been obtained by diagonalization of the energy matrix; matrix elements have been evaluated using expressions given in Chap. 2. A least-squares minimizing procedure (REI 73a, MEE 75c) has been applied to determine the coupling constants. The values for those constants were varied until the chi-square (χ^2) defined as

$$\chi^2 = \sum_i \left(\frac{\nu_c^{(i)} - \nu_o^{(i)}}{\Delta\nu^{(i)}} \right)^2 \qquad (3.1)$$

obtained an absolute minimum value; the symbols $\nu_c^{(i)}$, $\nu_o^{(i)}$ and $\Delta\nu^{(i)}$ are the calculated and observed frequency, and the experimental error of the i-th transition, respectively. The calculations, carried out on an IBM 370/155 digital computer, ultimately yielded coupling constants and their errors according to "error definition one", ED1, (REI 73a). Accuracies of the reported results were obtained by multiplying the ED1 errors with such a factor that at least a 95% confidence level was obtained according to the Tables of Fisher and Yates (FIS 63). This factor depends on the χ^2 and the number of degrees of freedom of the system.

Physical constants as given by Cohen et al (COH 73) have been used in the evaluation of the present results.

3.2 GROUND VIBRATIONAL STATE MEASUREMENTS; INTRODUCTION.

For all considered molecules in the (000) vibrational state, J=1 $|M_J|=0 \rightarrow 1$ Stark spectra have been observed. As only one rotational state has been considered it is not possible to obtain absolute values for the electric dipole moments without a reliable value for the electric polarizability anisotropy. The reason is that the second order Stark effect and the contribution due to the electric polarizability depend in the same way on the electric field strength. For the OCS isotopes the value $\alpha_{\parallel} - \alpha_{\perp} = 4.67(16)\text{Å}^3$, of Scharpen et al (SCH 70) for the most abundant species has been taken, while for $^{14}N_2{}^{16}O$ a value of $\alpha_{\parallel} - \alpha_{\perp} = 3.222(46)\ \text{Å}^3$ has been used (SCH 70). To our knowledge no accurate value of $\alpha_{\parallel} - \alpha_{\perp}$ for $^{35}Cl^{12}C^{14}N$ has been reported in literature, so that for this molecule only an absolute value for the electric dipole moment for J=1 can be given if the electric polarizability anisotropy is smaller than $5\ \text{Å}^3$.

Measurements of spectra in combined parallel electric and magnetic fields have been performed for N_2O and ClCN in the rotational state J=1. During these measurements some yet unexplained machine effect prohibited the normal high accuracy in the determination of the transition frequencies because larger errors in the determination of the magnetic field strength had to be accepted. At best an accuracy in the magnetic field of $2\text{x}10^{-4}$ can normally be obtained. For the present measurements an accuracy of only $1\text{x}10^{-3}$ for a field of about 8.7 kG could be claimed. Further discussion is given in Sect. 3.2.2b.

3.2.1 Carbonyl sulphide ($^{18}O^{12}C^{32}S$ and $^{16}O^{12}C^{33}S$); Stark spectra.

Because of the large improvement of the signal to noise ratio by employing a nozzle source, less abundant species of OCS could readily be measured without using enriched samples.

Stark effect measurements on $v_2=0$ states of $^{16}O^{12}C^{32}S$, $^{16}O^{12}C^{34}S$, $^{16}O^{13}C^{32}S$ were performed in the past by de Leeuw (LEE 70,71); we have reproduced these results and supplemented them by relative measurements on $^{18}O^{12}C^{32}S$ (natural abundance of 0.2%). The measurements on $^{16}O^{12}C^{33}S$ (natural abundance 0.75%) will be treated as a special case because of its hyperfine structure.

Measurements have been performed on EBR I machine using a 60μ diameter nozzle and backing pressure of 300 Torr. During the measurements the source was at room temperature. Line widths were about 6 kHz so that for $^{16}O^{13}C^{32}S$ only one somewhat broadened spectral line could be observed instead of the spin-rotation doublet with a separation of 3.1 kHz (LEE 70,71). The frequency of this broadened line has been treated in the calculations as the average of the doublet. The measured transition frequencies and dipole moments are listed in Table 3.1 and 3.2, respectively.

Table 3.1. Frequencies of the observed transitions $J=1 \rightarrow 1$ $\Delta M=\pm 1$ of the OCS-isotopes for the ground vibrational state at the electric field strength of 800.032(8) V/cm. All values are in kHz.

molecule	transition frequency
$^{16}O^{12}C^{32}S$	2044.96(5)
$^{16}O^{12}C^{34}S$	2097.62(5)
$^{16}O^{13}C^{32}S$	2052.39(7)
$^{18}O^{12}C^{32}S$	2175.82(10)

Table 3.1 continued
Observed and calculated frequencies in kHz for $^{16}O^{12}C^{33}S$ in the $v_2=0$ state.

F, M_F	→ F', M'_F	observed	obs.-calc.	exp. error
1/2,1/2	5/2,1/2	5577.71	0.00	0.10
5/2,1/2	3/2,1/2	8269.25	-0.06	1.00
5/2,3/2	3/2,3/2	7159.76	0.00	0.30
5/2,3/2	3/2,1/2	8144.58	-0.01	0.60
1/2,1/2	3/2,1/2	13847.02	0.00	0.10

The strong quadrupole interaction of the ^{33}S nucleus ($eQq_{11} \approx -29.13$ MHz) splits the J=1 rotational level into three hyperfine sublevels. In an external Stark field these levels split further. In order to get an idea about focusing properties we have calculated the energy levels as a function of the electric field strength from 0 to 3 kV/cm. This energy level diagram is given in Fig. 3.1. At low field strengths the energies of the F=5/2 and F=3/2 levels are depicted in the same figure with enlarged energy scales showing a changing character of the F=5/2, $M_F=1/2$ and F=3/2, $M_F=3/2$ levels.

These states possess positive Stark slopes at low fields and thus are the focused states while for high field strengths the Stark slope is negative resulting in rejection from the beam. That both possibilities really are encountered is proved by the fact that the transition from F, $M_F=1/2$, 1/2 (a focused state at all field strengths) to F, $M_F=5/2$, 1/2 and from F, $M_F=5/2$, 1/2 to F, $M_F=3/2$, 1/2 (a defocused state) both were observed.

From the five transition frequencies measured for J=1 (see Table 3.1 and also Fig. 3.1) the three constants eQq_{11}, $c_1^{(1)}$ and μ_{el} have been obtained. The results are given in Table 3.2.

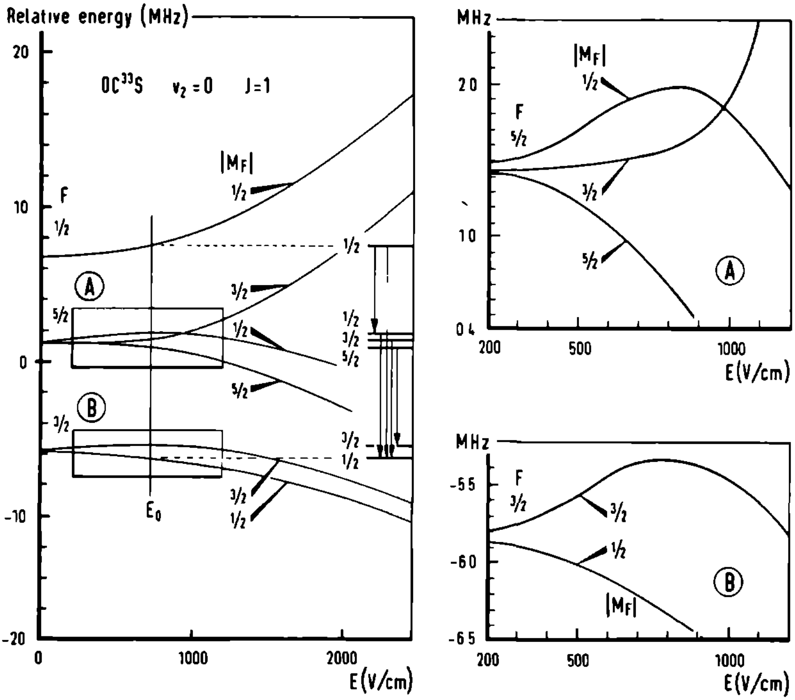

Fig. 3.1 Energy level diagram of $OC^{33}S$, $v_2=0$, $J=1$, and observed transitions at $E_o=800$ V/cm.

Table 3.2. Hyperfine coupling constants of $^{16}O^{12}C^{33}S$ and electric dipole moments of isotopic species of the OCS molecule in the ground vibrational state.

quantity	$^{16}O^{12}C^{32}S$	$^{16}O^{12}C^{33}S$	$^{16}O^{12}C^{34}S$	$^{18}O^{12}C^{32}S$	$^{16}O^{13}C^{32}S$
μ_{el}(rel.)	1.00000	1.00024(25)	1.00031(2)*	0.99904(3)	1.00017(2)*
μ_{el}(D)	0.71519(3)*				
eQq_{11}(kHz)		-29118.4(12)			
$c_{\perp}^{(1)}$(kHz)		0.87(5)			3.1(2)*

* from (LEE 70,71), see also REI 74c.

Commercial carbonyl sulphide (Matheson) with a purity of at least 97.5% has been used in the experiment. Quadrupole voltages of + and -13 kV have been applied and buffer field strengths of 3 kV/cm. With the 10 cm diameter C-field of EBR I machine a line width of 6.0 kHz has been obtained. Each line has been recorded with increasing and decreasing frequency for both C-field polarities. The line frequencies listed in Table 3.1 are the averaged values of these four. Typical signal to noise ratio was about 300 for $^{16}O^{12}C^{32}S$ at RC=0.1 s, 50 for $OC^{34}S$ (RC=1 s), 10 for $O^{13}CS$ (RC=1 s), 6 for ^{18}OCS at RC = 15 s and also 6 for the strongest $OC^{33}S$ line but at RC=4 s.

3.2.2 Nitrous Oxide($^{14}N_2{}^{16}O$)

3.2.2a Stark spectra.

An electric field strength of about 2.5 kV/cm has been applied to the C-field in order to obtain the J=1 → 1 $\Delta M=0$ and ±1 transition frequencies of N_2O. The measurements have been performed on EBR II machine. A backing pressure of 250 Torr and a 100µ nozzle has been used to produce an intense N_2O beam, monitored at m/e=44 with the quadrupole mass detector. Because of the small electric dipole moment of N_2O, high voltages on the quadrupole state selectors have been required for effective focusation. This requirement brought a confrontation with technical limitations of the apparatus because higher voltages than + and -30 kV on adjacent bars were hardly possible during a longer period. Optimum focusation demands even higher voltages. The same reason forced us to use a high C-field voltage to get enough Stark shift for the accurate determination of the electric dipole moment. A Fluke 332A (setting 1000 volts) and a Fluke 335A (setting 500 volts) voltage standard, calibrated by the Electronic Department of the Faculty, with a short time accuracy of 5 ppm, are connected in series to supply the Stark field voltage.

The calibration of field strength has been performed with OCS. The J=1 → 1, ΔM=±1 transition of $^{16}O^{12}C^{32}S$ has been observed at 17730.80(8) kHz. Using Eq. 4.2 of LEE 71 and for μ_{el} and $\alpha_{\parallel} - \alpha_{\perp}$ the values of 0.715189(7) D and 4.67(16) Å^3, respectively, electric field strength of 2357.19 V/cm has been obtained.

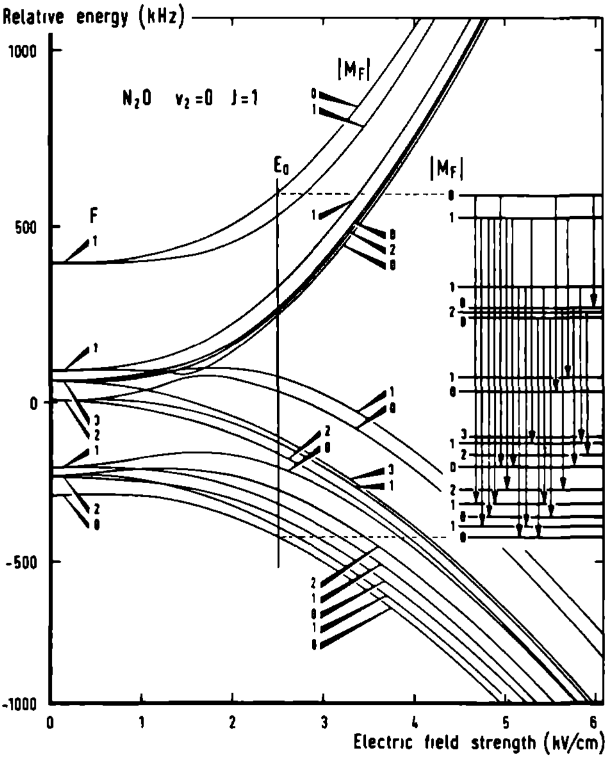

Fig. 3.2 Energy level diagram of N_2O ($v_2=0$, J=1) in electric fields and observed transitions at E_o=2357.19(2) V/cm.

The energy level diagram of the hyperfine levels in electric fields up to 5 kV/cm are given by Fig. 3.2 showing clearly the rather high fields needed to get reasonable Stark shifts of the levels. In this figure also the measured transitions have been depicted. Signal to noise ratio varied between 2 and 40 at an RC-time of 2 s and a sweep rate of 30 Hz/s for the 18 observed transitions. Frequencies of these transitions are given in Table 3.3. The line width was 2.5 kHz and experimental errors for most of the lines 150 Hz.

Table 3.3. Observed and calculated frequencies of N_2O in the ground vibrational state for J=1 at the electric field strength of 2357.19(2) V/cm. All values are in kHz.

$\|M_F\|$	$\to\|M'_F\|$	Observed	Calculated	obs.-calc.	Exp.error
1	1	833.35	832.99	0.26	0.5
0	1	833.35	833.33	-0.08	0.5
0	1	809.60	809.51	0.09	0.15
1	1	769.79	769.83	-0.04	0.15
0	0	732.53	732.49	0.04	0.15
1	2	732.53	732.37	0.16	0.15
0	1	668.84	668.99	-0.15	0.5
0	1	663.62	663.46	0.16	0.5
1	1	633.14	633.11	0.03	0.15
1	1	591.39	591.69	-0.30	0.15
0	0	582.69	582.56	0.13	0.3
1	1	569.82	569.95	-0.13	0.15
0	0	528.95	528.74	0.22	0.3
0	0	517.39	517.49	-0.10	0.15
2	2	458.93	459.14	-0.21	0.15
1	1	415.52	415.39	0.13	0.15
0	0	400.38	400.58	-0.20	0.30
1	1	391.80	391.80	0.00	0.15
2	2	353.48	353.20	0.28	0.15
0	0	331.87	331.90	-0.03	0.30

For the evaluation of the coupling constants, interactions for the J=0 through J=3 states have been retained in the calculations. The χ^2 for the fit was 14.5 for 20 spectral lines and five constants to adjust. The value for the spin-spin coupling constant has been calculated using the relation

$$d_T = \frac{\mu_o}{4\pi} \mu_N^2 g_{I_1} g_{I_2} r_{12}^{-3} \tag{3.2}$$

where μ_o is the permeability of free space, g_{I_1} and g_{I_2} the nuclear g-factors of the outer and inner N nucleus, respectively, and the distance between the nuclei r_{12}=1.126 Å. The resulting value for d_T=0.436 kHz. The ED1 errors (Sect. 3.1) are multiplied by a factor 1.4 to get 95% confidence intervals for the molecular constants as reported in Table 3.4. The first subscript 1(2) of the eQq constants and the superscript 1(2) of the c-constants refers to the outer (inner) nitrogen nucleus, while the second subscript 1 of the eQq constants refers to the zz-component of the q-tensor as defined in Eq. 2.24.

Table 3.4. Hyperfine constants and electric dipole moment of N_2O in the ground vibrational and J=1 rotational state.

constant	present result	others	ref.
μ_{ef}(D)	0.159771(23)		
μ_{el}(D)	0.160880(23)	0.160844(16)**	SCH 70
and			
$\alpha_{\parallel} - \alpha_{\perp}$ = 3.222(46)Å^3			SCH 70
eQq_{11}(kHz)	-773.76(27)	-776.7(10)	CAS 75*
eQq_{21}(kHz)	-267.58(38)	-269.4(18)	CAS 75
$c_{\perp}^{(1)}$ (kHz)	1.829(65)	2.35(20)	CAS 75
$c_{\perp}^{(2)}$ (kHz)	3.06 (12)	2.90(26)	CAS 75

*Casleton et al determined five constants from seven observed J=1 → 0 transitions yielding the reported 40% confidence intervals. Their errors multiplied by a factor 4.5 to get 95% confidence produces overlap of the hyperfine constants with our more accurate values.

**Electric dipole moment corrected for the "new" value of Planck's constant (COH 73).

3.2.2b Stark-Zeeman spectra

The electric field strength in the C-field region was the same as used for the Stark spectrum. For this electric field J=1 energy levels have been calculated as a function of the magnetic field strength up to 10 kG (Fig. 3.3). At high fields five

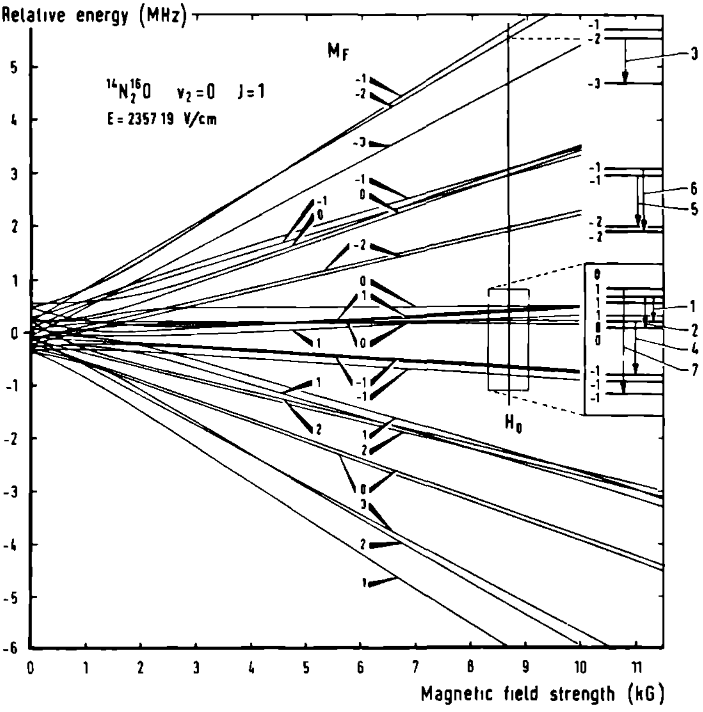

Fig. 3.3 Energy level diagram of N_2O (v_2=0, J=1) for E_o=2357.19(2) V/cm as a function of the magnetic field strength and observed transitions at H_o=8752.4(80) G. The numbers of the lines correspond with those in Table 3.5.

groups of levels belonging to the possible M_I-values (M_I is the sum of the components M_{I_1} and M_{I_2} of $\underline{I}_1$ and $\underline{I}_2$, respectively, along the external field axis). Because electric dipole transitions are considered only $\Delta M_{I_i}=0$ for i=1 and 2, transitions are possible. Again J=1, ΔM=±1 Stark-Zeeman transitions of OCS have been used for the calibration of the magnetic field $H= \Delta\nu/2g_{\perp}\mu_N$ where $\Delta\nu$ is the difference frequency of the $\Delta M=+1$ and $\Delta M=-1$ transitions, $g_{\perp}$ is the molecular g-value determined by de Leeuw (LEE 70,71) and μ_N the nuclear magneton. This value of H did not agree to within $2\text{x}10^{-4}$ with field strength measurements with an NMR probe (Bruker B-NM12). Changing the polarity of the H-field resulted in a discrepancy of the H-field values as determined with the two methods, which was different from that of the first chosen polarity. These difficulties, extensively discussed in internal reports (REI 75c, REI 76) forced us to enlarge the errors in the absolute magnetic constants because of a large uncertainty in the magnetic field strength, $1\text{x}10^{-3}$ for fields of about 8.7 kG. Table 3.5 presents the seven observed transition frequencies with experimental errors of 0.5 kHz. The numbers of the lines in Table 3.5 correspond with those in Fig. 3.3.

Table 3.5 Observed and calculated transition frequencies (in kHz) in N_2O $v_2=0$, $J=1$ in an electric field of 2357.19(2) V/cm and a parallel magnetic field of 8752.4(80) G. Experimental errors are 0.5 kHz.

No	observed	calculated	obs.-calc.
1	225.5	225.39	0.11
2	232.8	232.91	-0.11
3	837.6	837.44	0.16
4	844.5	844.28	0.23
5	961.2	961.39	0.19
6	1186.5	1186.47	0.03
7	1309.2	1309.43	-0.23

For the evaluation of the magnetic constants the hyperfine constants and electric dipole moment obtained from the Stark spectra have been taken and not further adjusted in the fit. Table 3.6 contains the best fit values for the magnetic constants. The χ^2 for the fit was 0.7. Because of the large experimental errors in the observed frequencies the values obtained for the anisotropic nuclear shielding are rather crude but do agree reasonably well with values determined for $^{15}N_2O$ by Bhattacharyya _et al_. (BHA 73); $\sigma_\perp^{(1)} - \sigma_\parallel^{(1)} = -367(12)$ ppm and $\sigma_\perp^{(2)} - \sigma_\parallel^{(2)} = -508(10)$ ppm, where the superscript 1(2) refers to the outer (inner) N nucleus.

Table 3.6. Magnetic constants of $^{14}N_2{}^{16}O$ for J=1 in the ground vibrational state.

constant	present value	FLY 69($^{15}N_2{}^{16}O$)
$g_\perp$	-0.07887(8)	-0.07606(10)
$\chi_\perp - \chi_\parallel$ (10^{-6}erg/G^{2}mole^{-1})	10.43(6)	10.10(15)
$\sigma_\perp^{(1)} - \sigma_\parallel^{(1)}$ (ppm)	-322(402)	
$\sigma_\perp^{(2)} - \sigma_\parallel^{(2)}$ (ppm)	-458(293)	

3.2.3 Cyanogen chloride ($^{35}Cl^{12}C^{14}N$)

Chemical corrosion and dangerous toxic properties required special arrangements for the production of a ClCN nozzle beam. A special stainless steel regulation system equipped with a DIRS No 6 regulator from "L'air liquide" was employed to reduce the cylinder pressure of 1.5 atm. to useable absolute inlet pressures of about 100 Torr. The complete inlet system has been placed inside a 4 m^3 large wooden dry box built around the source section of the EBR II machine. An electric fan installed on the roof of the building with a pump capacity of 750 m^3/h took care of the ventilation of the box.

With long gloves mounted onto the box the whole system inside could be handled from outside the box.

Inlet pressures of 60 Torr through a 100μ diameter nozzle yield optimum signal to noise for the spectral lines. Further increasing the pressure caused a decreasing line intensity.

3.2.3a Stark spectra.

For the measurements on ClCN in a Stark field a voltage of 300.000 V (Fluke 332A voltage standard) has been applied to the C-field. Calibration with OCS yields a field strength of E=471.439 V/cm for ClCN. A spectrum very rich in lines, about 3.0 kHz wide, has been observed. Because the Stark shifts at the applied field strength are still comparable with hyperfine splittings due to the large eQq of ^{35}Cl (≈ 83 MHz) there is some overlap of spectra for the different J states. Therefore some additional information on the lines was needed for determination of the J-state to which they belong. This extra information could be obtained from the Stark slopes $\partial\nu_o/\partial V$ of the lines. A voltage V applied to the C-field plates separated by a distance d yields a Stark field E=V/d. The Stark shift ν_o of a certain transition frequency can be written as

$$\nu_o = \alpha\,(\mu E)^2 = \alpha(\mu\frac{V}{d})^2 \tag{3.3}$$

where α depends on the transition in question. The Stark slope, then, is given by

$$\frac{\partial\nu_o}{\partial V} = \frac{2\alpha\mu^2 V}{d^2} = 2\,\frac{\nu_o}{V} \tag{3.4}$$

or 80, 19 and less than 10 kHz/V for the J=1, 2 and 3 states for V=300 V, respectively. With voltages of + and -1.75 kV on the quadrupole fields about 30 spectral lines of J=1 with signal to noise ratio between 3 and 30 (RC=1.9 s) have been accurately measured, all displaying Stark slopes of 20 kHz/V at least. The observed $\Delta M_F=0$ transitions had line widths of 1.5 kHz, the $\Delta M_F= \pm 1$ transitions of about 3 kHz. Experimental error of 0.5 kHz has been estimated for the $\Delta M_F= \pm 1$ lines, 0.2 kHz for the $\Delta M_F=0$ ones. Table 3.7 presents the observed transition frequencies.

In obtaining the calculated frequencies for J=1, interactions with J=0 through J=3 states have been taken into account. The χ^2 for the fit of 27 points and five constants to adjust was 20. To ensure a confidence level of at least 95% the ED1-errors have been multiplied by 1.4. The results are given in Table 3.8 together with those of other investigators. First subscript 1(2) of eQq and superscript 1(2) of $c_\perp$ refers to the ^{35}Cl(^{14}N) nucleus.

Table 3.7. Observed and calculated transition frequencies of $^{35}Cl^{12}C^{14}N$ in the ground vibrational and J=1 rotational state. The electric field strength was 471.439 V/cm. All values are in kHz.

$\lvert M_F\rvert \to \lvert M'_F\rvert$		observed	calculated	obs.-calc.	exp.error
0.5	0.5	865.25	864.78	0.47	0.20
0.5	0.5	998.98	998.89	0.09	0.20
2.5	3.5	5750.89	5750.98	-0.09	0.30
0.5	1.5	5980.34	5980.46	-0.12	0.30
2.5	2.5	6319.81	6319.74	0.07	0.20
1.5	1.5	6391.74	6391.90	-0.16	0.20
1.5	2.5	6868.54	6868.71	-0.17	0.30
1.5	1.5	16784.15	16784.24	-0.09	0.50
0.5	0.5	16863.76	16863.71	0.05	0.50
0.5	0.5	16997.78	16997.81	-0.03	0.50
0.5	0.5	17406.80	17407.26	-0.46	0.50
0.5	0.5	17540.77	17541.36	-0.59	0.50
2.5	2.5	21471.13	21471.25	-0.12	0.20
0.5	0.5	21521.28	21521.38	-0.10	0.20
1.5	1.5	22023.95	22023.96	-0.01	0.20
1.5	2.5	26095.97	26096.34	-0.37	0.30
0.5	1.5	26233.74	26233.86	-0.12	0.30
0.5	0.5	26298.42	26298.46	-0.04	0.20
0.5	0.5	26711.58	26711.33	0.25	0.20
0.5	0.5	37520.12	37520.30	-0.18	0.20
1.5	1.5	37632.28	37632.14	0.14	0.20
1.5	2.5	37628.27	37628.41	-0.14	0.30
1.5	1.5	42253.57	42253.49	0.08	0.20
0.5	0.5	42297.57	42297.39	0.18	0.20
0.5	0.5	42710.60	42710.25	0.35	0.20
0.5	0.5	42840.72	42840.94	-0.22	0.20
0.5	0.5	43253.72	43253.80	-0.08	0.20

The spin-spin interaction constant d_T has been calculated using the relation (3.2), resulting in a value of d_T=0.039 kHz if we use g_{I_1} and g_{I_2} as the nuclear g-factors for the ^{35}Cl and ^{14}N nuclei, respectively, and r_{12}=2.790 Å for the distance between the two nuclei.

Table 3.8. Hyperfine structure constants (in kHz) and electric dipole moment (D) of $^{35}Cl^{12}C^{14}N$ in the ground vibrational state for J=1.

constant	present result	others	reference
μ_{ef}	2.83312(15)	2.80	TOW 55
eQq_{11}	-83275.19(40)	-83390(200)	LAF 56
		-83285(20)	WHI 55
eQq_{21}	-3622.77(90)	-3370(260)	LAF 56
		-3620(10)	WHI 55
$c_\perp^{(1)}$	1.706(45)	3.0(15)	WHI 55
$c_\perp^{(2)}$	1.32(18)	2.5(10)	WHI 55

If the polarizability anisotropy is less than 5.0 Å^3 the effect on the measured frequencies is less than 0.1 kHz at the field strength used. In that case the effect of the polarizability anisotropy is at most 2x10^{-5} compared with the Stark shift due to μ_{el}. The value of the electric dipole moment reported in Table 3.8 may than be accepted as the absolute electric moment.

3.2.3b Stark-Zeeman spectra.

The same discrepancies as reported in Sect. 3.2.2b for the Stark-Zeeman spectra of N_2O appeared again for ClCN. Ultimately a magnetic field strength of 8731.4(9) G has been used as determined from the OCS transition frequencies in this field.

Determination of the field strength with the NMR probe resulted in a slightly different value. Because of this discrepancy an accuracy of $1\text{x}10^{-3}$ in the field strength has been retained. Experimental errors in the 21, $\Delta M=0$ transitions in combined parallel electric and magnetic fields as given in Table 3.9 have been determined from the experimentally obtained Zeeman slopes of the transition frequencies assuming an error in the field strength of $1\text{x}10^{-3}$.

Table 3.9. Observed and calculated $\Delta M_F=0$ transitions of $^{35}Cl^{12}C^{14}N$ in the $v_2=0$, J=1 state using a Stark field of 471.468(5) V/cm and a Zeeman field of 8731.4(87)G.

M_F	observed	calculated	obs.-calc.	exp. error
-0.5	45392.60	45394.03	-1.43	2.68
-0.5	44567.86	44568.30	-0.44	1.90
0.5	44508.98	44511.23	-2.25	2.20
0.5	44493.32	44495.72	-2.40	2.36
-1.5	44452.50	44452.47	0.03	2.44
0.5	42370.16	42370.69	0.53	0.48
0.5	42354.48	42355.18	0.70	0.40
-0.5	42192.20	42190.79	1.41	0.52
-0.5	41366.88	41365.06	1.82	0.94
1.5	41331.24	41332.59	-1.35	0.92
-0.5	40775.93	40778.27	-2.34	2.80
-1.5	40548.26	40549.02	-0.76	2.98
-0.5	26849.29	26848.06	1.23	2.00
-1.5	8300.56	8297.79	2.77	3.00
-1.5	27715.64	27713.47	2.17	1.48
-2.5	23005.22	23003.71	2.52	1.74
-1.5	26756.75	26757.15	-0.40	1.96
-1.5	25036.42	25036.80	-0.38	3.42
-1.5	23811.44	23810.02	1.42	1.94
-1.5	22852.51	22853.70	-1.19	2.44
1.5	35293.66	35292.75	0.91	2.20

The χ^2 for this fit was high (27.2) resulting in a confidence level of only 10%. If the $\sigma_{av}^{(2)}$ was also adjusted a dependent set of equations is obtained. Only two of the three constants g_J, $g_{I_1}(1-\sigma_{av}^{(1)})$, $g_{I_2}(1-\sigma_{av}^{(2)})$ could independently be varied in the fit. Including the term $\underline{\mu}_{el}\cdot\underline{v}\times\underline{H}$ in the Hamiltonian and adjusting the velocity v gave no improvement in the fit. If the anisotropic nuclear shielding constants were also varied a χ^2_{ν} 9 was obtained yielding confidence intervals of 95% but unreasonable values for the shielding factor of ^{14}N; 2860(320) ppm. Table 3.10 lists the "best" fit constants for Stark-Zeeman interactions. As in the case of N_2O only magnetic properties were varied, the hyperfine constants and electric dipole moment were set at the values of Table 3.8.

Table 3.10. Magnetic coupling constants of $^{35}Cl^{12}C^{14}N$ in the $v_2=0$, J=1 state.

constant	present result	EWI 72($ClC^{15}N$)
$g_{\perp}$	-0.04121(13)	-0.0385(2)
$g_{I_1}(\sigma^{(1)}_{av}-1)$	-0.547525(64)	-0.5476(10)
$\chi_{\perp}-\chi_{\parallel}$ (10^{-6} erg/G^{2}mole^{-1})	11.10(12)	10.8(5)

3.3 FIRST EXCITED BENDING VIBRATIONAL STATE MEASUREMENTS.

Several ΔJ=0, l-doublet transitions in the (01^10) vibrational state have been observed for five isotopic species of the OCS molecule, for $^{14}N^{14}N^{16}O$ and for $^{35}Cl^{12}C^{14}N$. Population of the first excited bending vibrational state relative to the ground state is given by the factor $e^{-h\omega_2/kT}$, where h is Planck's constant, ω_2 the bending mode frequency, k Boltzman's constant and T the absolute vibrational temperature in ^{o}K. Evaluation of this factor yields for the populations relative to the vibrational ground state 8.1% for OCS, 6.1% for N_2O and 15.1% for ClCN at a temperature of $300^{o}K$. Without employing nozzle beams measurements on $v_2=1$ states were possible only on $^{16}O^{12}C^{32}S$.

Zero field and Stark spectra have been observed for all mentioned molecules, Zeeman spectra only for the most abundant OCS isotope and for N_2O. Because of the linear Stark effect in the (01^10) state relatively low electric field strengths could be applied, so that higher order Stark contributions and also contributions of the electric polarizability gave frequency shifts much smaller than the experimental errors in the transition frequencies.

3.3.1 OCS isotopes.

Recent papers on OCS report the determination of electric and magnetic properties of $^{16}O^{12}C^{32}S$ in the (01^10) vibrational state measured by MBER spectroscopy (REI 72d) and of rotation-vibration coupling constants and electric dipole moments of the other isotopic species (REI 74c). For completeness the results obtained in these investigations together with all observed transition frequencies are given in this thesis. A re-evaluation of the spectra yields more accurate constants based on 95% confidence intervals.

3.3.1a Zero-field spectra

The $\Delta J=0$ l-doublet transition frequencies of $J=1$ through 12 of $^{16}O^{12}C^{32}S$ in the absence of external electric and magnetic fields are given in Table 3.11. For $OC^{34}S$ and $O^{13}CS$ only the lowest eight J states and for ^{18}OCS only the first seven rotational states have been observed. In the case of $O^{13}CS$ only $\Delta F=0$ transitions have been measured so that c-constants could not be obtained from the spectra. The measured $OC^{33}S$ spectrum consists of 23 transitions from $J=1$ up to $J=5$ (Table 3.11).

From the l-doubling transitions the vibration-rotation constants q_v and μ_v have been obtained (Table 3.12). For one isotope ($^{16}O^{12}C^{32}S$) also an upper limit for the absolute value for ΔH (see Eq. 2.12) of 8×10^{-4} Hz could be determined. The hyperfine structure constants of $OC^{33}S$ are given in Table 3.13. The errors listed there may differ from the ED1 errors given in

Table 3.11. Measured and calculated l-doubling frequencies in kHz in the $(01^{1}0)$ state for five isotopes of OCS.

molecule	J	obs. freq.	obs.-calc.	exp. error
$^{16}O^{12}C^{32}S$	1	12722.88	0.07	0.10
	2	38168.36	0.04	0.10
	3	76336.32	-0.02	0.10
	4	127226.48	-0.07	0.10
	5	190838.50	-0.04	0.10
	6	267171.86	0.06	0.10
	7	356225.85	0.14	1.00
	8	457999.60	0.03	0.10
	9	572492.46	-0.09	0.20
	10	699703.55	-0.18	0.20
	11	839632.20	0.11	0.20
	12	992276.00	-0.53	2.00
$^{16}O^{12}C^{34}S$	1	12137.73	-0.14	0.20
	2	36412.73	-0.06	0.20
	3	72825.07	-0.01	0.20
	4	121374.46	0.02	0.20
	5	182060.49	0.05	0.20
	6	243882.78	-0.01	0.20
	7	339840.58	-0.04	2.00
	8	436933.48	-0.07	1.00
$^{16}O^{13}C^{32}S$	1	13015.92	-0.27	0.50
	2	39046.83	0.02	0.50
	3	78093.36	0.03	0.50
	4	130154.95	0.01	0.50
	5	195231.06	0.07	0.50
	6	273321.35	0.02	0.50
	7	364425.17	-0.10	0.50
	8	468541.43	0.05	0.50
$^{18}O^{12}C^{32}S$	1	11306.55	0.55	0.50
	2	33917.95	0.03	1.00
	3	67835.50	-0.08	1.00
	4	113058.50	-0.20	1.00
	5	169586.85	-0.07	1.00
	6	237419.75	-0.06	1.00
	7	316556.85	0.05	1.00

Table 3.11 continued

$^{16}O^{12}C^{33}S$	J	F →	F'	observed	obs.-calc.	exp. error
	1	5/2	5/2	12360.85	0.24	1.00
		3/2	5/2	16075.90	-0.44	1.00
		5/2	3/2	8940.85	0.62	1.00
		3/2	3/2	12656.45	0.49	1.00
		3/2	1/2	18854.35	0.13	1.00
	2	7/2	5/2	40918.05	0.44	1.00
		7/2	7/2	37174.95	0.35	1.00
		3/2	5/2	39918.53	0.37	1.00
		1/2	3/2	40693.60	0.29	2.00
		3/2	3/2	37258.70	-0.59	1.00
	3	5/2	5/2	74577.40	0.24	0.50
		9/2	9/2	74419.35	0.10	0.50
		3/2	5/2	79802.85	0.25	0.65
		9/2	7/2	79953.91	-0.01	0.80
		5/2	7/2	77148.58	-0.10	0.50
	4	11/2	11/2	124088.06	-0.07	0.50
		11/2	9/2	130339.88	-0.27	0.50
		7/2	9/2	126461.80	-0.10	0.50
		5/2	7/2	130222.05	0.10	0.50
		7/2	7/2	124279.80	-0.61	1.00
	5	13/2	11/2	192789.80	0.16	0.50
		13/2	13/2	186178.53	0.07	0.50
		7/2	9/2	192690.20	-0.07	0.50

REI 72d and REI 74c, because now a 95% confidence level has been handled as criterion. The χ^2-s for the fits of OCS were 2.5, 0.6, 0.4, 1.2 and 3.7 for the isotopes in the same order as presented in Table 3.11.

Table 3.12. Vibration-rotation coupling constants and relative electric dipole moments of five OCS isotopes in the $(01^{1}0)$ state.

molecule	q_v(kHz)	μ_v(Hz)	ref*	μ_{el}
$^{16}O^{12}C^{32}S$	6361.413(3)	-4.27(3)	PI	1.00000
	6361.31(5)	-4.20(3)	MAK 67	
$^{16}O^{12}C^{34}S$	6068.802(10)	-3.93(26)	PI	1.00033(2)
$^{16}O^{13}C^{32}S$	6507.835(17)	-4.37(28)	PI	1.00067(2)
	6507.70(12)	-4.36(7)	MAK 67	
$^{18}O^{12}C^{32}S$	5653.009(45)	-3.74(96)	PI	0.99907(4)
	5652.88(8)	-3.47(4)	MAK 73	
$^{16}O^{12}C^{33}S$	6209.878(16)	-4.4(6)	PI	1.00012(9)

*References refer only to the vibration-rotation interaction constants. Electric dipole moments are all obtained in present investigations (PI).

Table 3.13. Hyperfine constants in kHz of $OC^{33}S$ in the $(01^{1}0)$ state, all from present investigations.

eQq_{11}	-28682.5(9)
eQq_{12}	- 1180.8(9)
$c_{\perp}^{(1)}$	1.16(4)
$c_{\parallel}^{(1)}-c_{\perp}^{(1)}$	11.5(3)
$c_{xx}^{(1)}-c_{yy}^{(1)}$	-0.12(6)

Fig. 3.4 shows the energies of $v_2=1$, $J=1$ hyperfine levels as a function of the Stark field strength. The zero field transitions of J=1 are shown in the insert of the figure. The figure is a good illustration of focusation properties in the excited bending vibration. It should be noted that all hyperfine levels belonging to the upper l-doublet state have either positive Stark slopes (corresponding with $|M_J|=1$ in the strong field case) and thus can be focused, or zero slopes which are not deflected

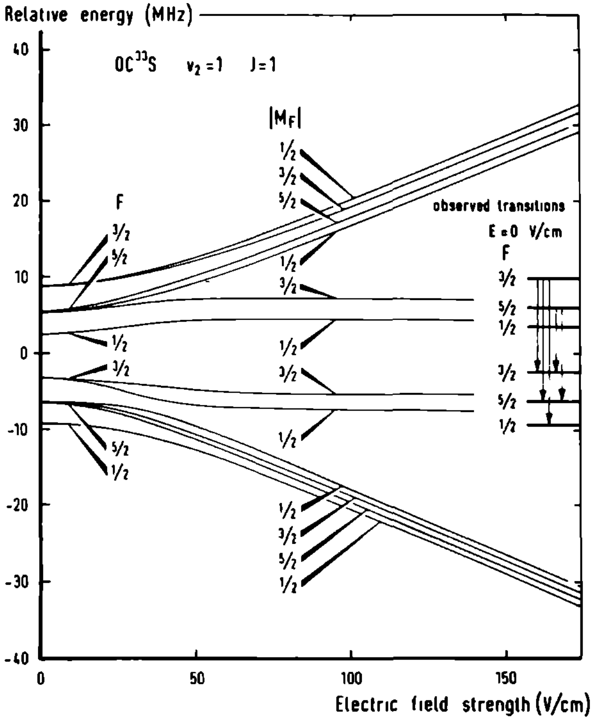

Fig. 3.4. Energy level diagram of $OC^{33}S$, $v_2=1$, $J=1$ and observed zero-field transitions.

(M_J=0). The lower $|M_J|$=1 l-doublet states have negative Stark slopes and are defocused while M_J=0 states have zero slopes and are not deflected. This clearly illustrates that as far as focusation properties are concerned the conditions are almost ideal for the observation of direct l-doublet transitions.

3.3.1b Stark spectra.

Stark measurements on $^{16}O^{12}C^{32}S$ were performed with EBR I machine using a 400μ nozzle and 10 Torr backing pressure. Electric fields of about 50, 100, 200 and 400 V/cm have been applied to investigate whether a J-dependence of the electric dipole moment could be measured for the J=1, 2 and 3 states. At high fields higher order contributions originating from $\Delta J=\pm 1$ interactions are not longer negligible. Also contributions of the electric polarizability become significant. Scharpens value of $\alpha_{\parallel} - \alpha_{\perp} = 4.67(16)Å^3$ for $v_2=0$ has been used (SCH 70). If all those contributions are taken into account no J-dependence of the electric dipole moment has been found.

The measured frequencies are tabulated in Table 3.14. The electric dipole moment has been determined relative to that of the ground state. The calculated frequencies have been determined using the value of $\mu_{el}(v_2=1)=0.704332$ D. All measured frequencies fall within a frequency interval calculated with electric dipole moments of 0.704312 D and 0.704352 D (REI 72a). No least-squares fit has been used in this calculation.

For the determination of the dipole moments of the other isotopes nozzle diameters of 100μ and backing pressures of 250 Torr have been used to produce strong beams. Asymmetric line shapes have been observed already at very low Stark fields. The shape of the line depends on the C-field polarity in that sense that the whole picture of the line is reversed if the polarity is changed. This phenomenon has not been encountered during the Stark measurements on $^{16}O^{12}C^{32}S$ where a 400μ nozzle was used. As there is also a line shape and line frequency dependence on the six-pole or four-pole voltages direct absolute measurements of the electric dipole moments were impossible. Only measurements relative to $^{16}O^{12}C^{32}S$ have been performed. At fields of 30 and 50 V/cm the J=1, $|M|=1 \rightarrow |M|=1$ transitions have been obtained for the three molecules $OC^{34}S$, $O^{13}CS$ and ^{18}OCS (Table 3.15) yielding the relative dipole moments as given in Table 3.12. As far as $OC^{34}S$ and $O^{13}CS$ are concerned those values have been confirmed by remeasurement on EBR II machine of the transitions J=1, $|M_J|=1 \rightarrow 0$ at 50 and 200 V/cm and also of the J=2, $|M_J|=2 \to 2$ and $|M_J|=1 \to 1$ transitions at 200 V/cm REI 73b).

Table 3.14. Observed transition frequencies for $^{16}O^{12}C^{32}S$ in the (01^10) state for J=1, 2 and 3 at different field strengths. Frequencies are in kHz and experimental errors 0.20 kHz if not otherwise mentioned.

E(V/cm)	J	$\lvert M\rvert \to \lvert M'\rvert$		observed	calculated
50	1	1	0	17271.9	17271.84
	2	1	0	38395.45	38395.23
		1	1	38623.04	38622.98
		2	1	39289.34	39288.21
		1	2		39290.76
		2	2	39956.7(1.0)	39955.98
	3	3	2	76707.0	76706.32
		2	3		76707.54
		2	1	76479.0	76478.72
		1	2		76479.46
100	1	1	0	25197.5	25197.47
	2	2	1	42419.87	42419.80
		1	2	42429.7	42430.03
		1	0	39060.8(1.0)	39060.45
	3	3	2	77804.3	77804.17
		2	3	77809.0	77809.05
		2	1	76905.2	76903.72
		1	2		76906.65
		1	0	76450.2	76450.03
200	1	1	0	42390.9	42391.12
	2	1	2	52845.9	52845.69
		2	1	52804.5	52804.80
		1	0	41524.1(1.0)	41524.28
	3	3	2	82030.0(1.0)	82029.82
		2	3	82049.6(1.0)	82049.35
		2	1	78572.9	78572.81
		1	2	78584.6	78584.53
400	1	1	0	77594.1	77593.66
		1	1	142381.8(1.0)	142382.06
	2	2	1	81274.7	81274.60
		1	2	81438.2	81438.17
		2	2	101956.6	101955.84
		1	0	49435.2	49435.35
		1	1	60756.8	60756.93
	3	3	3	104187.4	104187.17
		3	2	96948.2	96948.26
		2	3	97026.3	97026.38
		2	2	89787.5	89787.47
		2	1	84826.1	84826.13
		1	2	84873.1	84872.99

Table 3.15. Observed $|M_J|=1 \rightarrow 1$ Stark transition frequencies for OCS isotopes in the (01^10) J=1 state at different field strengths.

E(V/cm)	OCS	$OC^{34}S$	$O^{13}CS$	^{18}OCS
30	16581.73	16139.67	16811.71	15514.61
50	21818.76	21487.58	22000.46	21010.96

E(V/cm)	OCS	F	M_F →	F'	M_F'	$OC^{33}S$
100	37671.45	3/2	1/2	5/2	1/2	38099.11
	37671.35	3/2	1/2	1/2	1/2	40251.81
200	72047.46	3/2	1/2	5/2	1/2	72289.04
	72047.97	3/2	1/2	1/2	1/2	73952.36

The two transitions F, M_F=3/2, 1/2 → 1/2, 1/2 and 3/2, 1/2 → 5/2, 1/2 in the J=1 state of $OC^{33}S$ have been observed in Stark fields of 100 and 200 V/cm. Measurements again were performed relative to the J=1, $|M|=1 \rightarrow 1$ transition of $^{16}O^{12}C^{32}S$ as given in Table 3.15. Relative dipole moment for $OC^{33}S$ in the $v_2=1$ state is included in Table 3.12.

3.3.1c Zeeman spectra

Zeeman spectra of the J=3, 4 and 5 rotational states have been measured for the most abundant isotopic species at a magnetic field of about 8.5 kG. When an external magnetic field is applied each l-doublet state splits into 2J+1 M_J-sublevels. Between these sublevels the following transitions are possible: 2J $\Delta M_J=-1$ transitions, 2J $\Delta M_J=+1$ transitions and 2J+1 $\Delta M_J=0$ transitions. The $\Delta M_J=0$ transitions, however, could not be observed as separate lines at the maximum available field. The $\underline{\mu}_{el}\cdot\underline{v}\times\underline{H}$ term of the Hamiltonian gives line broadening because of the velocity distribution of the beam-molecules but also frequency shifts. The line broadening made high resolution for J=1 and 2 impossible at 8.5 kG. At lower fields the separation of the $\Delta M_J=\pm 1$ Zeeman components for these states was too small to resolve. The same difficulty was experienced for J-states higher than J=5 at maximum field thus leaving three J-states for which separated lines with normal line widths were possible (Table 3.16)

Table 3.16. Measured and calculated frequencies (in kHz) of OCS in the (01^10) vibrational state at a magnetic field of about 8 kG. The electric field E is calculated from $E=|\underline{v}\times\underline{H}|$.

H(kG)	E(V/cm)	J	M →	M'	observed	obs.-calc.	exp. error
7.953(1)	4.06	3	2	3	76455.3	0.36	0.3
			1	2	76461.4	0.27	0.3
			0	1	76467.4	0.31	0.3
			-1	0	76473.0	0.19	0.3
			-2	-1	76478.0	-0.29	0.3
			-3	-2	76483.0	-0.53	0.5
8.4522(3)	4.31	3	3	2	76210.3	0.25	0.3
			2	1	76206.0	0.33	0.3
			1	0	76201.5	0.47	0.3
			0	-1	76196.3	0.19	0.3
			-1	-2	76191.1	0.17	0.5
			2	3	76461.6	-0.02	0.3
			1	2	76468.4	-0.17	0.3
			0	1	76475.1	-0.15	0.3
			-1	0	76481.7	0.04	0.3
			-2	-1	76487.4	-0.40	0.3
			-3	-2	76493.7	0.03	0.3
8.4356(3)	4.30	4	3	4	127370.1	-0.52	0.5
			2	3	127375.1	0.00	0.3
			1	2	127379.7	0.11	0.3
			0	1	127384.1	0.03	0.3
			-1	0	127388.6	0.05	0.3
			-2	-1	127393.2	0.16	0.3
			-3	-2	127397.6	0.08	0.3
			-4	-3	127402.1	0.10	0.5
8.375(1)	4.27	5	4	5	190991.5	-0.28	0.5
			3	4	190994.6	-0.36	0.3
			2	3	190998.5	0.33	0.3
			1	2	191001.4	-0.01	0.3
			0	1	191004.8	0.11	0.3
			-1	0	191008.0	0.01	0.3
			-2	-1	191011.3	-0.03	0.3
			-3	-2	191014.7	-0.01	0.3
			-4	-3	191018.2	0.09	0.3
			-5	-4	191021.0	-0.55	0.3

H(kG)	E(V/cm)	J	M	→ M'	observed	obs.-calc.	exp. error
8.450(2)	4.31	4	-2	-3	127060.3	0.07	0.5
			-1	-2	127063.3	0.06	0.5
			0	-1	127066.0	-0.24	0.5
			1	0	127068.6	-0.64	0.5
			2	1	127071.9	-0.34	0.5
			3	2	127074.8	-0.44	0.5
			4	3	127078.3	0.06	0.5
			3	4	127370.6	-0.24	0.5
			2	3	127375.3	-0.04	0.3
			1	2	127379.9	0.06	0.3
			0	1	127384.4	0.06	0.3
			-1	0	127388.7	-0.13	0.3
			-2	-1	127393.4	0.07	0.3
			-3	-2	127397.5	-0.33	0.3
			-4	-3	127402.4	0.08	0.5
8.455(1)	4.31	5	4	5	190993.1	-0.03	0.5
			3	4	190996.3	-0.06	0.3
			2	3	190999.5	-0.13	0.3
			1	2	191002.8	-0.12	0.3
			0	1	191006.3	0.04	0.3
			-1	0	191009.5	-0.12	0.3
			-2	-1	191013.0	-0.02	0.3
			-3	-2	191016.4	-0.05	0.3
			-4	-3	191020.1	0.19	0.3
			-5	-4	191023.9	0.50	0.3

The experimental conditions were the same as described by de Leeuw (LEE 71). The magnetic field strength has been determined from the two known transitions in $v_2=0$, J=1 state measured before and after each group of lines of $v_2=1$. Magnetic constants have been derived from the frequencies with help of a least-squares procedure. In this fit program the velocity v was also used as an adjustable parameter resulting in a best fit value of 500 m/s (REI 71b).

The most probable beam velocity calculated from standard expressions was 350 m/s. In REI 72d, the badly known velocity was assumed to have a value somewhere between 350 and 500 m/s. Lateron we directly measured the beam velocity (REI 72c) and found the value of 500 m/s for it. The re-evaluated magnetic constants with their much smaller error limits are listed in Table 3.17.

Table 3.17. Magnetic properties of $^{16}O^{12}C^{32}S$ in the (01^10) state of vibration.

constant	present work	HUT 70
$g_\perp$	-0.02930(2)	-0.0285(6)
$g_\parallel - g_\perp$	0.09092(33)	0.0895(21)
$g_{xx} - g_{yy}$	0.000232(9)	0
$\chi_\perp - \chi_\parallel$ (10^{-6}erg/G^{2}mole^{-1})	9.50(8)	8.0(10)
$\chi_{xx} - \chi_{yy}$ (10^{-6}erg/G^{2}mole^{-1})	-0.13(3)	0

The transverse Stark effect $\underline{\mu}_{el}.\underline{v}x\underline{H}$ caused a shift of the spectral lines of about 3 kHz at 8 kG for J=3 and was therefore needed to explain the spectra. Unique identification of the spectral lines from the calculated magnetic energies was impossible with neither the sign of $g_{xx}-g_{yy}$ nor of $\chi_\perp - \chi_\parallel$ known. We have assumed the same sign for $\chi_\perp - \chi_\parallel$ as in the ground vibrational state, fixing herewith the sign of $g_{xx}-g_{yy}$.

3.3.2 Nitrous oxide

3.3.2a Zero field spectra

Until now no accurate value for vibration-rotation constants and no values at all for hyperfine constants in the first excited bending vibrational state of N_2O have been reported. The present investigations involve the determination of those molecular properties from ΔJ=0, l-doubling transitions of the three lowest rotational states. About 100 different transitions have been observed with signal to noise ratio of about 10 at RC=1.9 s. The line width was 2.5 kHz so that the top frequency could be determined to within 300 Hz. Backing pressures of 250 Torr and a nozzle diameter of 100μ have been used. Because of the small electric dipole moment it was very difficult to focuse higher J-states. Focusation of J=1 required +10 and -10 kV, J=2 +20 and -20 kV and so on. To prevent that transitions occurred in the buffer field region voltages on the buffers of 2-4 kV were applied. The 94 measured top frequencies for J=1, 2 and 3 are given in Table 3.18, together with the deviations from the frequencies calculated from the best-fit constants. All errors in frequency determination were set equal to 150 Hz unless stated otherwise.

Table 3.18. Observed and calculated transition frequencies (in kHz) of $^{14}N^{14}N^{16}O$ in the $(01^{1}0)$ state for J=1, 2 and 3 zero external fields.

J	F	→ F'	observed	obs. -calc.
1	1	2	47279.65	0.07
	1	1	47293.75	0.01
	3	2	47314.72	-0.07
	2	2	47341.12	-0.02
	2	1	47355.27	-0.04
	1	0	47385.77(20)	-0.04
	1	2	47402.01	0.09
	2	2	47413.56	0.12
	1	1	47416.16	0.08
	2	1	47427.62	0.02
	1	2	47448.13	-0.04
	0	1	47453.26	0.09
	3	2	47483.37	-0.01
	1	1	47488.11	0.03
	3	3	47500.29	0.01
	2	2	47509.70	-0.03
	2	3	47526.36	-0.27
	2	1	47549.65	0.01
	1	2	47570.56	0.05
	2	2	47582.11	0.08
	2	3	47599.05	0.12
	1	1	47610.53	0.11
	0	1	47647.65	0.14
	1	1	47739.57	0.06
	2	1	47801.26	0.19
	1	1	47862.04	0.19
	2	1	47873.46	0.09
	0	1	47899.03	0.09
2	2	2	142215.11(100)	0.12
	3	2	142238.18	0.06
	1	2	142267.50	-0.02
	3	4	142275.59	0.01

Table 3.18 continued

J	F	F'	observed	obs. -calc.
2	2	3	142299.38	0.10
	3	3	142322.44	0.02
	2	3	142361.86(100)	0.09
	1	1	142382.08	0.00
	3	3	142384.95	0.04
	2	2	142394.43	0.01
	3	2	142417.50	-0.05
	3	2	142439.86(100)	0.14
	3	4	142444.91	-0.04
	2	2	142471.63	-0.04
	4	4	142479.72	-0.09
	3	3	142491.72	-0.07
	1	2	142514.10	-0.04
	2	3	142523.71	-0.04
	4	3	142526.67(100)	0.03
	2	2	142536.45	-0.03
	1	1	142540.66	-0.02
	3	3	142553.97	-0.31
	2	1	142563.09	0.07
	0	1	142572.37	-0.03
	2	3	142586.22(100)	-0.02
	4	3	142588.88(100)	-0.26
	2	3	142620.02(100)	-0.75
	1	1	142660.96	0.05
	2	3	142683.33(100)	0.07
	1	2	142693.48	-0.09
	2	2	142715.74	-0.17
3	3	3	284562.04	0.07
	2	1	284597.61	0.09
	4	3	284612.89	0.02
	3	2	284626.78	-0.02
	2	3	284650.71	-0.05
	4	5	284654.58(150)	-0.02
	3	4	284679.94	-0.01
	4	4	284730.92	0.08
	3	4	284789.02(150)	-0.10
	2	2	284835.82	0.05
	4	4	284840.15(100)	0.14
	3	3	284854.77	0.05
	4	5	284881.20(100)	-0.53
	2	3	284902.67(50)	-0.10
	4	3	284905.44(50)	-0.17
	2	1	284915.02	0.05
	2	3	284927.57	0.09
	3	3	284935.91	-0.11
	5	5	284941.92	-0.06

Table 3.18 continued

J	F → F'		observed	obs. -calc.
3	4	4	284957.89(150)	-0.08
	1	1	284972.17	0.10
	3	3	284979.35	0.04
	2	2	284992.30	0.00
	3	4	285013.16	-0.10
	5	4	285018.12(150)	-0.10
	3	2	285044.26	0.13
	3	4	285121.05(100)	-1.38
	5	4	285127.30	-0.09
	4	3	285132.76	0.02
	2	2	285153.22	-0.01
	3	3	285188.04	0.01
	3	4	285206.48(150)	0.02
	1	2	285210.37	0.04
	2	3	285220.28	0.06
	3	3	285271.77	-0.29

Because of large vibrational effects on the quadrupole coupling constants interpretation of the spectrum was very difficult. The J=1 spectrum ultimately could be explained by a trial and error method. Assuming a certain order of the hyperfine energy levels the transition frequencies have been fitted by making use of the Stark slopes for the relevant energy levels. The levels as a function of electric field strength are shown in Fig. 3.5, for J=1. This figure provides valuable information about the focusing properties of a given level. Without this information it was not possible to obtain an unambiguous interpretation of the spectrum. With the best-fit constants for J=1 a preliminary calculation of the l-doubling transitions of the higher J-states became possible, converging eventually to a final identification of all measured transition frequencies.

Ten constants have been adjusted in the least-squares fit resulting in the best fit values as given in Table 3.19. The χ^2 of the fit was 32.0. The spin-spin constant d_T has been

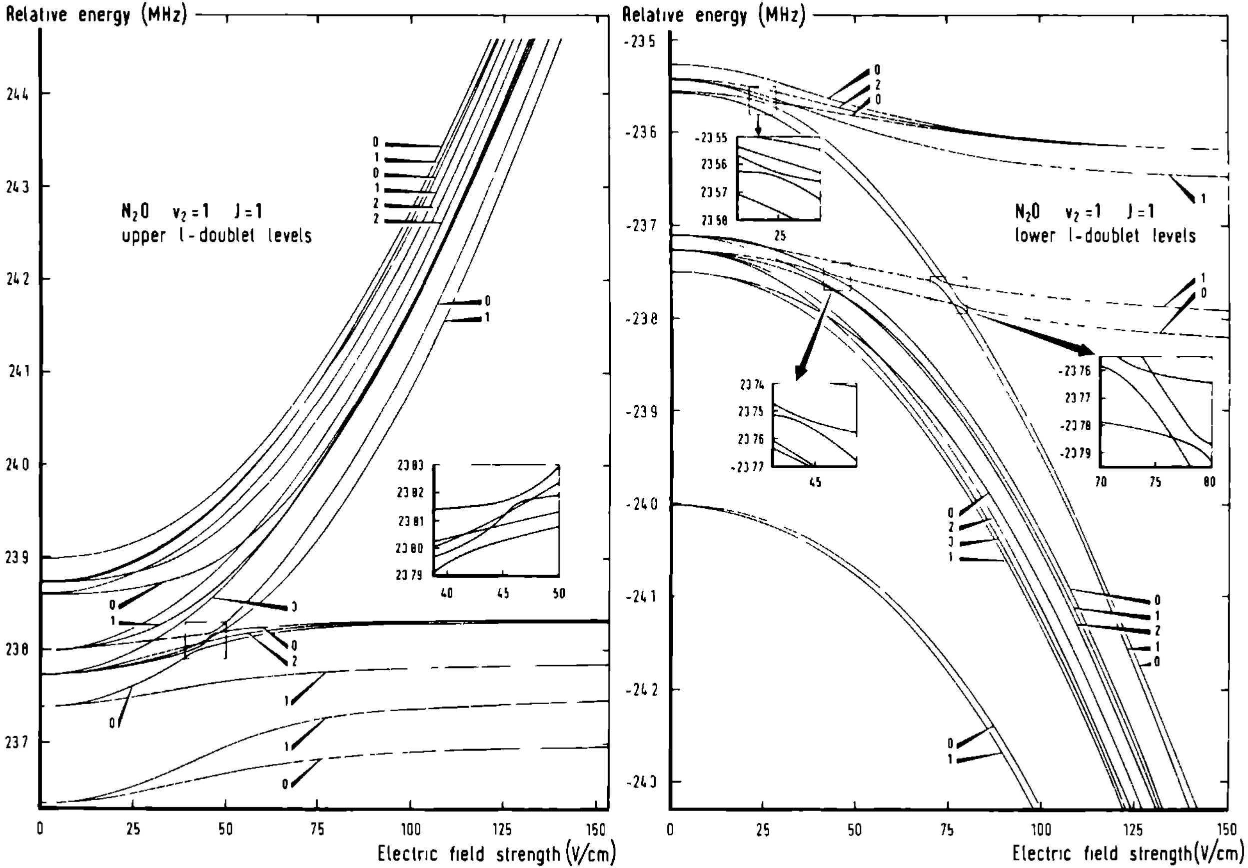

Fig. 3.5. Energy level diagram of the v_2=1, J=1 l-doublet of N_2O. The energy levels are labeled with their $|M_F|$-values.

fixed at the calculated value (d_T=0.436 kHz). Since variation of $d_{xx}-d_{yy}$ and $c^{(i)}_{xx} - c^{(i)}_{yy}$ for i=1 or 2 gave no further improvement of the fit these constants have been set equal to zero.

Table 3.19. Molecular constants of $^{14}N^{14}N^{16}O$ in the v_2=1 state. All values are in kHz except μ_{el} (in D).

constant	present value
q_v	23743.75(1)
μ_v	-0.032(1)
eQq_{11}	-886.53(12)
eQq_{12}	318.78(14)
eQq_{21}	-258.14(18)
eQq_{22}	- 60.84(18)
$c^{(1)}_{\perp}$	1.904(15)
$c^{(1)}_{\parallel}-c^{(1)}_{\perp}$	-1.78(7)
$c^{(2)}_{\perp}$	2.60(2)
$c^{(2)}_{\parallel}-c^{(2)}_{\perp}$	1.2(1)
μ_{el}(D)	0.173484(9)

Using the constants of Table 3.19 all energies and possible transitions for J=1 through 6 have been determined and reported in REI 75b.

3.3.2b Stark spectra

In a field of 300 V/cm fourteen ΔM_F=0 Stark transitions have been observed for J=1 in the (01^10) state. Calibration of the field has been performed with OCS. Nine lines of this group (Table 3.20) have been uniquely identified and used for the determination of the electric dipole moment in a least-squares fit. The best fit value is given in Table 3.19. The error quoted was determined by the accuracy of the absolute field strength. In the relative dipole moment determination an error of 1×10^{-5} is claimed. The transitions also have been recorded at 100 and 200 V/cm yielding frequencies fully in accordance with predicted values from the above value of μ_{el} in Table 3.19.

Table 3.20. Observed and calculated $\Delta M_F=0$ transitions of $^{14}N_2{}^{16}O$ in the (01^10) vibrational and J=1 rotational state. The applied field is 300 V/cm. Experimental errors in the frequencies are 0.15 kHz.

M_F	observed	obs. -calc.
1	54498.25	0.16
0	54492.63	0.13
1	54328.49	0.07
0	54275.53	0.04
2	54254.82	-0.03
1	54215.60	-0.09
2	54207.49	-0.06
0	54023.01	-0.13
1	54000.16	-0.11

3.3.2c Zeeman spectra

Absorption features for $v_2=1$, J=1, 2 and 3 states at magnetic fields of about 8.7 kG have been recorded. At such high fields coupling between $\underline{I}$ and $\underline{J}$ is broken down so that only $\Delta M_I=0$ transitions occur as in the $v_2=0$ states, resulting in three groups of lines corresponding with the $\Delta M_J=0$, +1 and -1 transitions. The observed spectrum in those groups is so rich in lines due to the magnetic and hyperfine splittings that no separate spectral lines could be identified. The alternative is to perform measurements in low fields and follow the lines as a function of the field strength until a reasonable Zeeman shift is obtained. In the present investigations a field of 93.7(2) G.

as calibrated from a $\Delta J=0$, $\Delta M_J=\pm1$ transition in the 1_{11} rotational state of SO_2 (ELL 76) has been applied to obtain the Zeeman spectrum of the $F=2 \rightarrow 1$ transition of $J=1$ at 47801.26 kHz. Especially this transition has been chosen because in its direct neighbourhood no other lines are present. In the field of 93.7 G the measured transition frequency of $M_F=1 \rightarrow 1$ was 47820.60(20) kHz. The Zeeman shift of this line is due to the g_I and g_J factors. The largest contribution comes from the known g_I factors. However the shift due to the molecular g-factor resulted in a large effect yielding a molecular g-value for $v_2=1$ $J=1$ of -0.0155(42). The molecular g-factor of this state (see Eq. 2.42) can be written as $\frac{1}{2}(g_{\parallel} + g_{\perp})$. Taking the value of $g_{\perp}$ of $v_2=0$ from Table 3.6 yields for the parallel component $g_{\parallel}=0.048(8)$.

At the field strength of 93.7 G several other components of the $F=2 \rightarrow 1$ transition have been observed to confirm above determination of the g-factor. Increasing the field strength resulted in overlap with other lines so that identification was not longer possible.

3.3.3 Cyanogen chloride

3.3.3a Zero field spectra

A first impression of the $v_2=1$ spectrum could be obtained from a calculation using the rather inaccurate value for the eQq_{11} of ^{35}Cl in $^{35}Cl^{12}C^{15}N$ determined by White (WHI 55) and a value for q_v of Burrus et al (BUR 56). Expected signal to noise ratio was about 10 times lower than for OCS under the same conditions. However, another factor 2 to 3 in S/N was lost because optimum backing pressure was about 60 Torr instead of 250 Torr as for OCS. Therefore the strongest $\Delta J=0$, $v_2=1$ transitions were measured with S/N of 4 at 1s time constant. Searches with long integrating times and slow sweep speeds

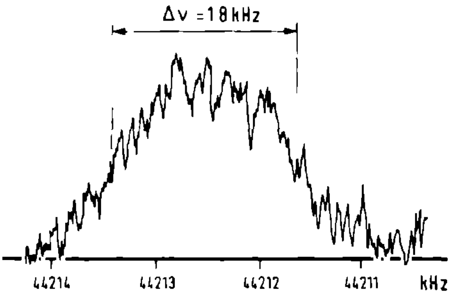

Fig. 3.6 Resonance of ClCN in the v_2=1, J=2 state for the F=7/2 → F=9/2 transition in the absence of external fields. The RC-time was 4s.

eventually resulted in 32 lines for J=2 and 21 lines for J=3 (Table 3.22). No J=1 transitions have been observed. The strongest ClCN line is shown in Fig. 3.6. Because vibrational effects on hyperfine levels were relatively small no hard problems have been encountered in the interpretation of the spectrum.

Table 3.21. Molecular constants of $^{35}Cl^{12}C^{14}N$ in the v_2=1 state. All values are in kHz except the electric dipole moment which is in Debye units.

constant	present work	others	references
q_v	7467.532(16)	7460.0(50) 7467.467	BUR 56 YAR 57
μ_v	-0.0183(15)	-0.01327	YAR 57
eQq_{11}	-82815.54(55)	-82825(15)	WHI 55*
eQq_{12}	-927.84(49)		
eQq_{21}	-3702.19(40)		
eQq_{22}	256.00(41)		
$c_\perp^{(1)}$	1.695(48)	3.5(6)	WHI 55
$c_\parallel^{(1)}-c_\perp^{(1)}$	7.38(35)	4.5(50)	WHI 55
$c_\perp^{(2)}$	1.243(67)		
$c_\parallel^{(2)}-c_\perp^{(2)}$	2.20(53)		
μ_{el}(D)	2.804(3)		

*The values from WHI 55 all refer to $^{35}Cl^{12}C^{15}N$.

Table 3.22. Observed and calculated frequencies of $^{35}\mathrm{Cl}^{12}\mathrm{C}^{14}\mathrm{N}$ in the $v_2=1$ state in zero external fields for J=2 and 3. Experimental error is 0.25 kHz.

J	F →	F'	observed	obs. -calc.
2	7/2	5/2	44064.13	-0.23
	7/2	9/2	44212.42	-0.23
	7/2	7/2	44687.36	0.00
	9/2	9/2	44756.34	-0.21
	5/2	5/2	44782.30	-0.12
	9/2	7/2	45231.23	-0.03
	5/2	7/2	45405.38	-0.05
	5/2	7/2	42156.32	0.05
	5/2	5/2	41533.24	-0.03
	3/2	5/2	41552.84	-0.07
	7/2	5/2	47335.19	0.06
	5/2	3/2	48039.37	0.13
	5/2	5/2	48053.21	0.02
	5/2	5/2	44804.20	0.17
	3/2	3/2	44809.85	0.13
	1/2	3/2	52148.79	0.21
	5/2	3/2	52175.15	0.01
	3/2	3/2	52194.77	-0.01
	5/2	7/2	52233.54	-0.13
	5/2	5/2	52432.17	0.00
	3/2	5/2	52451.82	0.01
	7/2	7/2	54764.61	-0.15
	7/2	5/2	54963.17	-0.09
	9/2	7/2	55308.55	-0.11
	5/2	3/2	55424.32	0.03
	5/2	5/2	55681.30	-0.03
	3/2	3/2	55037.68	0.19
	3/2	5/2	55051.32	-0.12
	1/2	3/2	44763.89	0.37
	5/2	3/2	44790.24	0.16
	3/2	5/2	44824.05	0.37
	3/2	5/2	45238.53	-0.31
3	5/2	5/2	89627.77	0.26
	7/2	7/2	89666.04	0.06
	3/2	3/2	89678.94	0.07
	11/2	11/2	89551.60	-0.17
	9/2	9/2	89474.39	-0.07
	7/2	7/2	106067.73	-0.16
	5/2	5/2	105500.13	0.22
	7/2	5/2	105346.72	-0.03
	11/2	9/2	105279.31	-0.08
	5/2	7/2	105072.93	0.09
	9/2	7/2	104977.47	0.04
	3/2	3/2	104343.14	0.04

Table 3.22 Continued.

J	F → F'		observed	obs. -calc.
	7/2	7/2	97516.52	-0.14
	5/2	7/2	97051.10	-0.01
	3/2	5/2	96964.20	-0.04
	7/2	9/2	96930.72	-0.23
	7/2	5/2	96795.70	0.04
	5/2	5/2	96330.13	0.01
	11/2	9/2	90361.74	-0.40
	3/2	5/2	90261.73	0.10
	7/2	5/2	90093.31	0.26

As in the case of N_2O ten significant molecular constants could be determined from the least-squares fit with the anisotropic spin-spin and c-constants set equal to zero. Table 3.21 lists the properties obtained.
The value of d_T has been calculated with Eq. 3.2 (d_T=0.039 kHz). The χ^2 was 20.5 for 53 lines and 10 variables. It should be remarked here that terms off-diagonal in J for the eQq_{11} and eQq_{21} interactions had to be taken into account to reach the best fit. If for example those terms were omitted the χ^2 rises up to about 800.

With the v_2=1 properties of Table 3.21 all possible $\Delta F=0$ and $\Delta F=\pm1$ transitions of J=1, 2 and 3 have been determined and reported in REI 76.

3.3.3b Stark spectra

One single Stark transition has been used for the rather inaccurate determination of the electric dipole moment. In a field of 10 V/cm, where the Stark shift of the lines is about 600 kHz seven v_2=1, J=2 lines have been observed at only one C-field polarity. Signal averaging techniques were used to get a detectable signal. The most intense line ($|M_F| = 5/2 \rightarrow |M_F'| = 7/2$) has been followed up to Stark fields of 20 V/cm in steps of 1 V/cm. At 20 V/cm a Stark shift of about 2.5 MHz is obtained demonstrating the quadratic character at low fields. Interpretation of the transition was unambiguous. Carefully obtained recordings of the line at 10 V/cm for both C-field polarities yield an averaged frequency of 52803.9(10) kHz. With the electric dipole moment deduced from this transition (Table 3.21 the entire Stark spectrum at 10 V/cm for J=2 has been computed and checked by measuring a second arbitrarily chosen line ($|M_F|=5/2 \rightarrow |M'_F|=5/2$) at 56428.95(200) kHz) to eliminate all doubts about interpretation. Because of very low signal to noise ratio already experienced in obtaining Stark spectra, measurements in external magnetic field did not look feasible.

3.4 MEASUREMENTS AND RESULTS ON KCN AND CsOH

Electric resonance measurements on KCN and CsOH have been discussed in details in internal reports (REI 70b; REI 74b; REI 75a). In this thesis we restrict ourselves to a short review of the best results thus far obtained. For all considered hot molecules the machine configuration described in WAC 67a (EBR I) has been employed apart from some small changes in the hot wire detector and the state selectors. An iridium wire (ø 0.25 mm) instead of tungsten ribbon (0.4x0.025 mm^2) and highly polished four- and six-poles in order to obtain higher voltages, have been used. As a preparation for KCN measurements KCl has been used to optimize the conditions for "hot beam" spectroscopy, yielding the well-known KCl spectra (WAC67a, WAC 67b) with signal to noise ratios of 20 at 0.1 sec time constant.

At optimum working conditions KCN spectra in zero external fields have been swept over the whole frequency range of 0 to 400 MHz. An impression of the observed spectrum is shown in Fig. 3.7 illustrating the typical saturated absorption pattern swept with high speed. Systematic optimizing of the variables

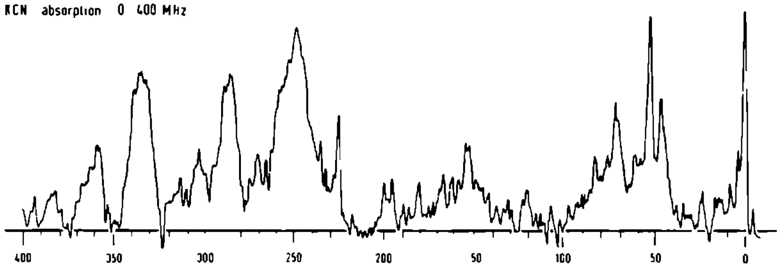

Fig. 3.7 Radio-frequency absorption spectrum of KCN in the 0-400 MHz range.

such as oven temperature, state selector voltages, RF power etc. did not yield absorption lines with the expected line widths of a few kHz. Comparison of transition probabilities for $v_2=1$ resonances of OCS and KCN shows that RF powers as used in the case of Fig. 3.7 are several orders of magnitude too high. Reduction of the RF power results in somewhat less broad absorption features, however, also in bad signal to noise ratio. Application of large integrating times at very slow sweep speed did not result in separate spectral lines.

The population of the lower rotational states in the $v_2=1$ vibrational state of KCN was compared with that of CsOH using molecular constants for CsOH from LID 67 (rotational constant) and ACQ 68 (vibrational frequencies) and for KCN, for want of something better, from matrix isolation studies (ISM 73). This comparison shows that the low-J levels of KCN are about five times less populated than those of CsOH.
The ΔJ=0 l-doubling spectrum of CsOH in zero external fields is probably much less complicated than that of KCN because of the simpler hyperfine structure. Comparison of CsOH with CsF makes a value of eQq of -1.25 MHz (for Cs) reasonable. This quadrupole

interaction together with the l-doubling (q_v=7.90 MHz; LID 67) provides a basis for a rough calculation of the zero field spectrum for v_2=1. The result of these calculations is a v_2=1 spectrum consisting of groups of lines with large frequency separations between the groups because of the large l-doubling constant and the relative small quadrupole splittings. However, the observed saturated RF spectrum showed the same behaviour like KCN. Optimizing procedures yielded also in this case the same negative results as for KCN (REI 75a).

CHAPTER 4

DISCUSSION OF RESULTS

4.1 INTRODUCTION.

In this chapter several molecular properties are deduced from the experimentally determined coupling constants of the $v_2=0$ and $v_2=1$ spectra of OCS, N_2O and ClCN. The molecular quadrupole moments and the nuclear shielding constants of OCS, N_2O and ClCN are deduced in Sect. 4.2 and 4.4, respectively. In Sect. 4.3 the sign of the electric dipole moment of N_2O and ClCN is determined. Sections 4.5, 4.6 and 4.7 are devoted to a discussion of the special features occurring in the excited bending vibrational state. It is shown in Sect. 4.5 that the traditional definition of various coupling constants parallel to the molecular axis (e.g. $c_{\parallel}$, $g_{\parallel}$) in analogy with symmetric top molecules can no longer be maintained. From the l-doubling constants of the isotopic species of OCS some Coriolis coupling constants are deduced in Sect. 4.6. Since no high quality ab-initio calculations have been performed on the reported molecules it is not possible to compare the present results with theoretical predictions. Experimental values of the nuclear quadrupole coupling constants and the molecular electric dipole moments for the different vibrational states are compared in Sect. 4.7 and a certain trend in vibrational effects is noticed. In Sect. 4.8 a new technique is proposed for the improvement of signal to noise ratio in high temperature MBER spectroscopy.

A complete survey of the measured molecular constants (of Chap. 3), together with the quantities derived from them in this chapter, are given in the appendix.

4.2 MOLECULAR QUADRUPOLE MOMENTS.

The molecular parameters $g_{\perp}$ and $\chi_{\perp} - \chi_{\parallel}$ as determined from the Zeeman spectra can be used to compute the molecular quadrupole moments of $^{14}N_2{}^{16}O$ and $^{35}Cl^{12}C^{14}N$. The parallel component of the molecular quadrupole moment Θ of a linear molecule is given by

$$\Theta_{\parallel} = -\frac{4m}{e}(\chi_{\parallel} - \chi_{\perp}) + \frac{h\mu_N}{2\pi B_o} g_{\perp} + me \sum_K \frac{Z_K^2 r_K^2}{m_K} \qquad (4.1)$$

Herein m and e is the electron mass and proton charge, respectively, m_K is the mass of the K-th nucleus and $Z_K e$ its charge, r_K is the length of the vector to the K-th nucleus from the molecular center of mass. The last term of Eq. 4.1, although small compared to the difference of the other two terms (contribution of this term to $\Theta_{\parallel}$ is 0.054, 0.026 and 0.054 in units of 10^{-26} esu cm^2 for OCS, NNO and ClCN, respectively), is not negligible in view of the high accuracy of the present measurements. The molecular quadrupole moments have been calculated using the Zeeman constants of Table 3.6 for N_2O and of Table 3.10 for ClCN. The results are given in Table 4.1.

Table 4.1. Molecular quadrupole moments in 10^{-26} esu cm^2 calculated from experimental Zeeman parameters. PI stands for present investigation.

molecule	$\Theta_{\parallel}$	reference
$^{14}N_2\,^{16}O$	-3.296(15)	PI
$^{15}N_2\,^{16}O$	-3.65 (25)	FLY 69
$^{35}Cl\,^{12}C\,^{14}N$	-4.01 (5)	PI
$^{35}Cl\,^{12}C\,^{15}N$	-3.87(100)	EWI 72
$^{37}Cl\,^{12}C\,^{15}N$	-4.01(100)	EWI 72

Though Eq. 4.1 is only valid in the equilibrium state of the molecule molecular quantities of the vibrational ground state have been used in the calculation of $\Theta_{\parallel}$. From the Zeeman measurements on OCS in the v_2=1 state (see Table 3.16) and from those in the v_2=0 state (LEE 70,71), collected in Table 4.2, it is obvious that neglect of vibrational effects in $g_\perp$ and $\chi_\parallel - \chi_\perp$ can introduce errors in $\Theta_\parallel$ of at most a few percents.

Table 4.2. Magnetic constants of $^{16}O^{12}C^{32}S$ for the v_2=0 (LEE 70,71) and v_2=1 states from Table 3.16.

constant	v_2=0	v_2=1
$g_\perp$	-0.028839(6)	-0.02930(2)
$\chi_\parallel - \chi_\perp$ (10^{-6} erg G^{-2} mole^{-1})	-9.37(1)	-9.50(8)
$\Theta_\parallel$ (10^{-6} esu cm^2)	-0.766(14)	-0.80(8)

The molecular quadrupole moment for the v_2=0 state of OCS (corrected value, see also TAF 73) was obtained by de Leeuw (LEE 70,71) from very accurate measurements. In view of the somewhat lower precision of the present v_2=1 measurements we have not been able to detect a significant change in the molecular quadrupole moment when the molecule is excited to the v_2=1 state. This statement is based upon the use of Eq. 4.1 for the v_2=1 measurements, too; the fact that there is no significant effect on Θ from vibrational excitation has convinced us that Eq. 4.1 does not introduce large errors when applied to v_2=0 states instead of to the equilibrium situation.

4.3 SIGN OF THE ELECTRIC DIPOLE MOMENT.

The isotopic dependence of the molecular $g_\perp$ value can be used to determine the sign of the electric dipole moment via the relation

$$\frac{h\mu_N}{2\pi}\left(\frac{g_\perp^{(2)}}{B^{(2)}} - \frac{g_\perp^{(1)}}{B^{(1)}}\right) = -2\mu_{el}\delta \qquad (4.2)$$

Herein δ represents the magnitude of the vector pointing from the center of mass of isotopic species (1) to the center of mass of isotopic species (2). It is assumed that internuclear distances and the electronic structure are the same for both isotopic species (i.e. the Born-Oppenheimer approximation is valid). Since no accurate Zeeman measurements have been performed by us on two isotopes of N_2O or ClCN measurements of other workers have been used in the calculations.

In the case of N_2O the value of $g_\perp$ determined by Flygare et al (FLY 69) for $^{15}N_2{}^{16}O$ (see Table 3.6) has been taken for the second isotope with internuclear distances of 1.126 Å for N-N and 1.191 Å for N-O. In that case a dipole moment of 0.52(45) D is obtained with the sign of μ_{el} opposite to that of δ resulting in an electric dipole moment polarity of (-)NNO(+). The actual value for μ_{el} of about 0.16 D lies well inside the range of the value obtained. For ClCN the measurements of Ewing et al on the $^{35}Cl^{12}C^{15}N$ as the second isotope (EWI 72) have been used to evaluate the sign of the dipole. The Cl–C and C-N distances have been taken to be equal to 1.631 and 1.159 Å, respectively. The result for the polarity is (+)ClCN(-), fully in accordance with the determination made by Ewing et al (EWI 72) from the $^{35}ClC^{15}N$ and $^{37}ClC^{15}N$ isotopes. However the value of μ_{el} calculated with Eq. 4.2 equals 8.3(17) D totally in disagreement with actual value of about 2.8 D. Accurate measurements of Zeeman spectra for two different ClCN isotopes are necessary to get a more reliable value of μ_{el} via the procedure followed here.

4.4 DETERMINATION OF THE NUCLEAR SHIELDING CONSTANTS IN ClCN, N_2O and OCS.

From the definitions of the molecular coupling constants (LEE 73, Table I) it can easily be deduced that

$$(c_\perp^{(K)})^e = \frac{2\mu_N g_K B}{\mu_B} \quad (\sigma_\parallel^{(K)} - \sigma_\perp^{(K)})^p \qquad (4.3)$$

where the superscript e and p refers to the electronic and paramagnetic contribution, respectively. The electronic part of the $c_\perp$-constant can be obtained by subtracting the calculated nuclear part $(c_\perp^{(K)})^n$ from the measured value for $c_\perp (=c_\perp^e + c_\perp^n)$. In the rigid rotor approximation the nuclear part is defined as:

$$(c_\perp^{(K)})^n = -\frac{e\mu_o\mu_N g_K B}{h} \sum_{L\neq K} \frac{Z_L}{r_{LK}^3} \left(r_{LK}^2 - \frac{1}{2}\left(x_{LK}^2 + y_{LK}^2\right)\right) \tag{4.4}$$

Herein $r_{LK}=|\vec{r}_L-\vec{r}_K|$, $x_{LK}=x_L-x_K$ and $y_{LK}=y_L-y_K$, where x_L and y_L are the x and y-component of $\vec{r}_L$. In first approximation x_{LK} and y_{LK} have been set equal to zero so that the sum in Eq. 4.4 simplifies to $\sum_{L\neq K} Z_L/r_{LK}$. The nuclear contribution to the $c_\perp$ constants of ^{35}Cl and ^{14}N in ClCN is -0.310 and -0.416 kHz respectively. With these $c_\perp^n$ values and the experimental $c_\perp$-constants the anisotropies in the paramagnetic shielding in ClCN have been obtained (Table 4.3, row 1 and 2, column 2). The diamagnetic parts of the shielding anisotropies have been calculated using the atom-dipole method by Gierke and Flygare (GIE 72). Using their results (row 3 and 4) and the paramagnetic shielding anisotropies (row 1 and 2) we obtained the values for the (total) nuclear shielding anisotropies given in row 5 and 6. For OC^{33}S the shielding constants are determined following the same approach as for ClCN (Table 4.3 column 3).

Table 4.3. Paramagnetic, diamagnetic and total nuclear shielding anisotropies in ppm for ^{35}Cl^{12}C^{14}N, ^{16}O^{12}C^{33}S and N$_2$O.

quantity	ClCN	OCS	NNO	NNO
$(\sigma_\perp^{(1)}-\sigma_\parallel^{(1)})^p$	-567(14)^a	-406(18)^a	-561(36)^b	-467(18)^a
$(\sigma_\perp^{(2)}-\sigma_\parallel^{(2)})^p$	-663(76)^a		-707(47)^b	-737(22)^a
$(\sigma_\perp^{(1)}-\sigma_\parallel^{(1)})^d$	71^c	81^c	194(38)	100(18)*
$(\sigma_\perp^{(2)}-\sigma_\parallel^{(2)})^d$	125^c		199(48)	229(24)*
$(\sigma_\perp^{(1)}-\sigma_\parallel^{(1)})$	-496	-325	-367(12)^d	
$(\sigma_\perp^{(2)}-\sigma_\parallel^{(2)})$	-538		-508(10)^d	

[a] Present investigation; *using the results of BHA 73 and the present paramagnetic constants; [b] CAS 75; [c] GIE 72; [d] BHA 73 (for $^{15}N_2O$).

Paramagnetic shielding anisotropies have been obtained also for N_2O following the same way as for ClCN. The results are given in Table 4.3 (column 5, rows 1 and 2) together with the results obtained by Casleton and Kukolich (CAS 75) in a beam-maser experiment (column 4). The present value for the paramagnetic shielding anisotropy of the outer N-nucleus is in sharp disagreement with the result of Casleton and Kukolich because of the earlier mentioned disagreement in the $c_\perp$-constants (see foot-note of Table 3.4). The value for the same constant of the inner N-nucleus overlap in both works. No ab-initio calculations of diamagnetic contributions are known for $^{14}N_2{}^{16}O$. Accurate values of the total $\sigma_\perp$ and $\sigma_\parallel$ for both nuclei have been reported by Bhattacharyya and Dailey (BHA 73) for $^{15}N_2O$ from which we have determined the anisotropies given in Table 4.3, rows 5 and 6. The diamagnetic contributions, for which no calculated values are available, can be obtained from the differences of the total and paramagnetic contributions. These diamagnetic parts (Table 4.3, rows 3 and 4) can serve as a test for future atom-dipole calculations.

4.5 ANISOTROPIES FOR AXES PERPENDICULAR TO THE MOLECULAR AXIS. Probable molecular structure for excited vibrational states.

In the present investigations values significantly different from zero have been obtained for the anisotropies (perpendicular to the molecular axis) for the spin-rotation constant, the nuclear quadrupole constant, molecular g-factors and magnetic susceptibility. If the configuration of the molecule is assumed to be linear and if the diagonal components of the molecular tensors $\underline{M}$, $\underline{G}$ and $\underline{\chi}$ are defined as in LEE 73,

Table I, then all nuclear contributions to the anisotropies for two mutually perpendicular axes both perpendicular to the molecular axis vanish. Because of symmetry of the electronic charge distribution around the z-axis in a $^1\Sigma$ state the electronic contributions for those two axes are equal and the contribution of the electrons to the anisotropy in azimuthal directions should be exactly zero.

Because non-zero azimuthal anisotropies have been measured it has to be concluded that not only symmetry of the nuclear frame but also of the electronic charge distribution around the molecular axis is broken down.

If for the excited bending vibrational states molecular properties like the components of the spin-rotation constant and the molecular g-factor ($c_{\|}$ and $g_{\|}$, respectively) along the molecular axis are considered the analogy with the symmetric top molecules no longer can be satisfied either. In the definitions of both $c_{\|}$ and $g_{\|}$ the moment of inertia around the molecular axis (I_{zz}) appears in the denominator. In the nuclear parts of the constants the numerator contains terms of the form $r_K^2-z_K^2$ which also vanish in a linear structure, while for the electronic parts L_z is a constant of motion and off-diagonal matrix elements $\langle 0|L_z|n\rangle$ all are zero. Thus in the definitions of both the electronic and nuclear parts of c_{zz} ($=c_{\|}$) and g_{zz}($=g_{\|}$) numerator and denominator are equal to zero and the constants are indeterminate. The problem can be circumvented by chosing a non-linear reference configuration resulting in a slightly asymmetric nuclear framework. In doing so, in fact one vibrational degree of freedom is treated like a rotation. Moss and Perry (MOS 73) state that in that case L_z is no longer a constant of motion and consequently also electronic contributions to the $c_{\|}$ and $g_{\|}$ can be explained.

Accepting this slight asymmetry an attempt has been made to calculate the bend angle. If the x- and z-axis are taken in the plane of the molecule with the z-axis parallel to the base of the obtuse-angled triangle formed by the three atoms in the molecule, then the y-axis points out of the molecular plane. For the moments of inertia the relation $I_z = I_y - I_x$ is then satisfied. For I_x and I_y the following expressions can be postulated if the observed l-doubling is purely an inertial-moment-effect:

$$I_x = \frac{h}{8\pi^2} \frac{1}{B + q_v(v_2+1)/4} \tag{4.5}$$

and

$$I_y = \frac{h}{8\pi^2} \frac{1}{B - q_v(v_2+1)/4} \tag{4.6}$$

If v_2 is set equal to 1, (the case we are primarily interested in) in Eqs. 4.5 and 4.6, and the relations $I_z = I_y - I_x$ and $B_z = h/8\pi^2 I_z$ are used we find for the rotational constant around the z-axis

$$B_z = \frac{B^2 - q_v^2/4}{q_v} \approx \frac{B^2}{q_v} \approx \frac{1}{2.6}\ \omega_2 \tag{4.7}$$

The last part of this equation has been deduced from results of the next section. With the information from Eq. 4.7 and internuclear distances as given for example by Townes (TOW 55 Table 2.1) angles of about 171° between the O-C and C-S bonds in OCS, between the N-N and N-O bonds in N_2O and between Cl-C and C-N bonds in ClCN are obtained, so that at least from the point of view of probable averaged bend structure no large discrepancies in vibrational effects between these molecules are expected (see Sect. 4.7). Anisotropies in azimuthal directions can also be explained with such a slightly asymmetric rotor model (see also HUT 70).

4.6 l-DOUBLING CONSTANTS, ESPECIALLY OCS

From the definition of the l-doubling constant q_{vJ} in Eqs. 2.11, 2.12 and 2.13 and the measurements of q_v for isotopic species of OCS it is not possible to determine the Coriolis coupling constants without knowing values for higher order vibrational effects. In Fig. 4.1 B_o^2/ω_2 is given as a function of q_v for the measured isotopic species of OCS. The values of B_o are taken from TOW 55, values for ω_2 from DOR 64 and the q_v values from Table 3.12. The uncertainty in B_o^2/ω_2 mainly can be ascribed to the error of ω_2, 1 part in 10^3 at most. Within this error all the B_o^2/ω_2 values lie on a straight line whose slope $(\omega_2 q_v/B_o^2)$ is 2.72 with an estimated error of 1% (solid circles). If instead of B_o the equilibrium value B_e is used another curve with the same slope (within the mentioned errors) should be found. Replacing q_v by q_e (Eq. 2.13) the slope also remains unchanged if we assume that the vibrational effects in q_v are the same for all isotopes. The estimated error of 1% in the slope thus represents the possible mutual differences in higher order vibrational effects for the different isotopic species. From the measured slope value and from the known B_o values (TOW 55) and bending vibrational frequencies calculated with Eq. II.200 of HER 45 using force constants and internuclear distances of normal OCS the until now unknown l-doubling constants q_v of less abundant OCS isotopes can be estimated to within 1%. Table 4.4 contains the B_o, ω_2 and q_v values. The less abundant isotopes are indicated in the figure by open circles.

Furthermore using Eq. 2.11 and neglecting higher order vibrational terms the slope can be written as

$$\frac{\omega_2 q_v}{B_o^2} = 2 + 8\left[\frac{\xi_{21}^2\omega_2^2}{\omega_1^2-\omega_2^2} + \frac{\xi_{23}^2\omega_2^2}{\omega_3^2-\omega_2^2}\right] = 2.72(3) \qquad (4.8)$$

With the sum rule $\xi_{21}^2+\xi_{23}^2=1$ and ξ_{21} and ξ_{23} as defined in TOW 55, Eq. 2.7, this relation can be used to obtain the values of ξ_{21}. For the isotopes for which ω_1,ω_2 and ω_3 are known the results of ξ_{21} are given in the last column of Table 4.4.

Table 4.4. Rotational constants B_o, vibrational frequencies ω_2, l-doubling constants q_v and Coriolis parameters ξ_{21} for OCS isotopes.

molecule	B_o(MHz)[a]	ω_2(cm^{-1})[b]	q_v(kHz)[c]	ξ_{21}[c]
${}^{16}O^{12}C^{32}S$	6081.492	527.0	6361.413(3)	0.174(12)
$O^{13}CS$	6061.886	511.4	6507.835(17)	0.182(12)
${}^{18}OCS$	5704.83	521.4	5653.01(5)	0.171(12)
$OC^{33}S$	6004.91	526.5	6209.87(2)	
$OC^{34}S$	5932.82	526.1	6068.80(1)	0.171(12)
$O^{14}CS$	6043.25	497.8	6650(60)	
${}^{17}OCS$	5883.67	524.4	5980(60)	
$OC^{35}S$	5865.2	526.1	5930(60)	
$OC^{36}S$	5799.67	525.8	5800(60)	
$O^{13}C^{34}S$	5911.73	510.8	6200(60)	

[a] TOW 55; [b] DOR 64; [c] Present investigations

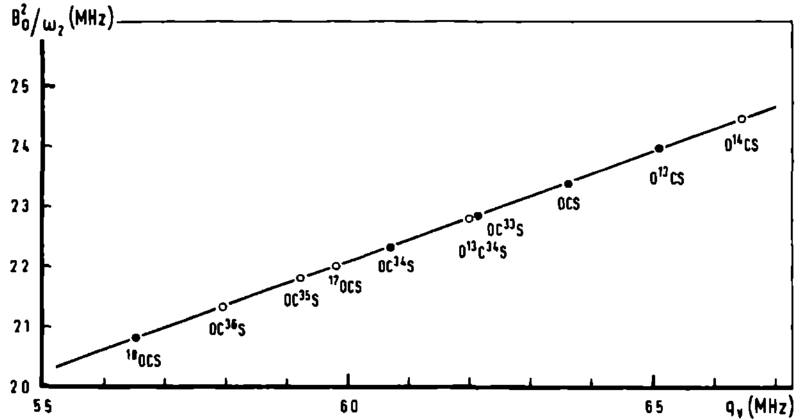

Fig. 4.1 Isotopic species of OCS: B_o^2/ω_2 (from TOW 55) against experimentally obtained l-doubling constants q_v (solid circles). Open circles indicate predicted points for the less abundant species.

A similar curve as in Fig. 4.1 can be constructed from the data available in literature for the group of nine HCN isotopes. Hydrogen and deuterium cyanides, also with the ^{13}C or ^{15}N isotope, have been measured by Törring (TOR 61) and tritium cyanide and its ^{13}C and ^{15}N species by De Lucia (DEL 75) The slope $(\omega_2 q_v/B_o^2)$, defined in the same way as for OCS, of 2.43 can be derived from the measurements with rather small deviations from this averaged value for the individual species. In both cases, for OCS as well as for HCN, only isotopic substitutions have been considered. However, if a group of molecules such as FCN, ClCN, BrCN and ICN is considered the values of B_o^2/ω_2 as a function of q_v lie again on a straight line whose slope is 2.5(2). The larger error is caused by the larger differences in internuclear distances and bond properties between the individual species, so that vibrational effects are different for the different molecules and can not simply be ruled out like for a group of isotopic species, by replacing q_v and B_o by q_e and B_e, respectively.

4.7 BENDING VIBRATIONAL EFFECTS ON NUCLEAR QUADRUPOLE MOMENTS AND ELECTRIC DIPOLE MOMENTS.

Comparison of the values for the nuclear quadrupole coupling constants and electric dipole moments of the OCS, N_2O and ClCN molecules in the ground and first excited bending vibrational state shows that vibrational effects may have a pronounced influence. In Table 4.5 are reproduced quadrupole constants and in Table 4.6 the electric dipole moments for several triatomic linear molecules in the (000) and (01^10) states. The data for HCN, mentioned in these tables, have been taken from TOM 70. As already mentioned in the definitions of q_{i1} and q_{i2} in Eq. 2.24 the first index i=1 refers to the nucleus with the largest quadrupole interaction, outer N nucleus in N_2O and Cl in ClCN. The second index 1 and 2 refers to the zz component and to the difference of the xx and yy components, respectively, of the q-tensor. Distortion of the molecule enhances or introduces probably certain interactions which are not measurable, though possibly present, for the ground state.

The method developed by Ramsey (RAM 52) for the calculation of vibrational effects for diatomic molecules by determining the R-dependence of the molecular constants, is not readily applicable to polyatomic molecules.

Table 4.5. Nuclear quadrupole constants (in kHz) and quadrupole asymmetry parameters,$_1$ η of linear triatomic molecules in the (000) and (01^10) vibrational states.

constant	$OC^{33}S$	$^{14}N^{14}NO$	$^{35}ClC^{14}N$	$HC^{14}N$
$eQq_{11}(v_2=0)$	-29118.4(12)	-773.76(27)	-83275.19(40)	-4707.89(8)
$eQq_{11}(v_2=1)$	-28682.5(9)	-886.53(12)	-82815.54(55)	-4807.9(19)
$eQq_{12}(v_2=1)$	-1180.8(9)	318.78(14)	-927.84(49)	395.1(27)
η_1(%)	4.116(6)	35.96(2)	1.1204(6)	-8.22(6)
$eQq_{21}(v_2=0)$		-267.58(38)	-3622.77(90)	
$eQq_{21}(v_2=1)$		-258.14(18)	-3702.19(40)	
$eQq_{22}(v_2=1)$		-60.84(18)	256.00(41)	
η_2(%)		23.57(7)	-6.914(12)	

Table 4.6. Electric dipole moments (in D) of linear triatomic molecules in the (000), (01^10) and (02^20) vibrational states.

molecule	$\mu_{el}(v_2=0)$	$\mu_{el}(v_2=1)$	$\mu_{el}(v_2=2)$
OCSe[a]	0.754	0.730	
OCS	0.71519(3)[d]	0.70433(3)[b]	0.6936(3)[e]
NNO[b]	0.160880(24)	0.173484(9)	
ClCN[b]	2.83312(15)	2.804(3)	
HCN[c]	2.9646(15)	2.9416(15)	2.8981(15)

[a] TOW 55; [b] Present investigation; [c] TOM 70;
[d] LEE 70, 71; [e] FAB 74.

Some trends, however, can be deduced from the present measurements. For a ^{14}N nucleus at one end of a molecule as in NNO (nucleus 1), ClCN (nucleus 2) and HCN (nucleus 1) an increment of the nuclear quadrupole constants eQq_{i1} by almost the same amount is observed when going from $v_2=0$ to $v_2=1$. In the case of HCN also the value for the (02^20) state is known to be -4899.0(21) kHz for eQq_{11} confirming the increasing trend as v_2 gets higher. For the single case of a ^{14}N in the middle of the triatomic molecule, as nucleus 2 in NNO, a slight decrease of the absolute nuclear quadrupole moment is seen.

The most striking phenomenon, however, is that relative vibrational effects for N_2O appear to be much larger than for other molecules. Moreover, the asymmetry parameter η_i defined as

$$\eta_i=q_{i2}/q_{i1}= \left(\frac{\partial^2V^{(i)}}{\partial x^2} - \frac{\partial^2V^{(i)}}{\partial y^2}\right) / \left(\frac{\partial^2V^{(i)}}{\partial z^2}\right) ,$$

which is a measure for the azimuthal anisotropy of the total field gradient is almost one order of magnitude larger than for other known triatomic molecules (Table 4.5). However, the parallel components of the electric field gradient tensors q_{i1} contain both nuclear and electronic contributions while the azimuthal anisotropy terms q_{i2} in the bend molecule model also contain electronic and nuclear contributions. Therefore, the ratio (η_i^e) of only the electronic contributions to the q_{i2} and q_{i1} seems a better quantity to compare for these triatomic molecules. The nuclear contributions to q_{i1} and q_{i2} are calculated with the expression $q_{i1}^n \approx \sum_K 2Z_K/r_K^3$ and $q_{i2}^n = \sum_K 3Z_K \times (x_K^2-y_K^2)/r_K^5$ (Table 4.7). With values for nuclear quadrupole moments Q from TOW 55 the experimental q_{i1}'s and q_{i2}'s can be calculated from the experimental eQq's. The values for the electronic contributions to the q_{ij}'s are then readily obtained from $q_i^e=q_i(\exp)-q_i^n$. The results are given in Table 4.7 together with the asymmetry parameters $\eta_i^e(=q_{i2}^e/q_{i1}^e)$ for the electronic charge contributions.

Table 4.7. Experimental values for the electric field gradients (in $Å^{-3}$) q_{i1} and q_{i2}, calculated nuclear contributions and predicted electronic contributions to q_{i1} and q_{i2}, nuclear quadrupole moments (TOW 55) in 10^{24} cm^2 and electronic asymmetry parameters η_i^e.

molecule	nucleus	Q	q_{i1}(exp)	q_{i1}^n	q_{i1}^e
ClCN	^{35}Cl	-0.085	28.0	3.42	24.58
ClCN	^{14}N	0.02	-5.8	9.19	-14.99
$N^{(1)}N^{(2)}O$	$^{14}N^{(1)}$	0.02	-1.28	11.1	-12.38
$N^{(1)}N^{(2)}O$	$^{14}N^{(2)}$	0.02	-0.37	19.3	-19.67
OCS	^{33}S	-0.067	12.3	3.95	8.35
HCN	^{14}N	0.02	-6.90	7.95	-14.85

molecule	nucleus	q_{i2}(exp)	q_{i2}^n	q_{i2}^e	η_i^e(%)
ClCN	^{35}Cl	0.314	0.039	0.275	1.1
ClCN	^{14}N	0.37	0.105	0.265	-1.8
$N^{(1)}N^{(2)}O$	$^{14}N^{(1)}$	0.46	0.137	0.323	-2.6
$N^{(1)}N^{(2)}O$	$^{14}N^{(2)}$	-0.088	0.22	-0.308	1.6
OCS	^{33}S	0.506	0.045	0.461	5.5
HCN	^{14}N	0.565	0.091	0.474	-3.2

From Table 4.7 it is now clear that the relative asymmetry in the electronic charge distribution because of vibrational effects does not show a deviating behaviour for N_2O compared with other linear triatomic molecules. The reason for the large relative vibrational and asymmetry effects in the eQq's of N_2O comes from the fact that for the q_{i1}'s, the parallel or zz-components of the electric field tensors, the nuclear and electronic contributions almost cancel each other, which is not the case in the other molecules considered. The nuclear contributions in q_{i1} are larger for N_2O than for the others because of the relatively small internuclear distances in that molecule. A slight distortion of the N_2O configuration then can cause large relative vibrational effects in the eQq's (e.g. $(eQq_{11}(v_2=1)-eQq_{11}(v_2=0))/eQq_{11}(v_2=0))$ though the absolute changes are of the same order as for other linear triatomic molecules (e.g. $eQq_{11}(v_2=1)-eQq_{11}(v_2=0))$.

A deviating behaviour is established for the electric dipole moments. From the five species for which electric dipole moments are known in at least two vibrational states N_2O possesses the largest relative vibrational effect. Moreover, while all molecules show a trend of decreasing dipole moments when going to higher excited bending states, the N_2O molecule behaves just the other way round. For OCS and HCN also (02^20) values for the dipole moments are known which confirm the decreasing character of μ_{el}'s when going to higher v_2's. We do not have any explanation for this strong vibrational effect in μ_{el} of N_2O. Incorrect interpretation of the spectra can be ruled out, completely. From the rather simple treatment in Sect. 4.5 no deviating behaviour for the other triatomic linear molecules could be found as far as averaged changes in the nuclear framework (bending angle) are concerned. A tentative conclusion is that probably relative large changes in electronic contributions occur when N_2O is excited to higher bending vibrational states. From the sign of the electric dipole moment and from the values of μ_{el} in the different bending vibrational states there are indications that negative charge moves from O to the outer N, if bending vibrations are excited.

4.8 MBER SPECTROSCOPY AT HIGH TEMPERATURES.

As has been stated in Sect. 1.5.1 appreciable gain in signal to noise ratio for gaseous species at room temperature has been achieved by increasing the pressure in the source well beyond 1 Torr. The velocity distribution is narrow and shifted to higher velocities, while the rotational temperature of the molecules in the beam is often much lower than the source temperature.

Gordon et al (GOR 71) employed jet sources also for high temperature atomic beams of K, Rb and Cs. Temperatures up to 900 °K corresponding to alkali vapour pressures of 350 Torr have been used. Random translational temperatures as low as 30 °K corresponding to narrow velocity distribution widths with a most probable velocity in the beam of 70% higher than in the oven have been achieved. Those conditions are favourable for polymerization even for loosely bound dimers, which is of course not advantageous for our purposes.

Better results can probably be obtained by mixing the gas in question with a large concentration of a light gas to produce a seeded beam with high kinetic energy (AND 67). Recent experiments on CsF seeded with Xe (BOR 75) showed clearly the possibility of lowering the rotational temperatures from 800 °K down to 6 °K. The population of the low rotational states was increased by up to two orders of magnitude.

Figs. 4.2, 4.3 and 4.4 illustrate the population distribution $f(\rho)$ of the effective dipole moments (ρ) for KCN, CsOH and OCS, respectively, for the same vibrational temperatures (T_{vib}) as used in the corresponding Figs. 1.4, 1.5 and 1.6, but now for the rotational temperature (T_{rot}) of 20 °K. It is clearly seen from these curves that at lower rotational temperatures high effective dipole moments, coming from low J-states are better populated than at higher rotational temperatures. For the low effective dipole moments, originating from higher J-states, it is just the other way round. The velocity distribution, indicated in Sect. 1.4 as $I(v)$, and hence also the distribution function $R(\rho V,v)$ becomes narrower. This can be seen as follows. With an $I(v)$, which is narrower and shifted to higher velocities, new state selector voltages V_o have to be

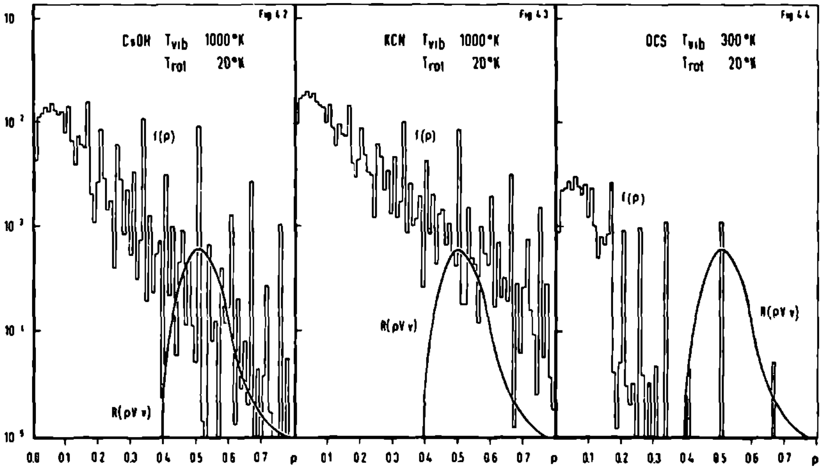

Figs. 4.2, 4.3 and 4.4 Population distributions of ρ for CsOH and KCN at a vibrational temperature of 1000 °K and a rotational temperature of 20 °K (Fig. 4.2 and Fig. 4.3, respectively) and for OCS at a vibrational temperature of 300 °K and a rotational temperature of 20 °K (Fig. 4.4).
The function R(ρV,v) (in arbitrary units) is chosen so that optimum focusation is obtained for ρ=½.

chosen to get a maximum for $\int_o^\infty R(\rho V_o,v)dv$. As can be deduced from Fig. 1.3 this maximum for $\int_o^\infty R(\rho V_o,v)dv$ will be obtained for an I(v) as described above if the function $S(\rho V_o,v)$ is also shifted to higher velocities (by chosing higher voltages V_o) so that the value of v for which $S(\rho V_o,v)$ has a maximum more coincides with the new most probable velocity. This results in the product function S(ρV,v)I(v) or also R(ρV,v) which is more intense in its maximum and narrower than without seeding. The expected detector signal is given by the product of R(ρV,v) and f(ρ) integrated over all ρ's and v's. From a qualitative comparison of these signals as obtained from the Figs. 1.4 through 1.6 and from Figs. 4.2 through 4.4 follows that roughly the same numbers of molecules are expected at the detector. Consequently the noise at a given mass, which is proportional to the square root of the number of molecules will be the same, with and without seeding. Then there will be a gain in signal to noise ratio because of a larger signal of the considered J-state coming from the better population of lower J-states. Lower noise contributions can only be achieved at extremely narrow velocity distributions assuming that no additional noise is introduced by the seeding. Extra noise could be produced by poor and fluctuating mixing of gases in the source. Our attempts of beam seeding thus far failed because of too low pumping speed in the source section of the present machine configuration. New experiments to be performed in the near future have either to confirm or to reject the applicability of seeded beam techniques for high temperature MBER spectroscopy.

Even if a reasonable signal to noise ratio can be achieved with the seeded beams the interpretation of the spectra may turn out to be very difficult if the vibrational and rotational effects on the coupling constants are weak so that hyperfine transitions in different states strongly overlap.

4.9 FINAL REMARKS.

This investigation demonstrates clearly the power of MBER spectroscopy in obtaining very accurate molecular properties of polyatomic molecules in excited vibrational states also.

A good understanding of the problems of extending the technique to high temperature polyatomic species has been acquired and proposals for future investigations are made. The succes in obtaining information about vibrational effects from the excited bending modes in linear triatomic molecules should stimulate the study of additional excited vibrational states of this class of molecules. The abundance of experimental data will provide very sensitive test points for theoretical calculations, which are badly missed at this time.

APPENDIX

Complete survey of the measured and derived molecular constants of all the isotopic species of OCS, N_2O and ClCN considered in this thesis. An explanation of the symbols is given below.

molecule	measured constants	derived quantities
$^{16}O^{12}C^{32}S$ ($v_2=1$)	$q_v, \mu_v, \Delta H, \mu_{el}$, $g_\perp, g_\parallel - g_\perp, g_{xx} - g_{yy}$, $\chi_\perp - \chi_\parallel, \chi_{xx} - \chi_{yy}$	Θ average bending structure ξ_{21}
$^{16}O^{12}C^{34}S$ ($v_2=1$)	q_v, μ_v, μ_{el}	ξ_{21}
$^{16}O^{13}C^{32}S$ ($v_2=1$)	q_v, μ_v, μ_{el}	ξ_{21}
$^{18}O^{12}C^{32}S$ ($v_2=0$)	μ_{el}	
$^{18}O^{12}C^{32}S$ ($v_2=1$)	q_v, μ_v, μ_{el}	ξ_{21}
$^{16}O^{12}C^{33}S$ ($v_2=0$)	eQq_{11}, $c_\perp^{(1)}, \mu_{el}$	$(\sigma_\perp^{(1)} - \sigma_\parallel^{(1)})^P, (\sigma_\perp^{(1)} - \sigma_\parallel^{(1)})$
$^{16}O^{12}C^{33}S$ ($v_2=1$)	$eQq_{11}, eQq_{12}, c_\perp^{(1)}$, $c_\parallel^{(1)} - c_\perp^{(1)}$, $c_{xx}^{(1)} - c_{yy}^{(1)}, \mu_{el}$	η_1, η_1^e, ξ_{21}
$^{14}N^{14}N^{16}O$ ($v_2=0$)	$eQq_{11}, eQq_{21}, c_\perp^{(1)}, c_\perp^{(2)}$, $\mu_{el}, g_\perp, \chi_\perp - \chi_\parallel$, $\sigma_\perp^{(1)} - \sigma_\parallel^{(1)}, \sigma_\perp^{(2)} - \sigma_\parallel^{(2)}$	Θ, sign of μ_{el}, $(\sigma_\perp^{(1)} - \sigma_\parallel^{(1)})^P, (\sigma_\perp^{(1)} - \sigma_\parallel^{(1)})^d$ $(\sigma_\perp^{(2)} - \sigma_\parallel^{(2)})^P, (\sigma_\perp^{(2)} - \sigma_\parallel^{(2)})^d$
$^{14}N^{14}N^{16}O$ ($v_2=1$)	$q_v, \mu_v, eQq_{11}, eQq_{12}$, $eQq_{21}, eQq_{22}, c_\perp^{(1)}$, $c_\parallel^{(1)} - c_\perp^{(1)}, c_\perp^{(2)}, c_\parallel^{(2)} - c_\perp^{(2)}$ μ_{el}, $(g_\parallel + g_\perp)$	average bending structure, influence of bending on electronic charge distribution, η_1, η_2, η_1^e, η_2^e

$^{35}Cl^{12}C^{14}N$ $(v_2=0)$	$eQq_{11}, eQq_{21}, c_\perp^{(1)}, c_\perp^{(2)}$, $\mu_{el}, g_\perp, g_{I_1}(\sigma_{av}^{(1)}-1)$, $\chi_\perp-\chi_\parallel$	Θ, sign of μ_{el}, $(\sigma_\perp^{(1)}-\sigma_\parallel^{(1)})^p, (\sigma_\perp^{(1)}-\sigma_\parallel^{(1)})$ $(\sigma_\perp^{(2)}-\sigma_\parallel^{(2)})^p, (\sigma_\perp^{(2)}-\sigma_\parallel^{(2)})$
$^{35}Cl^{12}C^{14}N$ $(v_2=1)$	$q_v, \mu_v, eQq_{11}, eQq_{12}$, $eQq_{21}, eQq_{22}, c_\perp^{(1)}, c_\perp^{(2)}$, $c_\parallel^{(1)}-c_\perp^{(1)}, c_\parallel^{(2)}-c_\perp^{(2)}, \mu_{el}$	average bending structure, $\eta_1, \eta_2, \eta_1^e, \eta_2^e$

EXPLANATION OF THE USED SYMBOLS

$q_v, \mu_v, \Delta H$	vibration-rotation coupling (or l-doubling) constants for vibrational state v
μ_{el}	electric dipole moment
$g_\perp, g_\parallel-g_\perp$, $g_{xx}-g_{yy}$	molecular g-factors; perpendicular to the molecular (z-)axis, anisotropy for parallel and perpendicular directions, and azimuthal anisotropy (for directions mutual perpendicular and both to the molecular axis)
$\chi_\perp-\chi_\parallel$	magnetic susceptibility anisotropy
$\chi_{xx}-\chi_{yy}$	azimuthal anisotropy in the magnetic susceptibility
eQq_{ij}	nuclear quadrupole coupling constant with e the elementary charge, Q the nuclear quadrupole moment and q the derivative of the electric field at the position of nucleus i, due to all charges outside this nucleus:

value of first index	$^{14}N_2{}^{16}O$	$OC^{33}S$	$^{35}ClC^{14}N$
1	outer N	^{33}S	^{35}Cl
2	inner N		^{14}N

	the second index j of q_{ij} refers to the zz-component if its value is 1, ($q_{i1}=\partial^2V/^{(i)}/\partial z^2$), and to the azimuthal anisotropy term if its value is 2, ($q_{i2}=\partial^2V^{(i)}/\partial x^2-\partial^2V^{(i)}/\partial y^2$), with $V^{(i)}$ the potential at nucleus i.
$c_{\perp}^{(i)}, c_{\parallel}^{(i)}-c_{\perp}^{(i)}$ $c_{xx}^{(i)}-c_{yy}^{(i)}$	spin-rotation coupling constants of nucleus i, perpendicular to the molecular axis, anisotropy for directions parallel and perpendicular to this axis and the azimuthal anisotropy
$\sigma_{av}^{(i)}$	average nuclear shielding constant of nucleus i
Θ	molecular quadrupole moment
$(\sigma_{\perp}^{(i)}-\sigma_{\parallel}^{(i)})$ $(\sigma_{\perp}^{(i)}-\sigma_{\parallel}^{(i)})^p$ $(\sigma_{\perp}^{(i)}-\sigma_{\parallel}^{(i)})^d$	anisotropy in nuclear shielding constants of nucleus i; total, paramagnetic and diamagnetic contribution, respectively.
η_i	asymmetry parameter, defined as $\eta_i=q_{i2}/q_{i1}$
η_i^e	asymmetry parameter of the electronic contributions only ($\eta_i^e=q_{i2}^e/q_{i1}^e$)
ξ_{2i}	Coriolis coupling constants for i=1 and 3, satisfying the sum rule $\xi_{21}^2+\xi_{23}^2 = 1$.

REFERENCES *

ACQ 68 N. Acquista and S. Abramowitz, J. Chem. Phys. 51, 2911 (1968)

AND 67 J.B.Anderson, Entropie 18, 33 (1967)

BHA 73 P.K. Bhattacharyya and B.P. Dailey, J. Chem. Phys. 59, 5820 (1973)

BOR 75 U. Borkenhagen, H. Malthan and J.P. Toennies, J. Chem. Phys. 63, 3173 (1975)

BUC 64 A. Büchler, J. Stauffer and W. Klemperer, J. Phys. Chem. 86, 4544 (1964)

BUC 67 A. Büchler, J. Stauffer and W. Klemperer, J. Chem. Phys. 46, 605 (1967)

BUR 56 C.A. Burrus and W. Gordy, Phys. Rev. 101, 599 (1956)

CAS 75 K.H. Casleton and S.G. Kukolich, J. Chem. Phys. 62, 2696 (1975)

CLE 73 E. Clementi, H. Kistenmacher and H. Popkie, J. Chem. Phys. 58, 2460 (1973)

COH 73 E.R. Cohen and B.N. Taylor, J. Phys. and Chem. Ref. Data 2, 663 (1973)

COR 73 L. Cornelis, QR 41 (1973) in Dutch.

DAB 73 O.B. Dabbousi, W.L. Meerts, F.H. de Leeuw and A. Dymanus, Chem. Phys. 2, 473 (1973)

DAV 75 R.E. Davis and J.S. Muenter, J. Chem. Phys. 61, 2940 (1974)

DEL 75 F.C. De Lucia, J. Mol. Spectr. 55, 271 (1975)

DEU 76 A.P.J. van Deursen, thesis, Katholieke Universiteit Nijmegen (1976)

DIJ 71 F.A. van Dijk, thesis, Katholieke Universiteit Nijmegen (1971)

---

* In the following "QR" stands for Quarterly Report of the Atomic and Molecular Research Group, Fysisch Laboratorium, Katholieke Universiteit, Nijmegen, The Netherlands. These reports are in English, if not stated otherwise, and available on request.

DOR 64 F. Dorman and C.C. Lin, J. Mol. Spectr. 12, 119 (1964)

DYK 74 T.R. Dyke and J.S. Muenter, Review of Molecular Structure and Properties, Series II. A.D. Buckingham Ed., Medical and Technical Publishing Co. Ltd., Lancaster (1974)

DYM 76 A. Dymanus, International Review of Science "Spectroscopy", Physical Chemistry Series 2, vol. 3 Ed. D.A. Ramsey, Butterworths, London 1976

EDM 60 A.R. Edmonds, "Angular Momentum in Quantum Mechanics", Princeton University Press, Princeton, New Jersey 1960

ELL 76 A.W. Ellenbroek and A. Dymanus, Chem. Phys. Lett. to be published

ENG 71 T.C. English, Rev. Sci. Instrum. 42, 1440 (1971)

EWI 72 J.J. Ewing, H.L. Tigelaar and W.H. Flygare, J. Chem. Phys. 56, 1957 (1972)

FAB 74 B. Fabricant and J.S. Muenter, J. Mol. Spectr. 53, 57 (1974)

FIS 63 R.A. Fisher and F. Yates, "Statistical Tables for Biological Agricultural and Medical Research", sixth edition, Ed. Oliver and Boyd, Edinburgh, London (1963)

FLY 69 W.H. Flygare, R.L. Shoemaker and W. Hüttner, J. Chem. Phys. 50, 2414 (1969)

FRE 66 K.F. Freed and J.R. Lombardi, J. Chem. Phys. 45, 591 (1966)

FRE 70 S. Freund, thesis, Harvard University (1970)

FRE 72 S.M. Freund, E. Herbst, R.P. Mariella Jr. and W. Klemperer, J. Chem. Phys. 56, 1467 (1972)

GIE 72 T.D. Gierke and W.H. Flygare, J. Am. Chem. Soc. 94, 7277 (1972)

GOR 71 R.J. Gordon, Y.T. Lee and D.R. Herschbach, J. Chem. Phys. 54, 2393 (1971)

HER 45 G. Herzberg, "Infrared and Raman spectra of polyatomic molecules", Van Nostrand Company, Inc., New York (1945)

HOW 70 B.J. Howard and R.E. Moss, Mol. Phys. 19, 433 (1970)

HOW 71 B.J. Howard and R.E. Moss, Mol. Phys. 20, 147 (1971)

HUT 70 W. Hüttner and K. Morgenstern, Z. Naturforsch. 25a, 547, (1970)

ISM 73 Z.K. Ismail, R.H. Hauge and J.L. Margrave, J. Mol. Spectr. 45, 304 (1973)

JUD 63 B.R. Judd, "Operator Techniques in Atomic Spectroscopy", McGraw Hill Book Company Inc., New York (1963)

KAI 70 E.W. Kaiser, J. Chem. Phys. 53, 1686 (1970)

KUI 75 P. Kuijpers, T. Törring and A. Dymanus, Z. Naturforsch. 30a, 1256 (1975)

KUI 76a P. Kuijpers, T. Törring and A. Dymanus, Chem. Phys. 15, 457 (1976) to be published.

KUI 76b P. Kuijpers, T. Törring and A. Dymanus, Chem. Phys. Lett. (1976) to be published.

KUS 39 P. Kusch, S. Millman and I.I. Rabi, Phys. Rev. 55, 1176 (1939)

LAF 56 W.J. Lafferty, D.R. Lide and R.A. Toth., J. Chem. Phys. 43, 2063 (1956)

LEE 70 F.H. de Leeuw and A. Dymanus, Chem. Phys. Lett. 7, 288 (1970)

LEE 71 F.H. de Leeuw, thesis, Katholieke Universiteit, Nijmegen (1971)

LEE 73 F.H. de Leeuw and A. Dymanus, J. Mol. Spectr. 48, 427 (1973)

LID 67 D.R. Lide and R.L. Kuczkowski, J. Chem. Phys. 46, 4768 (1967)

LID 69 D.R. Lide and C. Matsumura, J. Chem. Phys. 50, 3080 (1969)

LOV 71 F.J. Lovas and D.R. Lide Jr., Advances in High Temperature Chemistry, L. Eyring Ed., Vol. 3, Academic Press, New York (1971)

MAK 67 A.G. Maki and D.R. Lide, J. Chem. Phys. 47, 3206 (1967)

MAK 73 A.G. Maki and D.R. Johnson, J. Mol. Spectr. 47, 226 (1973)

MAT 69 C. Matsumura and D.R. Lide, J. Chem. Phys. 50, 71 (1969)

MEE 72 W.L. Meerts and A. Dymanus, J. Mol. Spectr. 44, 320 (1972)

MEE 75a W.L. Meerts, thesis, Katholieke Universiteit, Nijmegen (1975)

MEE 75b W.L. Meerts and A. Dymanus, Can. J. Phys. 53, 2123 (1975)

MEE 75c W.L. Meerts, QR 49 (1975)

MEE 76a W.L. Meerts, F.H. de Leeuw and A. Dymanus, Chem. Phys. (1976) to be published.

MEE 76b W.L. Meerts, Chem. Phys. 14, 421 (1976)

MOS 73 R.E. Moss and A.J. Perry, Mol. Phys. 25, 1121 (1973)

MUE 68 J.S. Muenter, J. Chem. Phys. 48, 4544 (1968)

MUE 75 J.S. Muenter, J. Mol. Spectr. 55, 490 (1975)

NIE 43 H.H. Nielsen and W.H. Schaffer, J. Chem. Phys. 11, 140 (1943)

NIE 51 H.H. Nielsen, Revs. Mod. Phys. 23, 90 (1951)

PEA 73a E.F. Pearson and M.B. Trueblood, J. Chem. Phys. 58, 826 (1973)

PEA 73b E.F. Pearson and M.B. Trueblood, Astroph. J. 179, L145 (1973)

POR 61 R.F. Porter, J. Chem. Phys. 35, 318 (1961)

RAM 52 N.F. Ramsey and E.M. Purcell, Phys. Rev. 85, 143 (1952)

REI 69 J. Reinartz, QR 25 (1969) in Dutch

REI 70a J. Reinartz, QR 26 (1970)

REI 70b J. Reinartz, QR 29 (1970)

REI 71a J. Reinartz, Monograph (1971) in Dutch

REI 71b J. Reinartz, QR 33 (1971)

REI 72a J. Reinartz, QR 34 (1972)

REI 72b J. Reinartz, QR 36 (1972)

REI 72c J. Reinartz, QR 37 (1972)

REI 72d J.M.L.J. Reinartz, W.L. Meerts and A. Dymanus, Chem. Phys. Lett. 16, 576 (1972)

REI 73a J.M.H. Reijnders, QR 40 (1973)

REI 73b J. Reinartz, QR 39 (1973)

REI 74a J. Reinartz, QR 42 (1974)

REI 74b J. Reinartz, QR 43 (1974)

REI 74c J.M.L.J. Reinartz and A. Dymanus, Chem. Phys. Lett. 24, 346 (1974)

REI 75a J. Reinartz, QR 46 (1975)

REI 75b J. Reinartz, QR 48 (1975)

REI 75c J. Reinartz, QR 49 (1975)

REI 76 J. Reinartz, QR 50 (1976)

SCH 61 C. Schlier, Fortschritte Phys. 9, 455 (1961)

SCH 70 L.H. Scharpen, J.S. Muenter and V.W. Laurie, J. Chem. Phys. 53, 2513 (1970)

STO 72 S. Stolte, thesis, Katholieke Universiteit, Nijmegen (1972)

TAF 73 H. Taft, P. Bhattacharyya, N. Smith and B.P. Dailey, Chem. Phys. Lett. 22, 113 (1973)

TOM 70 G.R. Tomasevich, thesis, Harvard university (1970)

TOR 61 T. Törring, Z. Physik, 161, 179 (1961)

TOR 73 T. Törring, J. Mol. Spectr. 48, 148 (1973)

TOW 55 C.H. Townes and A.L. Schawlow, "Microwave Spectroscopy", McGraw Hill Book Company Inc., New York (1955)

VER 69 J.A.Th. Verhoeven, thesis, Katholieke Universiteit, Nijmegen (1969)

WAC 67a R. van Wachem, thesis, Katholieke Universiteit, Nijmegen (1967)

WAC 67b R. van Wachem, QR 15 (1967)

WHI 55 R.L. White, Revs. Mod. Phys. 27, 276 (1955)

WIC 72 B.G. Wicke, R.W. Field and W. Klemperer, J. Chem. Phys. 56, 5758 (1972)

YAR 57 L. Yarmus, Phys. Rev. 105, 928 (1957)

YUT 62 A. Yutsis, I. Levinson and V. Vanagas, "The Theory of Angular Momentum", Israel Program for Scientific Translations, Jerusalem (1962)

ZOR 73 J.C. Zorn and T.C. English, Advances in Atomic and Molecular Physics, D. Bates and I. Estermann, Eds. Vol. 9, Academic Press, New York (1973)

SAMENVATTING

In dit proefschrift worden enkele drieatomige molekulen onderzocht met behulp van molekulaire bundel elektrische resonantie (MBER) spektroskopie.

Na uitgebreide metingen aan tweeatomige molekulen bij hoge temperaturen (∿1000 °K) in het verleden leek uitbreiding tot meeratomige molekulen bij deze temperaturen een voor de hand liggende stap. In dit onderzoek is gebleken dat de stap van tweeatomige naar de eenvoudigste meeratomige (n.l. de lineaire drieatomige) molekulen moeilijker is dan men op het eerste gezicht zou vermoeden. Het kenmerkende verschil tussen tweeatomige en lineaire drieatomige molekulen is dat deze laatste buigvibraties vertonen met relatief lage frekwenties, zodat de bezetting van de laagste quantum toestanden, zeker bij hoge temperaturen, zeer gering zijn. Dit betekent relatief zwakke signalen voor deze toestanden, waar we primair in geinteresseerd zijn. De bezetting van hogere vibratie- en rotatietoestanden is relatief hoog. Deze toestanden dragen zeer sterk bij tot ongewenste signalen op de detektor en leveren enerzijds een grote hoeveelheid moeilijk te identificeren spektraallijnen op en anderzijds een grote ruisbijdrage. Zodoende konden met de huidige techniek spektra van KCN en CsOH niet voldoende opgelost worden.

Om eerst meer ervaring op te doen met hogere aangeslagen buigvibraties zijn enkele molekulen uitgezocht die gasvormig zijn bij kamertemperatuur; OCS, N_2O en ClCN. Bij deze temperatuur bevinden ruwweg 90% van alle molekulen zich in de grondvibratie toestand en 10% in de eerste aangeslagen buigvibratie ($v_2=1$). Om spektra van deze molekulen in de $v_2=1$ toestand te kunnen waarnemen met voldoende signaal ruis verhouding worden nozzle bundels gebruikt. Deze techniek levert 1) meer voorwaarts gerichte bundels 2) smallere snelheidsverdelingen, zodat fokussatie effektiever verloopt en 3) invriezing van rotatievrijheidsgraden (Sektie 1.5.1).

De theorie van de spektra, welbekend voor de grondvibratie toestand, is uitgebreid (Hoofdstuk 2) voor de eerste aangeslagen buigvibratie. Resultaten van deze theorie zijn uitdrukkingen voor de frekwenties van de resonantie lijnen in termen van koppelingskonstanten; hyperfijn koppelingskonstanten en elektrische en magnetische momenten.

De gemeten spektra van verscheidene OCS-isotopen, van N_2O en ClCN in de grondvibratie en in de eerste aangeslagen toestand van de buigvibratie en hieruit verkregen waarden voor de koppelingskonstanten zijn gegeven in Hoofdstuk 3.

Uit de experimentele koppelingskonstanten kunnen molekulaire grootheden zoals molekulair kwadrupoolmoment, teken van het elektrische dipool moment, paramagnetische bijdragen tot anisotropie in de nukleaire shielding konstanten e.d. bepaald worden. Anisotropieën in richtingen loodrecht op de molekulaire as in de c-konstanten, g-faktoren e.a. en ook komponenten van enkele grootheden langs de molekulaire as ($c_{\parallel}$, $g_{\parallel}$) kunnen niet meer verklaard worden met een lineaire molekulaire struktuur.

Sterke relatieve buigvibratie effekten in nukleaire kwadrupoolmomenten en in het elektrische dipoolmoment zijn gesignaleerd in N_2O. Theoretische berekeningen aan dit soort molekulen in aangeslagen vibraties zijn een groot gemis op dit moment.

Voor hoge temperaturen MBER spektroskopie aan meeratomige molekulen wordt de toepassing van "seeded beams" kwalitatief beschouwd. Een verbetering van signaal ruis verhouding van de spektra is te verwachten. Toekomstige experimenten zullen moeten uitwijzen of deze winst in signaal ruis verhouding voldoende is om de spektra van bijvoorbeeld KCN te kunnen oplossen.

CURRICULUM VITAE

De schrijver van dit proefschrift werd geboren op 2 mei 1946 in Rimburg. Daar doorliep hij de lagere school, waarna de middelbare schoolopleiding gevolgd werd aan het St.Bernardinuscollege te Heerlen. In juli 1965 behaalde hij het diploma gymnasium β. Hierna ging hij Wis- en Natuurkunde studeren aan de Katholieke Universiteit in Nijmegen. Het kandidaatsexamen werd in januari 1968 afgelegd. Als afstudeerrichting koos hij experimentele natuurkunde binnen de werkgroep Atoom- en Molekuulfysika. Aan deze groep bleef hij ook na het doktoraalexamen in april 1971 als wetenschappelijk medewerker verbonden. Onder leiding van Prof. Dr. A. Dymanus verrichtte hij onderzoek aan drieatomige lineaire molekulen. De resultaten van deze studie worden gegeven in dit proefschrift.

Na reeds als kandidaatsassistent meegewerkt te hebben aan diverse werkkolleges in de wiskunde en natuurkunde, bestond zijn onderwijstaak na het afstuderen uit het assisteren bij het voorkandidaats natuurkunde praktikum en het geven van werkkolleges in de Algemene Natuurkunde voor chemiestudenten.

Sinds augustus 1976 is hij als natuurkunde docent verbonden aan de Lerarenopleiding van de Gelderse Leergangen in Nijmegen.

STELLINGEN

1

De grote afwijkingen van een Boltzman verdeling voor de rotatie-energieniveaus gemeten door Kukolich *et al.* in nozzlebundels van OCS zijn niet reëel.

S.G. Kukolich, D.E. Oates and J.H.S. Wang, J. Chem. Phys. 61, 4686 (1974)

2

Het optreden van een mogelijke negatieve "bending potential hump" voor CsOH is zeer twijfelachtig.

D.R. Lide and C. Matsumura, J. Chem. Phys. 50, 3080 (1969)
K. Yamada and M. Winnewisser, Z. Naturforsch. 31a, 139 (1976)

3

De overgangen $2_{12} \rightarrow 3_{03}$ en $4_{14} \rightarrow 5_{05}$ in ozon waarnaar Pochan *et al.* gezocht hebben zijn niet toegestaan vanwege het Pauli verbod.

J.M. Pochan, R.G. Stone and W.H. Flygare, J. Chem. Phys. 51, 4278 (1969)

4

De potentiaal zoals bepaald door Helbing *et al.* voor H_2-edelgassystemen is wel in staat gloryverschijnselen in de totale botsingsdoorsnede te beschrijven maar niet de ligging van de gebonden toestanden.

R. Helbing, W. Gardi and H. Pauly, Z. Physik, 208, 215 (1968)
J.P. Toennies, W. Welz and G. Wolf, J. Chem. Phys. 64, 5305 (1976) L. Zandee, Disc. Far. Soc. 62.

5

De funktie gegeven door Fisk *et al.* om de eindige levensduur van het bij een botsing gekreëerde komplex tot uitdrukking te brengen in de verhouding van intensiteiten verstrooid over 0 en 180 graden is niet korrekt. De met deze funktie bepaalde levensduren dienen ongeveer een faktor twee korter genomen te worden.

G.A. Fisk, J.D. McDonals and D.R. Herschbach, Disc. Far. Soc. 44, 228 (1967)
M.K. Bullitt, C.H. Fisher and J.L. Kinsey, J. Chem. Phys. 60, 478 (1974)

6

Voor "lineaire" molekulen, zoals OCS, N_2O en ClCN, kunnen de anisotropieën in de molekulaire koppelingskonstanten voor richtingen loodrecht op de molekulaire as evenals de komponenten van verscheidene koppelingskonstanten langs deze molekulaire as niet meer verklaard worden met een lineaire struktuur van het molekuul als dit zich in de eerste aangeslagen buigvibratietoestand bevindt.

7

In opgaven over elektriciteitsleer, waarin sprake is van een oneindig dunne cirkelvormige schijf met uniform verdeelde oppervlaktelading wordt een fundamentele fout gemaakt als niet vermeld staat dat het een isolator betreft.

I. Wolff, Grundlagen und Anwendungen der Maxwellschen Theorie I, Hochschulskripten 818/818a, Hochschultaschenbücher-verlag, Mannheim/Zürich (1968)

D. Halliday and R. Resnick, Physics I and II, John Wiley and Sons, Inc., New York (1966)

8

De mogelijkheid voor herhaalde publikatie van overzichtswerk is groter naarmate meerdere auteurs hieraan bijgedragen hebben.

J.C. Zorn and T.C. English, Advances in Atomic and Molecular Physics, vol. 9, D.R. Bates and I. Estermann, Eds., Academic Press, New York (1973)

T.C. English and J.C. Zorn, Methods of Experimental Physics, vol. 3B, Molecular Physics, D. Williams, Ed., Academic Press, New York (1974)

2 december 1976 J.M.L.J. Reinartz